The Pennsylvania State University

The Graduate School

Intercollege Program of Materials Science and Engineering

A THERMODYNAMICS BASED GUIDE TO ADDING HF TO A NI-SUPERALLOY TO IMPROVE OXIDATION RESISTANCE

A Dissertation in

Materials Science and Engineering

by

Austin J. Ross

Submitted in Partial Fulfillment
of the Requirements
for the Degree of

Doctor of Philosophy

December 2017

A dissertation of Austin J. Ross was reviewed and approved* by the following:

Zi-Kui Liu
Professor of Materials Science and Engineering
Dissertation Advisor, Committee Chair

Long-Qing Chen
Hamer Professor of Materials Science and Engineering, Engineering Science and Mechanics, and Mathematics

Vincent Crespi
Distinguished Professor of Physics, Materials Science and Engineering, and Chemistry

Ismaila Dabo
Assistant Professor of Materials Science and Engineering

Hojong Kim
Assistant Professor of Materials Science and Engineering

Suzanne Mohney
Professor of Materials Science and Engineering and Electrical Engineering
Chair, Intercollege Graduate Degree Program in Materials Science and Engineering

* Signatures are on file in the Graduate School

Abstract

This thesis focuses on the addition of the reactive element Hf to aid in the oxidation resistance of Ni-superalloys. Hf will improve the oxidation resistance of a given Al_2O_3 forming alloy when added to the alloy in small concentrations. However, when too much Hf is added, or rather when Hf is "over-doped", the oxidation resistance begins to worsen again. To date there is no design criteria for how much Hf should be added. The traditional value is around 0.1 at.%. This thesis looks to establish thermodynamic criteria for the addition of Hf based on consideration for the reactions at the alloy/Al_2O_3 interface.

The first part of this thesis is on the important Hf-Ni binary system. This system has been investigated several times in the literature but often using Hf sources contaminated by Zr. This work seeks to remodel the Hf-Ni system through the calculation of phase diagram (CALPHAD) approach based on first-principles calculations based in density functional theory (DFT) and additional experiments using high purity Hf. Diffusion couples in the Ni-rich portion of the Hf-Ni system were heat treated and analyzed at 1173.15, 1273.15 and 1373.15 K, respectively, to measure phase stability and Hf solubility in the fcc phase. The solubility observed in fcc Ni from Ni/$Ni_{50}Hf_{50}$ (at.%) diffusion couples is larger than that reported in previous experiments. These results are the only source fit to during modeling of the fcc solubility to avoid effects from Zr contamination. Data in the literature suggests that the high temperature crystal structure of the B33 NiHf phase is, in fact, the B2 structure. Because this phase has been observed to be in solid solution with the high temperature B2-NiTi, it has been modeled here as B2. Modeling of this phase was aided by first-principles calculations using special quasi-random structures (SQS).

.

Following this, the Ni-rich Al-Hf-Ni system and the Ni-rich Cr-Hf-Ni system are modeled to develop a Ni-rich model for the Al-Cr-Hf-Ni system. These models are based on experiments and first-principles calculations using density functional theory, both carried out in the present work. Thermodynamic models are developed with a focus on the fcc-γ, $L1_2$-γ', A2, B2, $L2_1$ and $P6_2m$-NiAlCr phases. Additional focus is placed on the η-Ni_7Hf_2 phase and the λ-Ni_3Hf phase, both with solubility of Al, Cr and Ni based on available work in the literature. Isothermal heat treatments are performed on alloys in the Ni-rich Al-Hf-Ni system and the Ni-rich Cr-Hf-Ni system in the range of 1273.15 K to 1473.15 K using high purity Hf to avoid Zr contamination. Density functional theory calculations are performed to obtain formation enthalpies for stoichiometric phases and the mixing enthalpies in the fcc-γ, $L1_2$-γ', A2, and B2 phases using SQS. Finite temperature properties of some end-members in the γ', $L2_1$ and $P6_2m$-NiAlCr phases are obtained by first-principles calculations. The current models replicate the present experiments in the Ni-rich Al-Hf-Ni and Cr-Hf-Ni systems well and agree with many features from other experimental investigations in the literature. These thermodynamic descriptions are then combined with thermodynamic models of the Al-Cr-Ni system and other binary models from the literature to form the thermodynamic description of the quaternary system. Good agreement is found between quaternary experiments and the calculations from the present thermodynamic description.

Over-doping is accompanied by precipitation of HfO_2 in and beneath the external Al_2O_3 layer, i.e. the co-existence of these two oxides at the alloy/Al_2O_3 interface. This equilibrium can thus be

used to determine the maximum Hf concentration which will result in HfO_2 precipitation. This Hf concentration is termed the "Hf-tolerance" and calculated with the alloy/Al_2O_3/HfO_2 equilibrium. The Al-Cr-Hf-Ni thermodynamic description is combined with the thermodynamic descriptions of Al_2O_3 and HfO_2 to study this equilibrium in terms of the Hf and Al activities in the alloy. The calculated Hf-tolerance is compared with available observations in the literature and is in good agreement. It is shown that the γ' phase plays a key role in increasing the Hf-tolerance.

Finally, the effects of other alloying elements on the Hf-tolerance is explored. In the present work interactions between Hf and other alloying elements in the fcc/$L1_2$ phase are obtained from DFT-based first-principles calculations. Since the ordered $L1_2$-Ni_3Al (γ') phase is already understood to be important for oxidation resistance, only elements with a solubility in the $L1_2$ phase of greater than 5 at.% at 1000 °C are chosen for study. The calculations confirm that Pt, Pd, Ru, Rh, and Si are the most beneficial alloying elements as reported in the literature experimentally. Given this information, the Al-Cr-Hf-Ni-Pt-O system is modeled, and used to calculate the Hf-tolerance in the Ni-rich Al-Hf-Ni-Pt and Al-Cr-Hf-Ni-Pt systems. Results from these calculations agree well with experimental observations.

In summary, this thesis provides a thermodynamic criterion on the maximum Hf contents on improving oxidation resistance of Al_2O_3 forming Ni-superalloys. This criterion is established by developing thermodynamic descriptions of several multicomponent systems including xxx using data from DFT-based first-principles calculations and experiments in the current work and the literature and by calculating the equilibrium between alloys/Al_2O_3/HfO_2.

Table of Contents

List of Figures

List of Tables

Acknowledgements

I would like to thank all my committee members for their input into this work. I would especially like to thank my advisor Dr. Zi-Kui Liu for all of his patience in helping me get this far. His energy was second to none and his optimism and faith in me was always appreciated. Additionally, I would like to express my gratitude to Dr. Thomas Gheno and Dr. Brian Gleeson for teaching me an incredible amount on high temperature oxidation during my projects with the Department of Energy.

My colleagues and friends were an incredible resource for me during my stay at graduate school. My education was all the richer for my interactions with them. In my research group I would like to thank all the researchers I had the pleasure of working with. However, I would like to especially single out Dr. Greta Lindwall and Dr. Xuan Liu for all their assistance. I truly would not be where I am today without them.

Finally, I would like to thank my wife and all of my family for believing in me.

Dedication

This dissertation is dedicated to my mother, Deborah Singer. She was the first who believed I could be a scientist.

1 Introduction

1.1 Introduction to High-Temperature Oxidation of Ni-Superalloys

Nickel-based superalloys are alloys which can retain their exceptional mechanical properties at temperatures up to 0.6 times their melting temperatures and in harsh environments[1]. In many cases, the ability of superalloys to resist damage in harsh environments comes from the presence of metallic coatings containing appreciable amounts of aluminum (Al), chrome (Cr) or typically a combination of both of these elements and other beneficial elements such as Hf and Y[1]–[4]. For high enough concentrations, Al and Cr give these metallic coatings the ability to form a dense, external layer of either Al_2O_3 or Cr_2O_3, depending on the relative concentration of each. These external oxide layers (scales) limit the transport of oxygen (O) to solid state diffusion through the oxide and oxide grain boundaries[2], [5], [6] which becomes the rate limiting step in oxidation at high temperatures. The establishment of a protective thermally grown oxide (TGO) scale is the main objective when designing protective metallic coatings[7]. At temperatures exceeding 1000 °C, Cr_2O_3 will begin to volatilize significantly through the formation of gaseous CrO_3[8]. The formation of gaseous $CrO_2(OH)_2$ occurs at even lower temperatures when Cr_2O_3 forming alloys are oxidized in mixtures of O_2 and H_2O[9]. Therefore, Al_2O_3 is the preferred protective layer at high temperatures. For this reason coatings rich in Al and aluminide compounds are often established on superalloy turbine blades through diffusion of Al into the superalloy surface. However, the chemistry of the aluminide deposition is determined by the underlying alloy composition and processing conditions. To offer greater control over the bond coat composition, overlay coatings containing a base component, typically cobalt (Co) or nickel

(Ni), with appreciable concentrations of Cr and Al and other minor additions (MCrAlY coatings) are used.

The type of TGO established on an MCrAlY coating will depend on the relative concentrations of Al and Cr. Pettit et al. observed three different oxidation morphologies in Ni-Al-Cr alloys depending on the alloying content[6], [10]: (i) formation of an external layer of NiO followed by internal Al-rich oxide precipitates growing into the alloy; (ii) formation of an external layer of a less noble oxide than the base alloy (e.g. Cr_2O_3), followed by Al-rich oxide precipitates forming internally in the alloy; and (iii) formation of an external layer of Al_2O_3 which is slow growing and desired in most applications. The formation of oxide precipitates into the alloy in groups (i) and (ii) is called internal oxidation. This type of oxidation provides little protection to the alloy and can embrittle the matrix[11], [12].

Since Al_2O_3 is the desired oxide for high temperatures it is important to achieve only the morphology that results in external Al_2O_3 growth during oxidation. This requires high concentrations of Al in the Ni-Al system[13]. However, elements like Cr can reduce the amount of Al required to form this external oxide[14]. These restrictions add another layer of complication when considering the design of MCrAlY systems and it becomes crucial to understand the underlying thermodynamics governing the phase behavior and oxidation behavior in this system.

1.2 Reactive Elements

Although Al_2O_3 offers excellent protection from oxidation at high temperatures, it does not come without its limitations. Perhaps the largest problem is that it is challenging to sustain the growth of an oxide on a metal during thermal cycling from high to low temperatures. This is due to the mismatch in thermal expansion coefficients between the metal and the oxide[1]. This thermal

cycling causes significant growth stresses at the oxide/metal interface and can lead to a loss of oxide adherence to the metal of even to catastrophic loss of the external oxide(spallation)[15]. This eventual spallation is due, in-part, to the fact that growth stresses scale with the thickness of the oxide[2]. Hence, one approach to reduce the onset of scale spallation is to simply reduce the growth rate of Al_2O_3 during oxidation.

Since Al_2O_3 grows primarily through ion movement in the Al_2O_3 grain boundaries, a popular method of reducing the growth of Al_2O_3 is through the use of elements which cluster in the grain boundaries and slow ion movement there[16]. The elements which do this most effectively in Al_2O_3 are Hf, Zr, and Y. Each of these elements have been found to reduce the growth rate by roughly a factor of two when added in small amounts (typically 0.05 to 0.1 at.%) in most Al_2O_3 forming alloys[16]. That Y is in the name MCrAlY speaks to the industrial effectiveness of adding small portions of these elements. However, there are two major challenges that face MCrAlYs today:

1) When too much reactive element is added to an alloy, the oxidation resistance of the alloy begins to worsen again.
2) Despite the fact that increasing the concentration of reactive element before this point translates to a better oxidation resistance[17], there is no actual criteria for how much reactive element you should add to an alloy.

The first challenge can become so severe that the oxidation resistance becomes worse than the oxidation resistance of the base alloy. This is usually termed “over-doping”. Over-doping is generally considered the leading cause of critical failure and spallation in reactive-element modified alloys[18].

1.3 Objectives

This work focuses primarily on Hf alloying additions to Ni-rich Al-Cr-Ni-Hf alloys to improve their oxidation resistance. Specifically, this work aims to establish a thermodynamic basis for predicting over-doping in a given alloy system in the disordered fcc phase (γ) and the ordered $L1_2$ phase (γ'-Ni_3Al). To do this it is important to focus not just on the stability of phases, but also on the activity of species in these phases and the specific equilibria resulting between neighboring phases. The calculation of phase diagram (CALPHAD) method offers an excellent means of achieving these features in a given alloy system[19]. This method brings phase equilibria and thermochemical equilibria together to define the Gibbs-energy space for a given system. In particular, this method can be coupled with first-principles calculations using density functional theory (DFT) to model thermodynamic properties that are either missing from experiments, or impossible to achieve experimentally[20].

Using the CALPHAD method and DFT the present work seeks to achieve the following:

I. A reliable description in the Ni-rich Al-Cr-Hf-Ni system of those phase boundaries directly affecting the activity of Hf in within the γ and γ' phase - i.e. the solubility of Hf in γ and γ' phases. This will entail:
    a. Thermodynamic modeling of the Hf-Ni system based on new experiments and first-principles calculations.

    and

    b. Thermodynamic modeling in the Ni-rich portions of the Al-Hf-Ni system and the Cr-Hf-Ni system.

II. A prediction of the onset of over-doping using thermodynamic considerations in the Ni-rich Al-Cr-Hf-Ni-O system.

III. A thorough, first-principles based search for other alloying elements which can improve the performance of Hf. This amounts to the following:

   a. The calculation of binary fcc solution phases and ordered $L1_2$ phases in the X-Hf system (X= Al, Co, Cr, Cu, Fe, Ga, Ge, Hf, Mn, Nb, Ni, Pd, Pt, Sc, Si, Ta, Ti, V, and Zn.)

   b. A thermodynamic model of the Ni-rich Al-Cr-Hf-Ni-Pt system based on first-principles and experiments.

   c. A prediction of the onset of over-doping using thermodynamic considerations in the Ni-rich Al-Cr-Hf-Ni-Pt-O system.

2 Computational methodology

2.1 Density Functional Theory

In recent years it has become more common to use ab-initio techniques over empirical models to obtain useful properties of molecules and crystal systems. This is made possible by computational quantum mechanics and the increasing computational power available to researchers. In quantum mechanics the energy of a time-independent system can be defined as follows:

$$H\psi(r_1, r_2, r_3 \dots r_N) = E\psi(r_1, r_2, r_3 \dots r_N) \qquad \textbf{Eq. 2.1}$$

H is the Hamiltonian operator which has eigenvalues corresponding to the energy, E, of the system with wave function $\psi(r_1, r_2, r_3 \dots r_N)$. There are many methods which attempt to build the wave function of a system. No matter what short-cuts these take it is likely to get cumbersome with increasing numbers of atoms. This is because a wave function will have variables of dimension and spin for *each* electron in that wave function. Another method is to calculate the properties of a system based on its electronic density. This is more manageable because it is only a function of spatial coordinates. Such an approach was made available by the work of Hohenberg and Kohn who formulated two main theorems. These are as follows[21]:

1. There exists a ground state electronic density function unique to the ground state of a system
2. Any trial electron density function will result in a functional which gives an energy equal to or greater than the ground state energy.

Kohn and Sham were able to construct a functional of the ground state energy based on these underlying assumptions and the construction of an electronic reference system. This electronic

reference system is one in which electrons do not interact. When in functional form, this equation may be represented as follows[22]:

$$\left[-\frac{1}{2}\nabla^2 + V_n(r) + V_{ee}(r) + V_{XC}(r)\right]\psi_i^{KS} = \varepsilon_i^{KS}\psi_i^{KS} \qquad \textbf{Eq. 2.2}$$

This equation is in Hartree units. The term ψ_i^{KS} is a Khon-Sham orbital analogous to the wave function orbitals in quantum mechanics. The term on the left hand side in square brackets is the Kohm-Sham operator. Here, $-\frac{1}{2}\nabla^2$ is the kinetic energy operator, $V_n(r)$ is the columbic potential between atomic nuclei, $V_{ee}(r)$ is the potential which results from an interacting gas of electrons distributed over some space, and the final term, V_{XC}, accounts for the unknown kinetic and potential contributions. This is the exchange-correlation potential. It is a functional derivative of the unknown energy contribution, $E_{XC}[\rho(r)]$, with respect to the electronic density:

$$\frac{\delta E_{XC}[\rho(r)]}{\delta\rho(r)} \qquad \textbf{Eq. 2.3}$$

Most improvements to DFT lie in designing exchange functionals to improve $V_{XC}(r)$. The simplest way of improving Eq. 2.3 is the local density approximation (LDA.) This functional assumes that the energy density at some point in the system with charge density $\rho(r)$ is given by energy density of an electron gas with the same charge density. Taking spins into account in this approximation results in the local spin density approximation (LSD or LSDA) which differentiates between the electron densities of spin up and spin down electrons[23]. A more sophisticated functional is found from the generalized gradient approximation (GGA.) This approximation takes both the electron density and its gradient at some point to compute the

energy functional but were initially only semi-empirical[24]. To get A non-emprical form of GGA by Perdew, Berke and Ernzerhof (called PBE) takes LSDA contributions in combination with physical approximations for the contributions made by the electron density gradient at a certain point[24]. This method loses some information about second-order electron density curvature compared to other functionals but represents a simpler form of approximations. Finally, more sophisticated still, is a weighted sum of GGA exchange-correlation energy and correction energies for columbic repulsions of each electron in the ψ_i^{KS} orbital. This is called a Hybrid functional. Hybrid functionals are used partly in this work because they significantly improve predictions for transition metal oxide formation enthalpies[25].

A number of useful properties are available if we can determine the ground state energy as a function of crystal volume and atomic position. For instance the enthalpy at 0 K of a binary structure composed of elements A and B can be obtained as follows:

$$\Delta H(A_aB_b) = E^{\gamma}(A_aB_b) - aE^{\alpha}(A) - bE^{\beta}(B) \qquad \textbf{Eq. 2.4}$$

γ is the phase (crystal structures) of the binary compound while α and β are the phases of the component elements. If α is the stable phase at standard pressure and temperature (SER) for each element then this gives us the enthalpy of formation. However, if $\alpha = \beta = \gamma$ then Eq. 2.4 calculates the enthalpy of mixing[26]. To gain information regarding the mixing enthalpy one must resort either to a dilute calculation (where A outnumbers B greatly or vice versa) or use a structure which sufficiently mimics a disordered structure. These enthalpies will find application in the CALPHAD method as will finite temperature information obtained by exploring further ground state properties.

We can also obtain properties about the system by manipulating the volume of crystal unit cells and calculating the corresponding cohesive energy. When a number of these points have been calculated they are fit to an equation of state (EOS.) Typically the equation of state is given as Birch-Murnaghan EOS or else some variation of this fitting[27][28]. The original Birch-Murnaghan fitting is given as follows:

$$E(V) = a + bV^{-2/3} + cV^{-4/3} - dV^{-2} + eV^{-8/3} \quad \textbf{Eq. 2.5}$$

Calculations performed by Shang et al. found that for some Ni systems setting e=0 yielded the most accurate results[27]. This 4 parameter EOS will be used throughout for this reason. Having energy as a function of volume grants us the ability to manipulate this function to yield other useful physical properties. These are as follows:

$$P(V) = -V\frac{\partial E(V)}{\partial V} \quad \textbf{Eq. 2.6}$$

$$B(V) = -V\frac{\partial P(V)}{\partial V} \quad \textbf{Eq. 2.7}$$

$$B'^{(V)} = \frac{\partial B(V)}{\partial P} = \frac{\partial B(V)}{\partial V} \Big/ \frac{\partial P(V)}{\partial V} \quad \textbf{Eq. 2.8}$$

$$B''(V) = \frac{\partial^2 B(V)}{\partial P^2} \quad \textbf{Eq. 2.9}$$

This method relies on a uniform expansion in all directions. In a similar manor the lattice can be distorted by specific elongations of the lattice in various directions. In this way one can obtain a stress strain response and a set of compliance coefficients:

$$\sigma_i = C_{ij}\varepsilon_j \quad \textbf{Eq. 2.10}$$

Calculations details for this method can be found in recent work by Shang et al.[29] and will not be discussed in the current work.

2.2 Finite Temperature Thermodynamics from DFT

Many properties may be calculated from the ground state structures calculated in DFT. In this paradigm we are calculating properties which are valid (at least in the assumptions and approximations of DFT) at 0 K. For temperatures above 0 K we must calculate the Helmholtz free energy, $F(V,T)$, by breaking it into contributions from the total energy at 0 Kelvin, E^{0K} and into the electronic and vibrational contributions to F:

$$F(V,T) = E^{0K}(V) + F_{electronic}(V,T) + F_{vibrational}(V,T) \qquad \textbf{Eq. 2.11}$$

For solid phases, we can easily convert between the Helmholtz energy and the Gibbs free energy by addition of the term PV (that is, with a Legendre transformation.) The difference between these two energies will be negligible since the low pressure and the low pressure response of the solid. The ability to convert between the Gibbs free energy and the Helmholtz free energy is necessary for later CALPHAD modeling if we are to include finite temperature information from DFT.

2.2.1 Vibrational Contribution: Phonon Method

If the perturbation of an atom is small enough then it will readily return to its equilibrium position. This is just the assumption we make in the harmonic approximation. Consider a system of oscillators each of mass M_i each with displacement $u(i)$ from equilibrium. If we make a

change in variables $e(i) = u(i)\sqrt{M_i}$ then the Hamiltonian (total energy) of this system can be expressed as[30]:

$$H = \sum_i \frac{1}{2}\left(\frac{de(i)}{dt}\right)^2 + \sum_{i,j} \frac{1}{2} e^T(i) D(i,j) e(j) \qquad \textbf{Eq. 2.12}$$

Where if $\Phi(i,j)$ is the force constant matrix with 3x3 dimensions:

$$D(i,j) = \frac{\Phi(i,j)}{\sqrt{M_i M_j}} \qquad \textbf{Eq. 2.13}$$

The eignenvalues λ of the matrix $D(i,j)$ are related to the normal mode frequencies, ν, by:

$$2\pi\nu = \sqrt{\lambda} \qquad \textbf{Eq. 2.14}$$

Having ν described for a system allows us to build $g(\nu)$ - the density of states (DOS.) And finally we can describe the vibrational contribution to the free energy:

$$F_{vibrational}(V,T) = k_B T \int_0^\infty \ln\left(2\sinh\left(\frac{h\nu}{2k_B T}\right)\right) g(\nu) d\nu \qquad \textbf{Eq. 2.15}$$

Where h is Plancks constant and k_B is Boltzmann's constant. Real systems will exhibit anharmonic behavior. To deal with this, what is known as the qausiharmonic approximation is made where phonons frequencies, and by extension the force constant matrix, are given a dependence on volume[31]. In the end this only change the eigenvalues of $D(i,j)$ and the expression for the vibrational free energy in Eq. 2.15 remains unchanged.

This structure has easily been adopted into DFT calculations through the Alloy Theoretical Automated Toolkit (atat[32].) The force constant matrix can be built in two ways: either through the supercell method or through the linear response method. The former technique offers advantages in speed. Perturbations in a structure containing several repeat groups of the primitive cell (the supercell) are used to evaluate the force constant matrix. The linear response technique seeks direct evaluation of $D(i,j)$ through perturbation theory.

2.2.2 Vibrational Contribution: Debye Method

Even less computationally intensive than the phonon method for obtaining $F_{vibrational}$ is the Debye Method. The implementation of which depends primarily upon the Debye temperature - Θ_D. This is the temperature at where the highest normal mode frequency is activated. If we take the speed of sound to be $\sqrt{B/\rho}$ where B is the system bulk modulus and ρ is the density then with respect to the equilibrium bulk modulus, B_0, and the equilibrium volume, V_0, and average system mass, M, the Debye temperature is:

$$(\Theta_D)_0 = V_0^{\frac{1}{6}}\left(\frac{6\pi^2\hbar^3}{k_B^3}\right)^{\frac{1}{3}}\left(\frac{B_0}{M}\right)^{\frac{1}{2}} \qquad \textbf{Eq. 2.16}$$

This is an extension of the Debye temperature originally implemented by Moruzzi et al. where the Debye temperature was given as a function of lattice separation[33]. This does not always agree well with experiment so a scaling factor, s, and the Grüneisen parameter, γ, for anharmonicity at volume V are introduced[34]:

$$\Theta_D(V) = s\left(\frac{6\pi^2\hbar^3}{k_B^3}\right)^{\frac{1}{3}}\left(\frac{B_0}{M}\right)^{\frac{1}{2}}V_0^{\frac{1}{6}}\left(\frac{V_0}{V}\right)^{\gamma} \quad \textbf{Eq. 2.17}$$

The Grüneisen parameter is given in terms of the first pressure derivative of the equilibrium bulk modulus[35]:

$$\gamma = \frac{1}{2}\left(1 + \frac{\partial B(V_0)}{\partial P}\right) - \chi \quad \textbf{Eq. 2.18}$$

Where χ is either 0 or 1 for low temperatures and 2/3 for high temperatures. The scaling factor need not be a fitting factor. By considering an average between the longitudinal and transverse speeds of sound in terms of the Poisson ratio, ν_p, one can define the scaling factor as[35]:

$$s = 3^{\frac{5}{6}}\left[4\sqrt{2}\left(\frac{1+\nu_p}{1-2\nu_p}\right)^{\frac{3}{2}} + \left(\frac{1+\nu_p}{1-2\nu_p}\right)^{\frac{3}{2}}\right]^{-\frac{1}{3}} \quad \textbf{Eq. 2.19}$$

Hence Eq. 2.17 is expressed entirely in terms we can calculate from DFT. The equilibrium volume, bulk modulus, and first pressure derivative of the bulk modulus can all be obtained from the EOS fitting while the poisons ratio can be calculated from the elastic stiffness matrix in Eq. 2.10[36]. Finally the calculated value for Θ_D can be used to obtain vibrational Helmholtz free energy:

$$F_{vibrational}(V,T) = \frac{9}{8}k_B\Theta_D(V) - k_BT\left[D\left(\Theta_D(V)\right) + 3\ln\left(1 - \exp\left(-\frac{\Theta_D(V)}{T}\right)\right)\right] \quad \textbf{Eq. 2.20}$$

where D(x) is a function given by:

$$D(x) = \int_0^x \frac{udu}{\exp u - 1} \qquad \textbf{Eq. 2.21}$$

While this is encouraging, in some cases it is not practical to calculate the elastic stiffness matrix. Moruzzi et al. performed a fit to several different cubic metals and found that a scaling factor of 0.617 represented a good average velocity of sound in these systems. This value will be used for cubic crystal structures when no other scaling factors can be determined.

2.2.3 Thermal Electronic Contribution

The thermal electronic contribution to the free energy is important for systems where there exists a sizable distribution of electrons near the Fermi level. The electronic internal energy at volume V and temperature T in a system with Fermi level ε_F is:

$$U_{electronic}(V,T) = \int_0^\infty g(\varepsilon) f(\varepsilon,T,V)\varepsilon d\varepsilon - \int_0^{\varepsilon_F} g(\varepsilon) f(\varepsilon,T,V)\varepsilon d\varepsilon \qquad \textbf{Eq. 2.22}$$

where

$$f(\varepsilon) = \frac{1}{\exp\left(\frac{\varepsilon - \mu(T,V)}{k_B T}\right) + 1} \qquad \textbf{Eq. 2.23}$$

$g(\varepsilon)$ is the electronic DOS and $f(\varepsilon,T,V)$ is the Fermi-Dirac distribution. The electronic chemical potential is chosen in way that conserves the total number of electrons in a system[37]. The electronic contribution to the free energy is determined by subtracting the term $TS_{electronic}$ from Eq. 2.22 where

$$S_{electronic}(V,T) = \int g(\varepsilon)G(f(\varepsilon,T,V))d\varepsilon \qquad \textbf{Eq. 2.24}$$

and

$$G(x) = x\ln x + (1-x)\ln(1-x) \qquad \textbf{Eq. 2.25}$$

2.3 Thermodynamic Modeling

To model the thermodynamics of a system one must have a reasonable description of the possible phases atoms can adopt. In thermodynamic modeling we are interested in controlling the natural variables temperature, T, pressure, P, and composition, n. These are the natural variables of the Gibbs energy. Each phase has its own distinct Gibbs energy and which phases are present in the system is determined by the state which results in a global energy minimum for the system at fixed T, P and n.. The Gibbs energy of a phase Φ in the CALPHAD computational structure is given per mole and represented as a polynomial function of temperature given with respect to $\sum H_m^{SER}$ - the molar enthalpy at 298.15 K of the standard states of the phase's component elements. Thus:

$$^{\circ}G_m^{\Phi} - \sum H_m^{SER} = a_0 + a_1T + a_2T\ln T + \sum_2^n d_nT^n \qquad \textbf{Eq. 2.26}$$

For modeling the diffusion of atomic species it is necessary to have both a thermodynamic description of each phase and a description of the tracer diffusivities of each element in these

phases. Various approximations are typically made to create a complete description of the physical situation.

2.4 Compound Energy Formalism

The CALPHAD method relies on a simple description of the phases in a system. This description is called the compound energy formalism[38]. In this formalism, distinct symmetry-related positions in the crystal structures are collected into "sublattices." Mixing occurs between those species which predominantly populate those positions. For instance, the intermetallic compound Ni_3X in the Al-Ni-Ti system could be broken up into the sublattice structure $(Ni)_3(Al,Ti)_1$ since Ti preferentially mixes on the Al sites and has less preference for the Ni sites. Of course, the reality is more complex. Some Ni will be present on the second sublattice and some Al and Ti will be present on the first. Regardless, the choice is a good first approximation given the site preference of each element. The fraction of species on each sublattice is called the site fraction and will change based on the composition of the system. In this example the site fraction of Ni, y_{Ni}, is always 1 while the site fraction of Al and Ti on the second sublattice varies by the relation $y_{Al} + y_{Ti} = 1$. Hence, in this structure the sublattice has two extremums of composition corresponding to Ni_3Ti and Ni_3Al. These are called end-members and are used to define a Gibbs energy surface of reference, $G_m^{s.r.}$, in the system. For a sublattice structure with s sublattices, each sublattice i will have n_i components and can be given a stoichiometric coefficient m_i. This is written out as:

$$\left(c_1, c_2, \ldots c_{n_1}\right)_{m_1} \left(c_1, c_2, \ldots c_{n_2}\right)_{m_2} \ldots \left(c_1, c_2, \ldots c_{n_s}\right)_{m_s} \quad \textbf{Eq. 2.27}$$

The components c can be any atom, ion, or vacancy. These components can also represent more complex compounds but this will not be covered here. The Gibbs energy surface of reference for this sublattice structure is:

$$G_m^{s.r.} = \sum_{i=1}^{M} \left({}^{\circ}G_{end}^{i} \prod_{j=1}^{s} y_{z_j}^{j} \right) \qquad \textbf{Eq. 2.28}$$

Where M is the number of end-members for this sublattice, ${}^{\circ}G_{end}^{i}$ is the Gibbs energy of one mole of the ith end-member, and z_j is the whichever of n_j components occupies the jth sublattice for that end-member. The quantity M is the permutation of possible sublattices and is simply:

$$M = \prod_{i=1}^{s} n_i \qquad \textbf{Eq. 2.29}$$

The molar Gibbs energy for the phase is obtained by adding an ideal mixing term and an excess term, ${}^{E}G_m$, to $G_m^{s.r.}$. In this structure the molar Gibbs energy would be:

$$G_m = \sum_{i=1}^{M} \left({}^{\circ}G_{end}^{i} \prod_{j=1}^{s} y_{z_j}^{j} \right) + RT \sum_{i=1}^{s} \left(\sum_{j=1}^{n_i} m_i y_{c_j}^{i} \ln y_{c_j}^{i} \right) + {}^{E}G_m \qquad \textbf{Eq. 2.30}$$

For an end-member with n components, $\{c_1, c_2, \ldots c_n\}$, the Gibbs energy of the end-member can be given with respect to the component standard state Gibbs energies ${}^\circ G_{c_i}^{stst}$. Accounting for vacancies, the concentration of each component c_i per mole formula unit is:

$$\chi_{c_i} \sum_{c_i \in j}^{s} m_j (1 - y_{Va}^j) \qquad \textbf{Eq. 2.31}$$

where χ_{c_i} is the mole fraction of c_i in the system and the summation only covers those sublattices which contain c_i. With this, we can write out the Gibbs energy of the end-member with respect to the standard states of its n components.

$${}^\circ G_{end} = \sum_{i=1}^{n} {}^\circ G_{c_i}^{stst} \left(\chi_{c_i} \sum_{c_i \in j}^{s} m_j \left(1 - y_{Va}^j\right) \right) + \Delta_f {}^\circ G_{end} \qquad \textbf{Eq. 2.32}$$

The Gibbs energy of formation in the CALPHAD method is parameterized as a polynomial of temperature, as in Eq. 2.26[39].

$$\Delta_f {}^\circ G_{end} = a_0 + a_1 T + a_2 T \ln T + \sum_{2}^{n} d_n T^n \qquad \textbf{Eq. 2.33}$$

This expression simplifies to the Neumann-Kopp rule when only $\boldsymbol{a_0}$ and $\boldsymbol{a_1}$ are non-zero. ${}^\circ \boldsymbol{G_{end}}$ can also be expressed simply as a polynomial temperature sum. In CALPHAD the excess term, ${}^{\boldsymbol{E}}\boldsymbol{G_m}$, is described by a Redlich-Kister expansion of components interacting in a particular sublattice. For binary interactions of components $\boldsymbol{z_j}$ and $\boldsymbol{z_k}$ mixing on the $\boldsymbol{i}$th sublattice:

$${}^E G_m = \sum_{l \neq i}^{M'} \prod y_{z_l}^l \left(\sum_{j=1}^{n_i - 1} \sum_{k=j+1}^{n_i} y_{z_j}^i y_{z_k}^i \sum_{p=0}^{m} {}^p L_{z_j, z_k} \left(y_{z_j}^i - y_{z_k}^i \right)^p \right) \qquad \textbf{Eq. 2.34}$$

$$M' = \frac{\prod_{j=1}^{s} n_j}{n_i} \qquad \textbf{Eq. 2.35}$$

The parameters ${}^{p}L_{x_j,x_k}$ are the interaction parameters accessible during CALPHAD modeling. The term $\prod_{l \neq i} y_{z_l}^{l}$ gives the product of site fractions in sublattice $l \neq i$ each with component z_l corresponding to M'th permutation. ${}^{p}L_{x_j,x_k}$ can be (and often is) given a linear temperature dependence:

$${}^{p}L_{z_j,z_k} = {}^{p}A_{z_j,z_k} + {}^{p}B_{z_j,z_k}T \qquad \textbf{Eq. 2.36}$$

The above equations can be modified and extended to account for other effects such as charge neutrality in ionic compounds and magnetism. The reader is directed to other sources for a discussion on these, and other, effects [39], [40]. Information for pure elements and compounds can be found from work by Dinsdale on the pure elements and in many commercial thermodynamic databases[41]. These will typically account for pure element data. When the Gibbs energy is not available for a certain phase, phase boundary and thermochemical data are used to adjust parameters from Eq. 2.33 and Eq. 2.36 for that phase.

3 A first principles based assessment of the Hf-Ni system

3.1 Introduction

The Hf-Ni system is of key importance to high temperature oxidation resistant alloys where the Hf has been observed to reduce the growth rate of protective oxides and improve scale adherence [16]. In MCrAlX overlay coatings (M=Ni, Co or Fe and X=Y,Hf,Zr, or La), platinum diffusion aluminides (e.g. MDC-151L) and Ni-base superalloys (e.g. Rene N5), this alloying element has proven to be especially beneficial with residence in the Ni3Al($L1_2$) [42] and NiAl (B2)[43] ordered intermetallics phases. Both of these phases are rich in Al, making them important for forming a protective oxide layer of α-Al_2O_3 during oxidation. High temperature coatings and alloy microstructures typically contain significant fractions of one or all of the following phases: fcc($A1$), Ni3Al(L12) and $B2$[44]. Therefore, it is of great importance to understand the solubility of Hf in the fcc-Ni phase as it will have a large impact on the underlying thermodynamics relevant to oxidation. It also especially important to consider the stability of the bcc (A2) solution phase and the B2 phase in the Hf-Ni system since the thermodynamics from this binary system will play an important role in the reactivity of Hf during oxidation in the β phase.

Hf-Ni is also considered an important binary system for shape memory applications. The Ti-Hf-Ni system has been long considered a rich source of shape memory compositions and due to the relative low costs of these alloys[45]. In part, the large stability range of the B2-NiTi phase plays a role in alloy design. It has been suggested that NiTi forms a complete solid solution with NiHf at high temperatures but the high temperature phases rich in Hf could not be analyzed after quenching[46]. Although it is likely that this phase is, indeed, the B2 phase, no experiments have yet confirmed this without extrapolation. Confirmation of this phase stability will offer

justification not only to thermodynamic models but also to first-principles based Gibbs energy descriptions of this phase which model it as the B2 phase. Finally the Hf-Ni is important to consider due to the strong stability of NiXHf2 Huessler and NiXHf half Huessler phases for several alloying elements X and because of the eutectics often present in those Hf-Ni-X systems [47]–[49].

The Hf-Ni system has been modeled several times in the literature. It was recently modeled in by Wang et al using new experimental diffusion couples[50]. Then, the system was re-modeled by Zhang et al[51] in the Ni-rich Al-Hf-Ni system where it was found that solubility was required in the Ni_7Hf_2 phase to match experimental observations in the ternary system. Finally a first-principles based assessment was carried out by Berche et al[49] with little focus on experiments. Unfortunately many thermochemical experiments in the literature used by Wang et al used Hf containing ~2-3 wt.% Zr. This is not ideal for equilibrium measurements and phase boundary measurements as Zr may alter the phase boundary of the system or stabilize a phase which would not have otherwise been present. Although it is not wise to discard these equilibria measurements entirely, some uncertainty must be attributed to the position of phase boundaries – especially for the equilibrium between fcc-A1 and Ni_5Hf which will have a large impact on the resulting activity of Hf in the fcc-A1 solution phase. While not all experimental data in the literature reports the presence of Zr in their Hf samples, it is seems likely that Zr contamination is more probable in older experiments given the cost in detecting and removing Zr from Hf[52].

The present theoretical and experimental work seeks to expand the previously investigated (1) first principles in this system, (2) the phase stability and solubility of Hf in this system using high purity Hf, and (3) the high temperature NiHf phase. Finite temperature, first-principles calculations are carried out on select Ni-rich intermetallic phases to obtain Gibbs energies for

each of these phases. Special quasi-random structures (SQS) calculations were performed to obtain enthalpies of mixing in the fcc-A1, bcc-A2 and B2 phases. This information is implemented in the computation of phase diagrams (CALPHAD) remodeling of this system. Diffusion couple experiments are utilized to confirm the stability of the Hf_3Ni_7 phase and confirms a larger solubility of Hf in fcc Ni compared to previous experiments. First-principles calculations of the B33-NiHf and B2 phases shows the expected results that the B2 phase is mechanically stable and has a higher calculated molar entropy compared to the B33 phase. This suggests the possibility of B2 being the high temperature stable phase.

3.2 Literature Review

Although the Hf-Ni system has been investigated many times, results often came with the presence of Zr impurities in the Hf used. For instance, investigations into equilibria in this system by Hajjaji et al.[53], Svechnikov et al.[54] Bsenko et al.[55] contained ~2.5, ~0.65, and ~3 wt.% Zr in the starting Hf alloys, respectively. Investigations into the formation enthalpies of intermellatic compounds by Selhaoui et al.[56], Bencze[57], contained ~2.3 and ~2.52 wt.% Zr in the starting Hf alloys. An additional complicating factor is that Hf has a very high solubility for O[58] whichonly briefly addressed by Guo et al. [59], [60]. The most recent collection of the literature in this system are included in the thermodynamic re-modeling by Wang et al.[50]. While many sources re listed, the details of these experiments are not fully summarized. What follows is an in-depth discussion of the literature, a discussion of experiments by Wang and a discussion of some of the newer experiments in this system.

3.2.1 Equilibria

The Ni-rich Hf-Ni system has been investigated by Bsenko et al.[55] where the Hf-Ni system was studied between 65 and 80 at.% Ni using x-ray diffraction (XRD) to study equilibria for

samples given heat treatments at temperatures between a 1173.15 and 1593.15 K. Differential thermal analysis (DTA) of arc-melted samples was also used to tabulate the invariant reactions within this composition range. Svechnikov et al.[54] and Yeremenko et al[61] both performed DTA to measure the liquidus of the system from 0 to 100 and 0 to 50 at.% Ni respectively. Yeremenko reported performing additional equilibria measurements at 1473.15, 1373.15 and 1273.15, however only data at 1375.15 K is reported.

Wang performed diffusion couple experiments at 1123 and 1173 K for 1440 and 1200 hours. Electron probe micro-analysis (EPMA) measurements were performed to analyze present phases, Hf solubility in fcc-Ni, Ni solubility in hcp, and solubility in the $NiHf_2$ phase. Hajjaji et al.[53] also studied the solubility of Hf in fcc-Ni using XRD and transmission electron microscopy (TEM) in the temperature range of 773.15 to 1373.15 K. Notably, heat treatment times for measurements in this study were unspecified except at 1333 K with a heat treatment time of 24 hours.

3.2.2 Thermochemical Data

Experiments by Bencze[57] using Knudsen effusion cell spectrometry represents the most extensive investigation of the thermochemical information of the solid phases in the Hf-Ni system. This data set includes Gibbs energies of formation, enthalpies of formation, associated activities and, to a lesser extent, phase stabilities at 1418 and 1473.15 K. Selhaoui et al.[56] and Guo et al. [59], [60] both measured formation enthalpies of compounds via direct synthesis calorimetry for a range of temperatures between 1050 and 1350 °C and at 1204 °C, respectively. The most recent thermochemical investigation into the liquid phase was carried out by Popoprigora et al.[62], [63] on the Hf-Ni melts at 1770 $\pm$5 K using calorimetry. Earlier

calorimetry measurements were also carried out Selhaoui et al.[56] at 1473 and 1633 K, and by Sudavtsova and Sharkina[64] at 1877 K. Additionally, Popoprigora et al. also report that there is calorimetry data at 1873 K in a thesis by P. G. Agraval. this data was taken from Popoprigora et al. for comparison but was not fit to since the thesis was unavailable at the time the present modeling was performed.

3.2.3 First-principles Data

The formation enthalpy of the known compounds in the binary system was investigated by Berche[49] in a larger investigation of the Hf-Ni-Sn system. Calculations were performed in vasp using settings intended to attain reasonable accuracy for values of the compound formation enthalpy. However, this study did not investigate the B2 phase or the L12 phase and did not include enthalpies for the disordered fcc-A1 and bcc-A2 solution phases. Additional sources of compound formation enthalpies for select compounds are also available from high-throughput DFT calculations such as work using AFLOW[65].

3.2.4 Experimental Evidence of the B2 Phase

In the investigation by Wang et al the high temperature allotrope of NiHf is modeled by the crystal structure is not explicitly identified as the B2 phase. This is largely due to the fact that there has been no direct observation of this phase in the literature. Experiments performed by Yeremenko et al[61] in the Hf-Ni-Ti system suggests a complete solid solution between β-NiTi and the high temperature NiHf through phase relations of quenched alloys and DTA measurements. However it was not possible for Yeremenko et al[61] to quench this phase from high temperature and only the low temperature B33 allotrope was ever resolved during

experiments. There are also other experiments by Eremenko et al.[66] which studied solid solutions between NiZr and NiHf. A complete solid solution was observed for the B33 phase at low temperatures and a large solution range for a high temperature phase of B2 was also suggested but, yet again, it was too difficult to quench this phase[66].

3.2.5 Non-stoichiometric Compounds

As stated before, Wang et al. observed appreciable solubility in the Hf_2Ni phase. Some off stoichiometry and slight solubility was also observed in the Hf_2Ni_7 phase with compositions as low as 21.7 at.% Hf with solubility ranges of 0.3 at.%. While it is possible that this is within the realm of measurement error it is worth noting since several ternary investigations also noted noticeable solubility in this phase. Experiments by Nash and West[67], [68], Khorunov et al.[48], and Zhang et al[51] all noted that those compositions nearest to Hf_2Ni_7 in equilibrium with other phases were rich in Ni. In this work a model for this phase is adopted from corresponding work in a larger investigation into the Ni-rich Al-Cr-Hf-Ni system and a suggested solubility is added based on first-principles and fitting in the ternary system.

3.3 Thermodynamic Models

3.3.1 Stoichiometric Intermetallic Phases

When full thermochemical information on a stoichiometric compound Hf_ANi_B is available the molar Gibbs energy of this phase, $G_m^{Hf_ANi_B}$, can be given as:

$$G_m^{Hf_ANi_B} - \left(\frac{A}{A+B}\right) H_{Hf}^{SER} - \left(\frac{A}{A+B}\right) H_{Ni}^{SER} = a + bT + cT\ln T + dT^2 + \frac{e}{T} + fT^3 \quad \textbf{Eq. 3.1}$$

where a through f are constants and H_i^{SER} is the enthalpy of element i in the standard element reference state. When this information is not available experimentally it can be also be calculated using first principles. However this is not always considered necessary and a in some cases a simpler approach employing a Kopp–Neumann type approach is used. In such cases the Gibbs energy is given as:

$$G_m^{Hf_ANi_B} - \left(\frac{A}{A+B}\right) H_{Hf}^{SER} - \left(\frac{A}{A+B}\right) H_{Ni}^{SER} = \left(\frac{A}{A+B}\right) G_m^{Hf} + \left(\frac{B}{A+B}\right) G_m^{Ni} + A^{Hf_ANi_B} - B^{Hf_ANi_B}T \quad \textbf{Eq. 3.2}$$

Where $A^{Hf_ANi_B}$ and $B^{Hf_ANi_B}$ are values used to fit the available formation enthalpy and entropy, respectively, and the heat capacity is given by the mechanical mixture of the individual elements.

3.3.2 Solution phases

The solution phases modeled here are the bcc-A2 phase, the fcc-A1 phase, the hcp-A3 phase, and liquid phase. All models considered here use the compound energy formalism (CEF) and solution phases are modeled with mixing on a single symmetry equivalent sublattices[38]. For each of the solid solution phases the sublattice is occupied by both Ni and Hf with sublattice model $(Ni,Hf)_a(Va)_b$ where a and b represent the relative stoichiometry for lattice sites and modeled interstitial sites, respectively. Mixing occurs between those compounds representing

extremes in sublattice occupation (end-members): Ni_aVa_b and Hf_aVa_b. The Gibbs energy of the solution phase is constructed using contributions from the mechanical mixing of these end-members, configurational entropy and an excess term. The excess Gibbs energy, G_m^{ex} is considered using a Redlich-Kister polynomial:

$$G_m^{ex} = \sum_i \sum_{j>i} x_i x_j \sum_\nu {}^\nu L_{i,j} \left(x_i - x_j\right)^\nu \qquad \textbf{Eq. 3.3}$$

Where ${}^\nu L_{i,j}$ is the νth order interaction parameter between species i and j expanded out in mole fraction of these components: x_i and x_j respectively. In this work the interaction parameters are expanded to the first order of T:

$${}^\nu L_{i,j} = {}^\nu A_{i,j} + {}^\nu B_{i,j} T \qquad \textbf{Eq. 3.4}$$

Where ${}^\nu A_{i,j}$ is used to fit the solution Gibbs energy to the excess enthalpy and ${}^\nu B_{i,j}$ to the excess entropy for a given phase. No work modeling the magnetism of the solution phases was required in this work and hence this is not discussed here.

3.3.3 Non-Stoichiometric Intermetallic Phases

Wang et al observed significant solubility in the Ni_1Hf_2 phase and thus modeled this phase using the sublattice model $(Ni,Hf)_1Hf_2$ with the assumption that Ni could dissolve further Hf. This model is adopted in this work with Ni_1Hf_2 and Hf_1Hf_2 end-members adjusted using first-principles calculations. Aside from this, the model is the same as the one found in Wang et al.[50]. The Ni_7Hf_2 phase is modeled using the sublattalice model: $(Ni)_7(Hf,Ni)_2$. The details of this model are presented elsewhere.

3.3.4 The Order-Disorder Model

The order disorder model in this work describes the A2 to B2 transformations and the fcc to L12 transformations. It should be noted that while L12 and A2 are not stable in this work it is still important to model these for higher order systems where these phases are stable such as the Ni-Al-Hf[69] system and the Ni-Cr-Hf[48], [70] systems. The model used in this work to describe these transformations is the one developed by Ansara[71] and Dupin[72]. While a more physical version of this model uses four sublattices this this paper will use the two sublattice (2SL) model for both the B2 and L12 ordered phases given the wide-spread application of this model. Within this model for a disordered phase Θ and an ordered phase Θ′ the Gibbs energy of the ordered phase, $G_m^{\Theta'}$ is treated as the Gibbs energy of the disordered solution phase, $G_m^{\Theta'}$, with a contribution from the difference between an ordering contribution with a given number of sublattices $\Delta G_m^{\Theta'}$ and an ordering contribution where the site fractions of species i and j, y_i and y_j, on sites s1 and s2 are fixed to the mole fraction of these components in the system: $\Delta G_m^{\Theta'}(y_i^{s1} = x_i, y_j^{s1} = x_j, y_i^{s2} = x_i, y_j^{s2} = x_j)$. The full form of the ordering contribution can be found elsewhere and will not be discussed here.

The interactions and end-members of the ordered energy contribution are modeled using the concept of bond energies between elements i and j, $U_{i,j}$, on a given sublattice. For the Hf-Ni system there are three ordered compounds considered in the 2 SL model. The Gibbs energy of these compounds is given as:

$$G_{\mathrm{HfNi_3}} = 3U_{HfNi} + \alpha_{\mathrm{HfNi_3}}$$
$$G_{\mathrm{Hf_2Ni_2}} = 4U_{HfNi} \qquad \textbf{Eq. 3.5}$$
$$G_{\mathrm{Hf_3Ni}} = 3U_{HfNi} + \alpha_{\mathrm{Hf_3Ni}}$$

Where the α terms represent changes in the bonding environment between each compound[73]. U_{HfNi} and the α terms are used to fit to available thermochemical and phase equilibria data in the same way that interaction parameters are:

$$U_{HfNi} = A_U^{HfNi} + B_U^{HfNi}T \quad \textbf{Eq. 3.6}$$

And

$$\alpha_{\mathrm{i}} = A_i + B_iT \quad \textbf{Eq. 3.7}$$

In the 4SL model there is an equivalency between sublattice configurations due to the symmetry between wycoff sites in the L12 phase and B2 phase. This results in equivalency between end members of the 4SL model, e.g.: $G_{i:j:j:j} = G_{j:i:j:j} = G_{j:j:i:j} = G_{j:j:j:i}$, and interactions in the 4SL model, e.g.: $L_{i,j:j:j:j} = L_{j:i,j:j:j} = L_{j:j:i,j:j} = L_{j:j:j:i,j}$. Since the 2SL model represents a simplification of the more complex 4SL model, modifications to the energy surface of the 2SL model are made through relations in the interaction parameters to account for this equivalency. The full form of these relations can be found elsewhere.

3.4 First-Principles Methodologies

3.4.1 Finite Temperature Calculations

Although first principles calculation have already been carried out by Berch et al.[49] it is of interest to calculate the finite temperature properties of the B2 phase, the low temperature HfNi allotrope and the high temperature compound $NiHf_2$. The $NiHf_2$ is of interest since it will come in equilibrium with the B2 phase at high temperatures and this will play a role in determining the extent of the solid solution of the B2 phase. All calculations are carried out in the Vienna ab

initio software package (vasp 5.3.3) using the projector augmented wave (PAW) method and a planewave cut-off of 400 eV. Electronic exchange and correlation is described using the generalized gradient approximation via the implementation by Perdew, Burke, and Ernzerhof (PBE). The recommended PAW potentials by vasp are used for Hf and Ni are used in this work[74]. Brillouin zone integration was carried out using the tetrahedron-bloch method with the fully automatic function of k-mesh generation provided by vasp. A length of 80 was provided for all calculations within this method[74]. This kpoint method results in a variable kpoint per reciprocal atom (kppra) value but the smallest kppra was 5000 which should result in acceptable accuracy. All calculations used an energy plane-wave cut-off of 400 eV.

Finite temperature information is obtained using the approach detailed by Shang and Wang[27], [75] where the Helmholtz free energy, $F(V,T)$, is taken as the sum of the 0K energy, E^{0K}, the vibrational Helmholtz free energy, $F_{vib}(V,T)$, and the thermal-electronic Helmholtz free energy, $F_{T-ele}(V,T)$. In this work $F_{vib}(V,T)$ is obtained with the quasi-harmonic Debye model as described by Shang et al. where a Debye temperature, $\Theta(V,T)$, is calculated using X structures at different volumes to obtain the Energy as a function of volume, $E^{0K}(V)$, through a four parameter Birch-Murnaghan equation of state fitting. A scaling factor for $\Theta(V,T)$ to account for the crystal anisotropy of a given phase was calculated using the methods described by Shang et al.[76].

3.4.2 SQS Calculations

Once again, all SQS calculations were carried out in vasp using the same setting described above. A2-bcc mixing enthalpies were calculated using binary structures developed by Jiang et al.[77] fcc mixing was calculated using structures developed by Wolverton et al.[78] and B2

mixing was calculated using structures developed by Jiang et al.[79]. All calculations followed a three tiered relaxation scheme during vasp structure calculations: 1st only volume was allowed was relax, 2nd volume and shape were allowed to relax, and 3rd volume, shape and ion position were allowed to relax. Mixing enthalpies were only kept if the corresponding structure kept its crystal symmetry. This was tested using radial distribution functions to assess the symmetry of the structures.

3.5 Experimental Methodologies

The experiments were performed using an HfNi ingot of nominally equiatomic composition, $Hf_{50}Ni_{50}$ (at. %), received from the Materials Preparation Center of Ames Laboratory[80]. The ingot was made by argon arc melting, drop cast into a 10 mm diameter rod, and homogenized for 6 h at 1200 °C plus 48 h at 1150 °C in vacuum.

3.5.1 Diffusion Couple

Diffusion couples were made between the HfNi alloy and pure Ni in order to study phase equilibria in the Ni-rich half of the HfNi system. The Ni specimens were taken from a high purity (99.999 %), 1 mm thick plate received from Goodfellow. Specimens of dimensions 4 x 4 x 1 mm were ground using SiC papers, polished with diamond suspensions down to a 3 μm finish, and ultrasonically cleaned in ethanol. Couples were made by placing Ni and HfNi specimens in a BN clamping device, and heat treating the assembly 30 min at 1100 °C (900 °C couple) or 1 h at 1150 °C (other couples) in laboratory air. After slow cooling, the couples were vacuum-encapsulated in quartz capsules and annealed at 900, 1010 and 1100 °C for 500, 190, and 100 h, respectively. The diffusion heat treatments were terminated by water quenching.

Polished sections of the heat-treated couples were prepared by standard metallographic procedures. Composition profiles were measured by electron probe micro-analysis (EPMA)

using a JEOL JXA-8530F field emission gun instrument. The measured intensities were converted to concentrations via a built-in ZAF calibration procedure, using pure Hf and Ni as standards. A step size of 5 μm was used for overall scans of the diffusion regions, and 1 μm steps were used for detailed scans of the Ni/$HfNi_5$ interface region.

3.6 Results and Discussion

3.6.1 Results from First-Principles

A list of calculated enthalpies formation at 298.15 K, $\Delta H^{298.15K}$ and entropies at 298.15 K, $S^{298.15}$, are given in Table 3.1. Data by Berche[49] is given for comparison. Formation enthalpies from Berche agree well with the present calculated values. Only some compound entropies were calculated due to a limitation on resources. The entropy at 298.15 K for the NiHf B2 phase is higher than the entropy for the B33-NiHf phase while the formation enthalpy for the B2 phase is higher than the B33 phase. This is the expected behavior for the thermodynamics of high-temperature and low temperature phases. The difference in the formation enthalpy is around 8 kJ, however, and it is difficult to ascertain directly from first-principles if this is surmountable for the B2 phase based on the entropy difference between these two phases and the accuracy of the present vibrational calculations.

Calculated mixing enthalpies for the fcc and A2 and B2 solutions are presented in Table 3.2. Also included are the formation enthalpies of the ordered B2 and L12 compounds with respect to their respective disordered solutions. The mixing enthalpy is asymmetric for both phases. Mixing was more positive for dilute Hf-rich calculations compared to dilute Ni-rich calculations. Indeed, there is a sign change between the two extremes in composition in the fcc phase. This is most likely caused by the size mismatch between each element. This may explain why the sign does not flip on the bcc portion of the diagram since the A2 Hf phase has a greater equilibrium

volume than the fcc phase and can therefore accommodate more strain in the lattice. The ordering contributions are much more negative compared to the disordered solutions, as expected.

3.6.2 Experimental Results

3.6.2.1 Diffusion couples

The phases present after annealing of the diffusion couples, identified from the composition profiles, are summarized in Table 3.3 (partial oxidation of the 1010 °C couple prevented reliable identification of the complete sequence at that temperature). Micrographs and composition profiles obtained from the 900 °C couple are given in Figure 3.1 as an example. This information is compared to diffusion couple work by Wang in the same table. Phase observations are in good agreement. Detailed analysis of the Ni/$HfNi_5$ interface region allowed the Hf solubility in γ-Ni to be determined; the measured values are given in Figure 3.7 and will be discussed below.

3.6.3 Results from CALPHAD Optimization

Thermochemical information from first-principles and experiments as well as phase equilibra data were optimized with the PARROT module of Thermo-Calc. First-principles information was optimized to first to obtain initial formation enthalpies and entropies. Following this experimental information was fit to simultaneously with first-principles information. First principles enthalpies of formation were given an error of 10% of the enthalpy value per mole-atom to be used during least-squares fitting. It should be noted that the actual error could be much higher than this depending on the type of system[81].

3.6.3.1 Intermetallic stability

A plot of the formation enthalpies calculated from the present model at 1413.15 K and 298.15 K compared to experimentally determined enthalpies of formation and calculated enthalpies of formation is given in Figure 3.2. Data by Benscze at 1413.15 K was not fully reproduced at this temperature. This was due to a closer fit to first principles data in this work in the fcc phase and the result of fitting to the available invariant reactions and liquidus information. However, the present modeling matches the observed trend in the formation enthalpy with increasing Hf concentration by Benscze. Only two compounds fall on the convex hull according to DFT: B33-NiHf and Ni_3Hf (R-3m). In the present modeling these phases are also the only ones present on the convex hull at 298.15. However C15b-Ni_5Hf is stabilized at 302 K and this phase is so close to the convex hull as to be practically stable at low temperatures in the present predictions. Calculated molar entropies from the present modeling for the Ni3Hf (L12), B33, B2, C16, and C15b phases is given in Figure 3.3 compared to values obtained from first-principles calculations. Calculated trends in entropy are replicated in the present model but the magnitude of entropy was not. The C15b phase required a higher entropy to match observed invariant equilibria with the liquid and the C16 phase required a decrease of ~10 J/mol-atom-K at 298.15 K. The entropy difference between B33 and B2 modeled in this work was much larger compared to the value calculated from first-principles. Although it is possible that this is related to uncertainty in the equilibria near this phase, it is more likely caused by sources of error in the bonding described between B33 and B2 through the PBE, PAW potentials.

Ni activities measured by Bencze compared to the calculated activities in the present model are shown in Figure 3.4. Good agreement was achieved during optimization to this data. However, optimization to the activity represented by the equilibria between B2 and the liquid was not

possible. Agreement was also worse on the Hf-rich portion of the diagram. However, there was a large degree scatter in the experimental values for samples with low Ni activities.

3.6.3.2 Thermochemical data in the liquid phase

The enthalpies of mixing at 1770 K, partial enthalpy of mixing at 1770 K, and the enthalpy of mixing with respect to liquid Ni and solid hcp at 1743 is plotted in Figure 3.5a, b and c respectively. The collected mixing enthalpies were fit to during optimization and, hence, the resulting mixing enthalpy is an average of experimental values. Disagreement occurs with higher Hf concentrations between datasets. This is why partial enthalpy calculations by Podoprigora et al. and Sudavtsova et al. disagree with the present model and why experimental partial enthalpies agree well for low Hf concentration in the liquid.

3.6.3.3 The liquidus and sources of disagreement in this work

The Hf-Ni phase diagram is plotted in Figure 3.6. Invariant reactions agree well with the collected experimental invariant reactions with the exception of those between B2 and the NiHf2 phase. The disagreement between Yerkemenko's DTA and Svechinkov's DTA data is stark with a difference of roughly 200 K between the two experiments near 66 at.% Hf. Hf has a higher melting point than Zr, 2504 against 2128 K, and it is likely that compounds containing Hf will have a higher melting point than corresponding compounds containing Zr. Work by Eremenko[66] showed that liquidus between NiZr and NiHf was roughly a linear interpolation between the melting points of these two compounds: 1543.15 and 1778.15 K, respectively. The liquidus surface should not be drastically different between NiHf2 and NiZr2 so of the two datasets, assuming no error between datasets, measurements by Yeremenko are more likely to be

contaminated by Zr. However it was not possible to fit to this data and capture the surrounding eutectics. Hence near the NiHf2 phase DTA data by only Yeremenko was used to fit the liquidus in this region. The catatectic on the Hf-rich portion was subsequently affected with a calculated value of 1802 which is much higher than 1428 K suggested by Yeremenko. While it is possible to adjust the liquid energy in this region of the phase diagram to yield an acceptable fit to the measured phase boundaries and catatectic reaction, this would require a more intricate model such as the assosciate model or the modified quasichemical model[82]. It is the opinion of the authors that more experimental work is needed with high purity samples in the Zr-rich portion before these more complex parameters are to be tried.

3.6.3.4 Hf solubility in fcc Ni and the L12 phase

The Ni-rich portion of the Hf-Ni phase diagram displaying the equilibrium between the fcc solution phase and Ni_7Hf_2 phase from 800 K to 1600 K with experiments from this work and work by Hajjaji[53], Wang[50], and Svechnikov[83] is given in Figure 3.7a. The solubility measurements in this work were larger than the solubility measured by Hajjaji. This may be due to the Zr present in the samples but it may also be due the heat treatment by Hajjaji which was not stated. If these heat treatment times were sufficiently small it may be that the experiments did not yet reach equilibrium. Indeed, heat treatments of 1200 and 1440 hours by Wang yield solubility measurements close to the present results. Hence, the present fitting was performed only with respect to the experiments in this work. Because the previous work by Wang fit to work by Hajjaji, this resulted in a higher solubility compared to the present model and resulted in disagreement with their measured solubility.

The fit performed to SQS information along with the calculated metastable diagram resulting from this paper's fitting is given in Figure 3.7b. The asymmetric mixing did not require major modification during solubility fitting and the L12 enthalpy with respect to the fcc phase was able to be replicated to a reasonable degree without α terms. This asymetric mixing is consistent with the chemically similar Ni-Ti[84] and Ni-Zr[85] models, each of which had a more negative mixing enthalpy on the Ni-rich portion of the diagram.

3.6.3.5 The A2 and B2 phase

Given the confirmation of the B2 phase by high-temperature synchrotron, the high temperature NiHf phase was, indeed, modeled with this crystal structure with a transition temperature of 1146.97 °C in accordance with measurements of ~1150°C by Yeremenko[61]. The parameters for the B2 phase were adjusted based on the surrounding equilibrium in the system. Good agreement was found possible with the surrounding transition temperatures and experimental liquidus obtained. Good agreement is also found with DTA data from Svechinkov[83] and from Yeremenko[46] near 50 at.% Hf. However, there are unaccounted transitions in the present description between the NiHf phase and the $NiHf_2$ phase. It is likely that this is caused by a wider solubility range for Ni in this phase at higher temperatures. Since this could not be confirmed it was not addressed further here.

A plot of the mixing enthalpies resulting from SQS calculations and the metastable diagram A2-B2 diagram is given in Figure 3.8a and b respectively. A fit of the A2 mixing enthalpy was not possible simultaneously with the B2 enthalpy with respect to the A2 end-members and the modeled liquidus. Reasonable fits were obtained to the B2 phase. As with the metstable fcc-L12 diagram, here no spurious high temperature ordering can be observed.

3.7 Conclusions

A thorough investigation into the nickel-rich portion of the Hf-Ni system was performed using both first-principles calculations and experiments. New experiments used very pure Hf for all experiments to avoid Zr contamination. Diffusion couple experiments were carried out at 1173.15, 1273.15, and 1373.15 K to confirm the phase stability observed in previous experiments and to measure the Hf solubility in fcc Ni. This solubility is of key importance to understanding and predicting the Hf activity in Ni-rich alloys containing Hf as a component to improve the oxidation resistance of the alloy. CALPHAD modeling was carried out using phase stability data from these diffusion couples and from the literature, thermochemical data in the literature and calculated thermochemical data from first principles. The resulting phase diagram and thermochemical properties agree well with available experiments.

First principles thermochemical data at 0K and finite temperatures provided a physical basis for the modeling of experimentally observed phases and unstable phases having the L12 crystal structure. This description of the $L1_2$ phase in this system is important for extrapolations into higher-order systems. Special quasi-random structures were used to obtain mixing enthalpies in the fcc-A1 and bcc-B2 systems and these were used as a basis for solubility modeling in the fcc-A1 phase.

The stability of the B2 phase is also important to oxidation resistant alloys given the prominence of the B2-NiAl phase in high-temperature alloys and coatings. Special quasi-random structures were used to model the bcc phase and the B2 phase was modeled as a solution phase in tandem with modeling of the A2-bcc phase. The stability range of the B2 phase fit using first-principles will provide important groundwork for future models built to design shape-memory alloys.

Table 3.1. Calculated and entropies at 298.15 K, , $S^{298.15}$, of enthalpies formation at 298.15 K, $\Delta H^{298.15K}$ including calculated mixing enthalpies for the fcc and A2 solutions

Phase	Volume	ΔH (kJ/mole-atom)	ΔH[49] (kJ/mole-atom)	$S^{298.15}$ (J/mole-atom·K)
Ni (fcc-A1)		0		--
Ni5Hf (C15b)		-33.67		27.4825
Ni7Hf2		-45.18		--
Ni7Hf3		-48.88		--
NiHf (B33)		-50.00		38.8575
NiHf (B2)		-41.77		40.29
NiHf2		-32.88		51.5817
Hf (hcp-A3)		0	0	38.8683
Ni_3Hf ($L1_2$)		-51.41	--	29.0286
$NiHf_3$ ($L1_2$)		-1.60	--	--

Table 3.2. Calculated and entropies at 298.15 K, , $S^{298.15}$, of enthalpies formation at 298.15 K, $\Delta H^{298.15K}$ including calculated mixing enthalpies for the fcc and A2 solutions

	ΔH (kJ/mole-atom)		ΔH (kJ/mole-atom)
$Ni_{32}Hf_1$ (bcc-A2)	-9.13	$Ni_{32}Hf_1$ (fcc-A1)	-6.75
$Ni_{0.75}Hf_{0.25}$ (bcc-A2)	-17.06	$Ni_{0.75}Hf_{0.25}$ (fcc-A1)	-6.45
$Ni_{0.5}Hf_{0.5}$ (bcc-A2)	-8.81	$Ni_{0.5}Hf_{0.5}$ (fcc-A1)	-6.46
$Ni_{0.25}Hf_{0.75}$ (bcc-A2)	-8.06	$Ni_{0.25}Hf_{0.75}$ (fcc-A1)	3.65
Ni_1Hf_{32} (bcc-A2)	-1.30	Ni_1Hf_{32} (fcc-A1)	2.24
NiHf (B2)	-55.15	Ni_3Hf ($L1_2$)	-49.68
$Ni_{0.5}(Hf_{0.5}Ni_{0.5})_{0.5}$ (bcc-B2)	-29.94	$NiHf_3$ ($L1_2$)	3.59
$Hf_{0.5}(Hf_{0.5}Ni_{0.5})_{0.5}$ (bcc-B2)	-10.22		

Table 3.3: Phases of the Ni-rich half of the HfNi system observed after annealing of the Ni/HfNi diffusion couples.

T (°C)	850[50]	900[50]	900*	1100*
Ni	x	x	x	x
$HfNi_5$	x	x	x	x
Hf_2Ni_7	x	x	x	x
$HfNi_3$	x	x	x	x
Hf_3Ni_7				x
Hf_7Ni_{10}	x	x	x	x
Hf_9Ni_{11}	x	x	x	x
HfNi	x	x	x	x

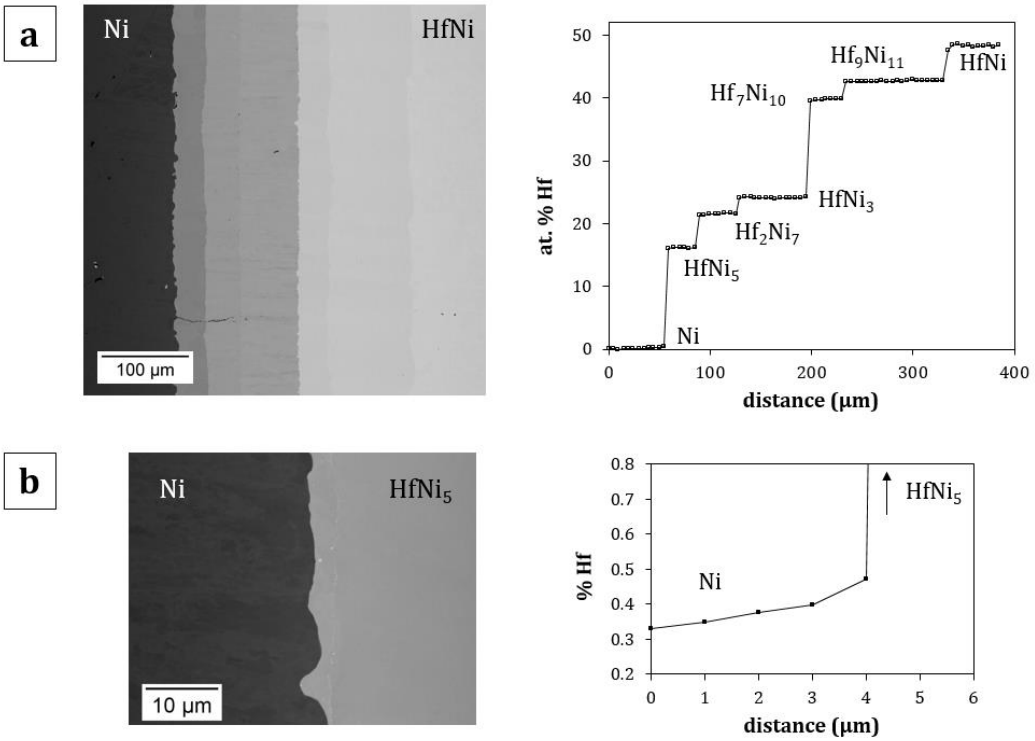

Figure 3.1. Micrograph and composition profile obtained from Ni/HfNi diffusion couple annealed 500 h at 900 °C. (a): overview; (b): detailed analysis of the Ni/$HfNi_5$ interface region.

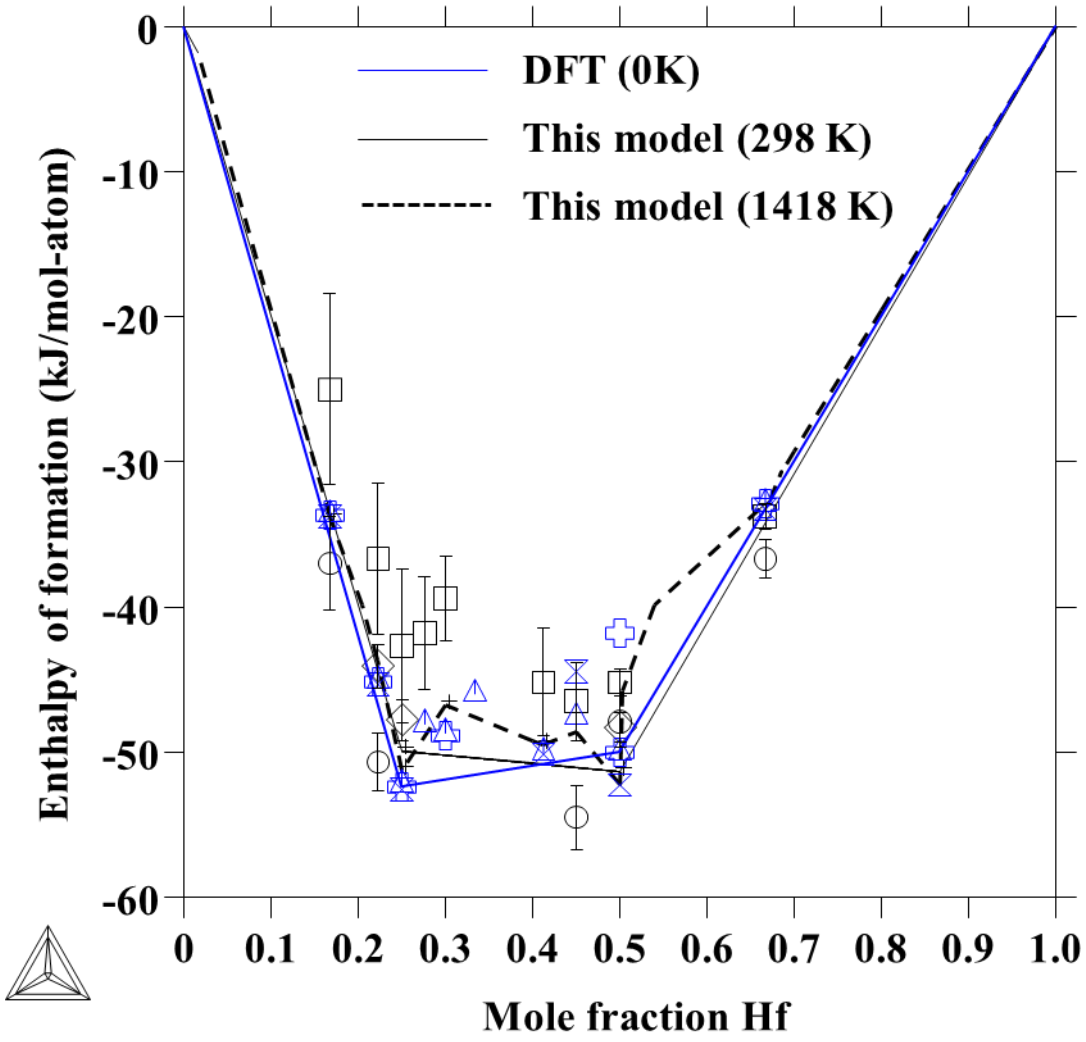

Figure 3.2. Formation enthalpy of compounds at 0K by first-principles and at 298 and 1418 K as calculated from the present model. Comparison is made to experiments with reported error bars by Bencze (□), Guo (◇), and Selhaoui (○) and first-principles calculations in this work (✚), and by Berche (△) and Curtarolo (⧖).

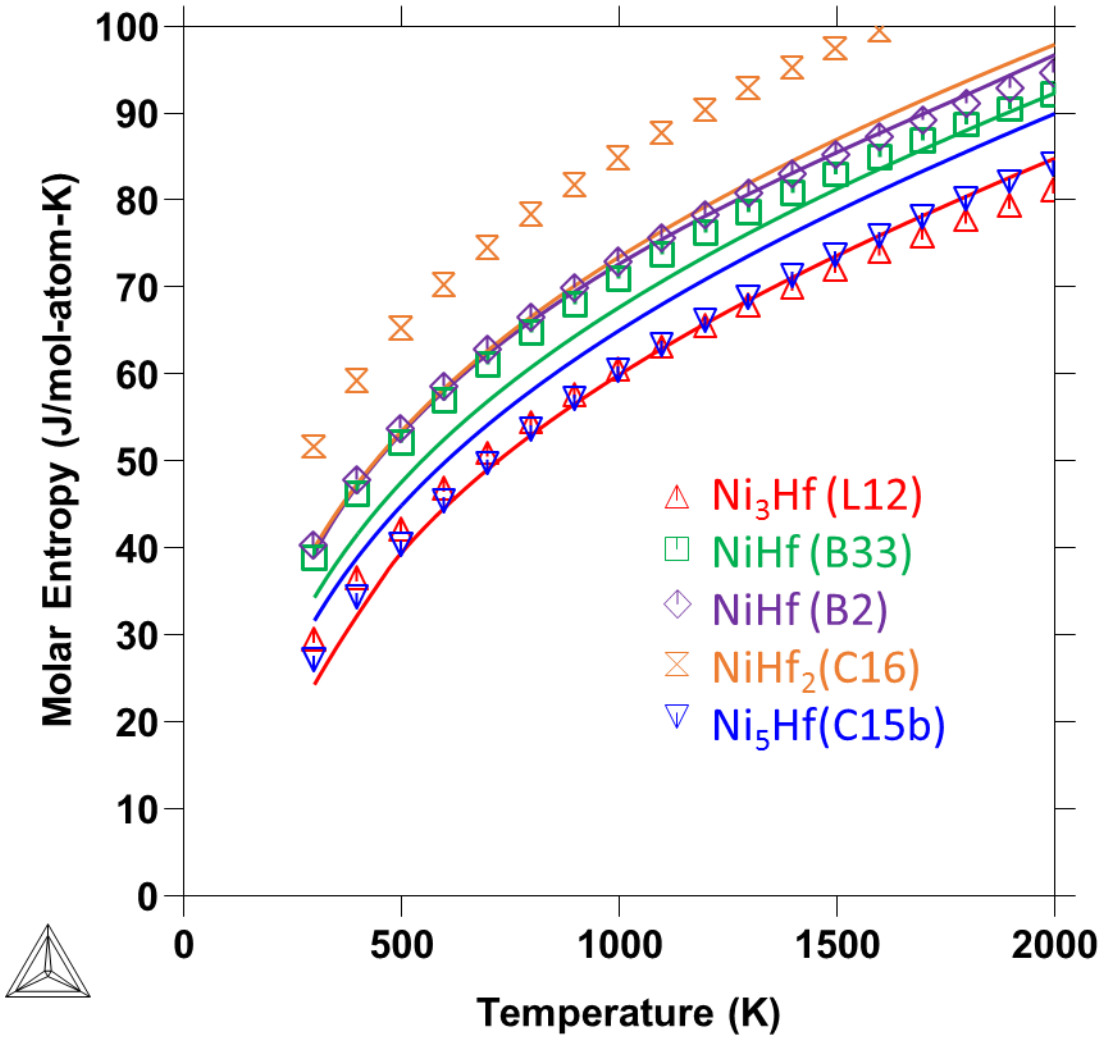

Figure 3.3. Calculated molar entropy for the compounds Ni3Hf (L12), NiHf (B33), NiHf (B2), NiHf2 (C16), and Ni5Hf (C15b) (solid lines) and calculated molar entropies for compounds from first-principles, finite temperature calculations (symbols).

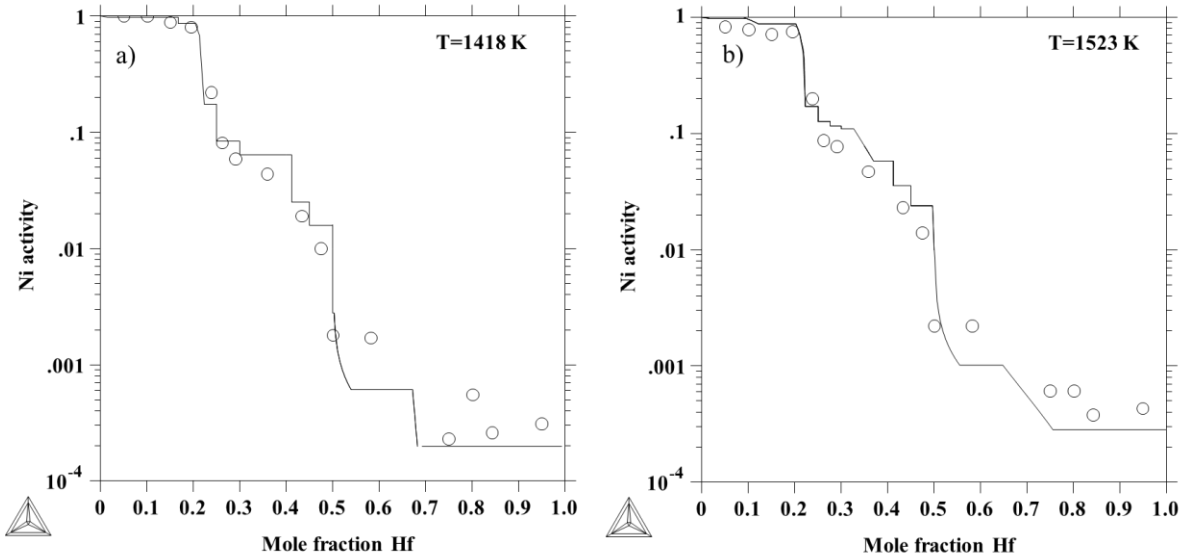

Figure 3.4. Calculated Ni activies from this work at 1418 and 1523 K compared to measurements by Bencze (○) with a Ni reference state of fcc at the given temperature in each case.

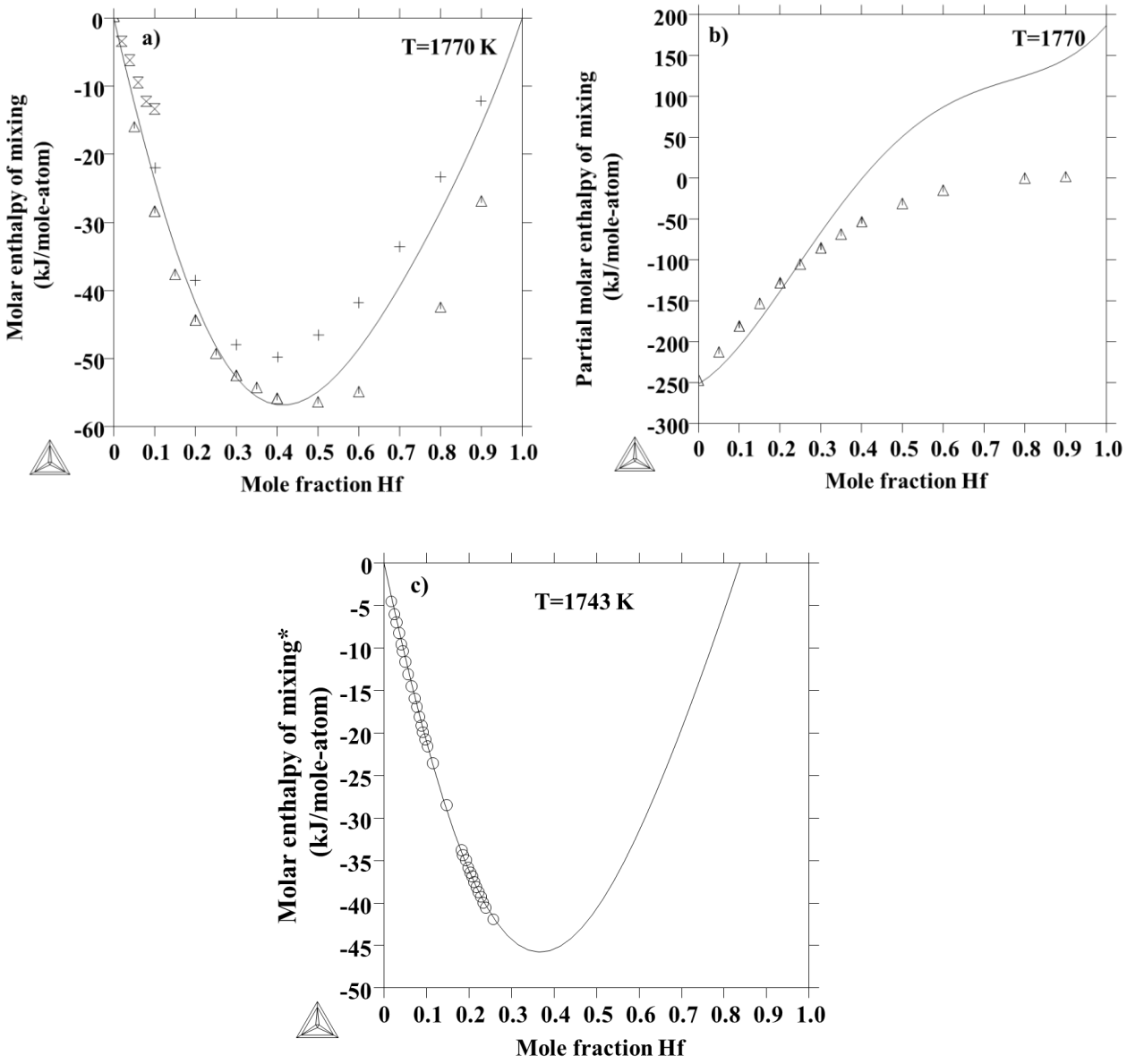

Figure 3.5. Thermochemical calculations in the liquid phase: a) the molar enthalpy of mixing at 1770 K compared to experiments by Podoprigora and Sudavtsova[62], [63] **at 1770 K (⧋) and Sudavtsova**[64] **at 1877 K (+) and thesis work cited by Podoprigora and Sudavtsova**[62], [63] **(⧓) b) calculated partial molar enthalpy of mixing compared to Podoprigora and Sudavtsova at 1770 K**[62], [63] **(⧋) and c) calculated molar enthalpy of**

mixing (*with respect to solid hcp Hf and liquid Ni) at 1743 K compared to data by Selhaoui[56] **at this temperature (○)**

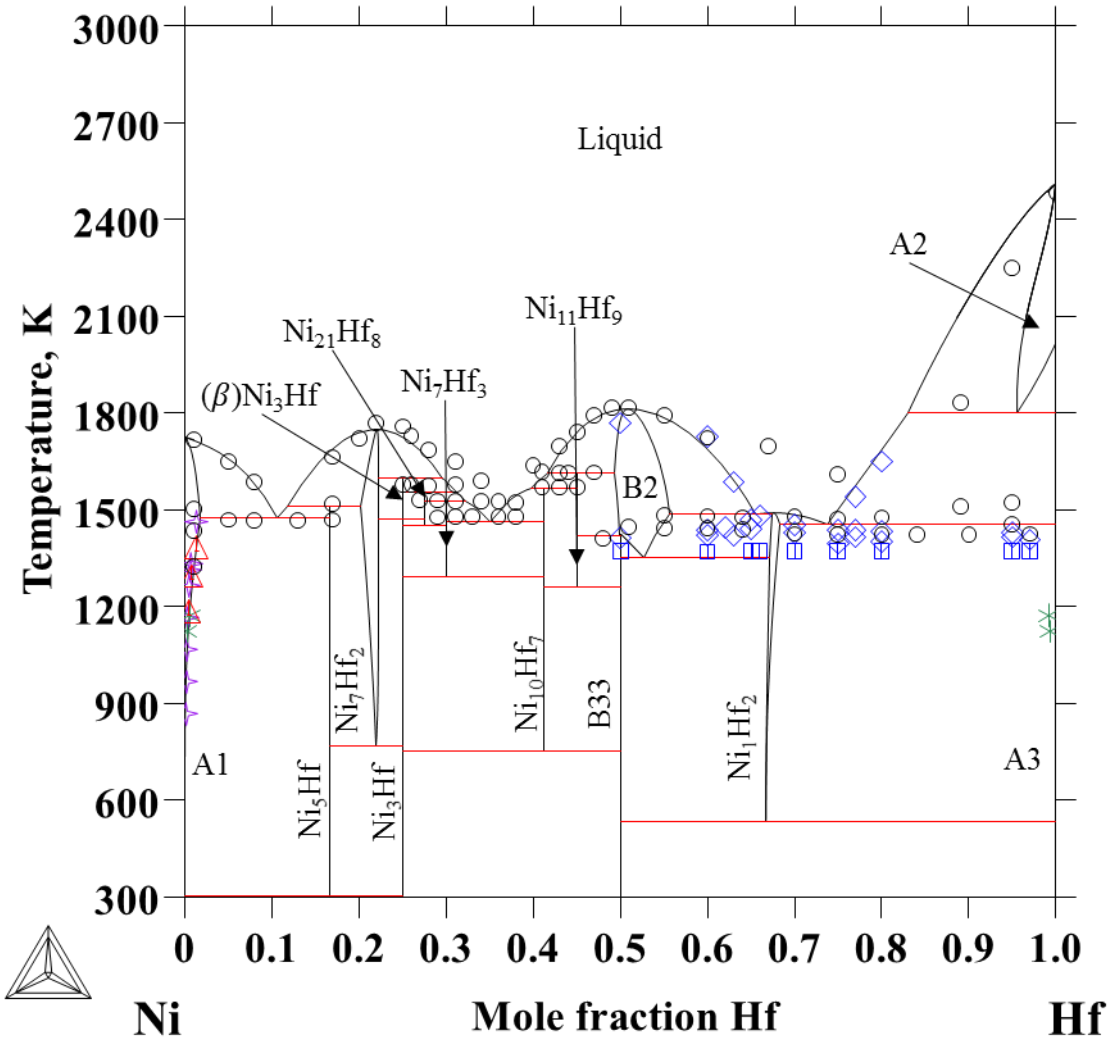

Figure 3.6. Hf-Ni phase diagram from 300 to 3000 K plotted with DTA data by Svechnikov et al.[54]**(○) DTA data, two phase observations, and single phase observations by Yeremenko**[61] **(◇, ◫, and □ respectively) and solubility measurements by Wang et al.**[50] **(✳) solubility measurements by Hajjaji et al. (✧) and solubility measurements from this work (◬).**

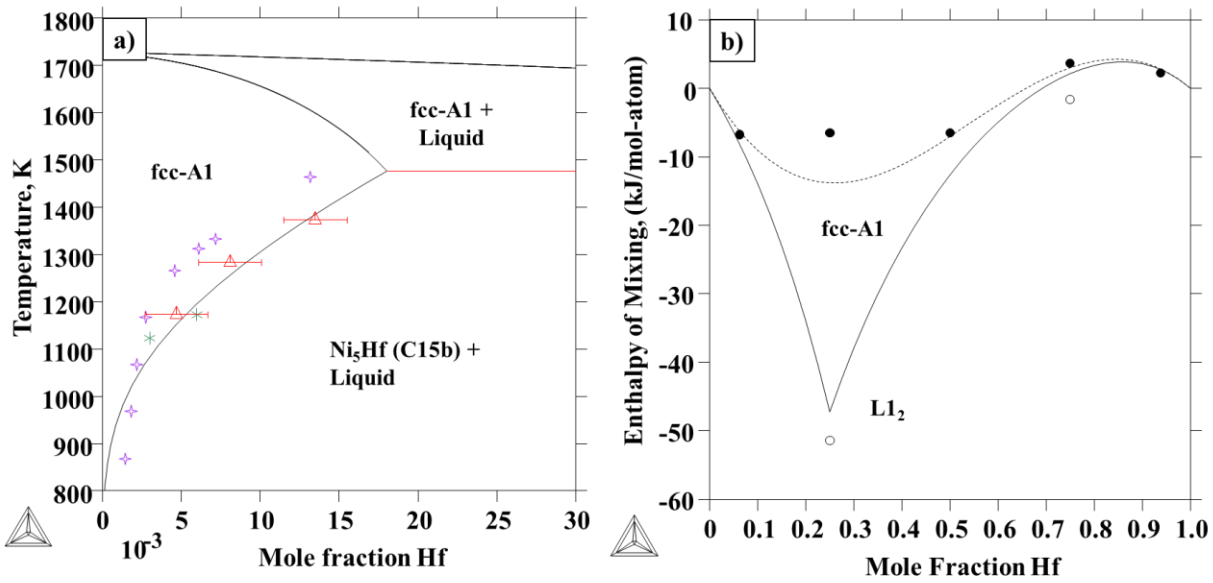

Figure 3.7. a) Solubility of Hf in fcc (A1) Ni and b) calculated mixing enthalpy of the fcc A1 phase and the L12 phase resulting from CALPHAD optimization plotted with calculated mixing from first-principles from this work for each phase (● and ○ respectively). Solubility measurements by Wang et al.[50] **(✳) solubility measurements by Hajjaji et al. (✧) and solubility measurements from this work (△).**

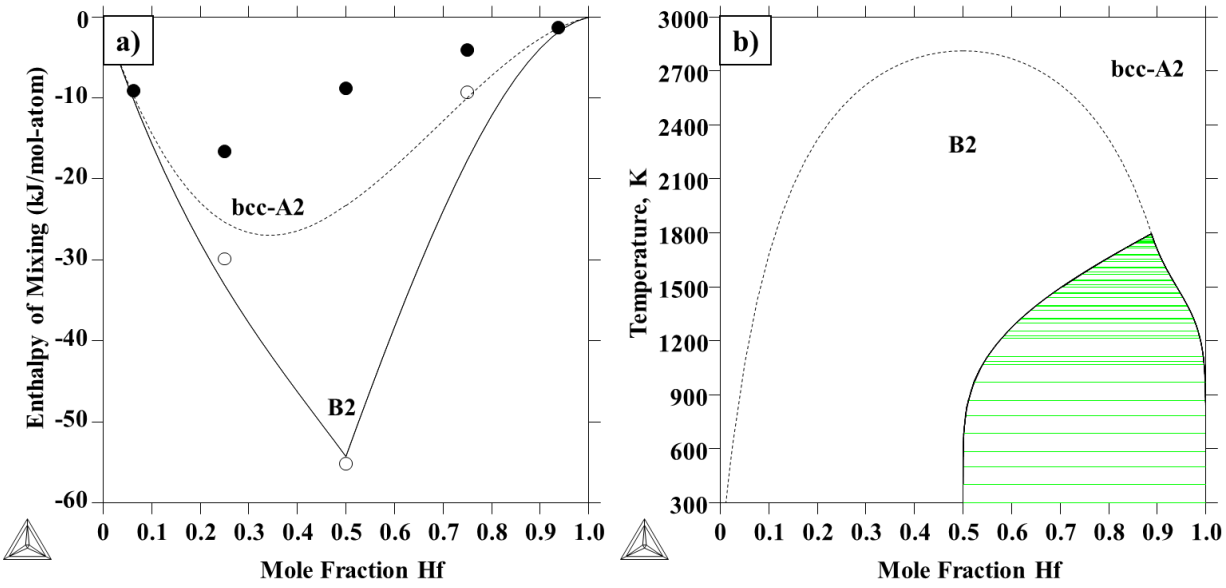

Figure 3.8. a) calculated mixing enthalpy of the bcc-A2 phase and the B2 phase resulting from CALPHAD optimization plotted with calculated mixing from first-principles from this work for each phase (● and ○ respectively) and b) the metastable A2-B2 phase diagram. A dotted line shows the second-order phase transition between bcc-A2 and B2.

4 Modeling the Ni-Al-Hf and Ni-Cr-Hf systems – towards a model of the Ni-Al-Cr-Hf system

4.1 Introduction

Hf in MCrAlYs has the largest impact on the thermally grown oxide (TGO) layer established on the MCrAlYs prior to field use. The addition of this Hf has been found to reduce the growth rate and improve the adhesion of the TGO[16], [86]. The Al concentration in MCrAlYs is often high and understanding the thermodynamics and phase behavior at higher temperatures is important to achieving optimal mechanical properties between the MCrAlY and the underlying alloy[15]. Furthermore, the prediction of oxidation behavior requires an in-depth understanding of how the activity of the component elements in the MCrAlY coating changes with compositional changes. Hence, it is important to understand the thermodynamics for any given MCrAlY system.

The system of interest in the present study is the Ni-Al-Cr-Hf system. For MCrAlY coatings in this quaternary system, the Ni-rich ternary Al-Cr-Ni, Al-Hf-Ni, and Cr-Ni-Hf systems are of primary importance. An extensive description of the Al-Cr-Hf system is available in the literature[72] but improvements of the Al-Hf-Ni and Cr-Ni-Hf systems are possible. Both these systems were first studied by Kaufman and Nesor[87] who combined the at the time available binary subsystems to study expected liquidus projections. Recently, the Al-Hf-Ni system was remodeled by Zhang et al.[51] using phase boundary data from their own equilibration experiments at 1160°C, phase boundary data by Nagarajan[88] at 1130°C and phase boundary data at 1000 °C by Nash and West[67]. Unfortunately the Hf used in experiments by Nash and

West contained approximately 3 at.% Zr making the accuracy of the phase boundaries somewhat questionable. In-fact, the binary model of the Ni-Hf system by Wang[50] adopted by Zhang et al. has this same issue, since many of the experimental data for the Hf-Ni system accounted for by Wang[50] also contained approximately 3 at.% Zr. Furthermore, the Ni-Cr-Hf by Kaufman et al.[87] contains outdated phase models which are not compatible with the current models.

Due to the few temperatures investigated (1000 °C, 1130 °C and 1160 °C) and the contamination issue, this work seeks to remodeled the Al-Hf-Ni system while using new experimental data at temperatures between 900 °C and 1200 °C. The binary Ni-Hf system has previously been remodeled using a new, extensive set of experiments [ref?] and this description will be used adopted in the current work. The Ni-rich Ni-Cr-Hf system is also remodeled accounting for new experimental data between 900 °C and 1200 °C to improve the solubility of Hf in the γ phase. The new ternary models developed in this work are combined with available ternary and binary models in the literature and used to study phase equilibria in the Ni-rich portion of the Ni-Al-Cr-Hf system. Finally, the developed description is applied in the thermodynamic model developed by Gheno et al. [42] to predict the onset of HfO_2 precipitation at the interface between the TGO and the alloy. The Ni-Al-Cr-Hf-O description used for these calculation is included in the supplementary material (TDB file).

4.2 Literature Review

4.2.1 Binary Models

In the current work the thermodynamic descriptions of the binary Al-Hf and Cr-Hf systems are by Wang et al.[89] and Pavlů et al. [90], respectively, are adopted without change. Our previous model for the Ni-Hf system model is also adopted in the present work.

4.2.2 Ternary Models and Experiments

The ternary Al-Cr-Ni system by Dupin [72] is adopted in the current work and details of the experimental data relevant for this system is not repeated here. In the case of the Al-Cr-Hf system, only one set of experimental equilibrium data is available in the literature in regards to the solution between the laves phases Al_2Hf and Cr_2Hf[91]. A two phase region is observed after annealing for 800 hours at 800 °C and no solid solution is observed. Due to the lack of thermodynamic information, this system will not be considered in the present study and constructed only from the binary systems. However, a review of the relevant literature for the Al-Hf-Ni and the Cr-Hf-Ni systems is given below. A summary of the experiments available in the literature, along with analysis techniques, and important experimental information is given in Table 4.5.

4.2.2.1 Al-Hf-Ni

The Al-Hf-Ni system has been reviewed several times[69][92], [93][94] due to its technological importance. While the number of experimental works is plenty, judging their quality is complicated by the fact that Hf often contains non-negligible fractions of Zr. For instance, Nash and West[68] performed experiments on Ni-rich samples where they reported that the starting Hf contained ~3 at.% Zr and 0.38 at.% of other impurities. Furthermore, Miura et al.[95] performed experiments on the Ni-rich samples where the initial Hf was reported to contain up to 5wt.% of

contaminants. The only other study which reported its Zr was by Albers et al.[96] where Hf contained 2-3 at.% Zr.

The problem with the Zr containing Hf is due to the high cost of removing Zr from Hf[52]. For instance, a recent report on the Hf-Pt system also contained ~3 at.% Zr impurity in Hf samples used for creating alloys[97]. It is also possible that Hf used for early experiments [refs] even contained greater Zr concentrations than reported given the difficulty in distinguishing Hf from Zr during purification.

Appreciable amounts of impurities like Zr in the starting Hf material adds uncertainty to reported phase boundary positions. For this reason, equilibria data by Nash and West [68] and Miura et al. [95] is only compared to and not explicitly accounted for during CALPHAD modeling in this work. Additionally, given the difficulties in producing pure Hf, work not reporting the component purities is only compared to and not used during modeling with the exception of selected studies reporting melting temperatures. This includes thermochemical work on the enthalpies of formation of alloys in the Al-Hf-Ni system by Hu and Nash[98] and work by Ochiai et al[99] on the solubility of Hf in the ordered γ' phase at 1000 °C. Only experiments by Zhang et al. at 1130 ° C are considered in this work since this study reported a Hf purity of at-least 99.9 wt%. Nagaraja et al.[100] also reports a purity of Hf of at least 99.9 wt%. However, they report a four phase equilibrium which would violate the Gibbs-phase rule for a ternary system at constant pressure and temperature[40] and consequently, it must be assumed that either the samples were not at equilibrium (which is unlikely given the long annealing times and high

temperatures) or that there was sufficient Zr present to create a four phase equilibrium in the quaternary Al-Hf-Ni-Zr system.

The Al rich portion of the system was recently studied using high purity Hf by Mudryi and Shved[101]. Alloys were annealed at 300 °C and 800 °C and the equilibria of several ternary compounds were observed using X-ray diffraction analysis. The Hf-rich portion of the diagram was studied by Markiv et al.[102] and their results are comparable to the results by Mudryi and Shved. However, samples prepared by Markiv were held in a silica crucible and Si might have contaminated these samples during annealing. Neither of these datasets are used explicitly in the present work.

4.2.2.2 Cr-Hf-Ni

The Cr-Hf-Ni system was reviewed by Gupta in 2001[103] and again in 2010[104]. Most equilibrium information reviewed available comes from work by Nash and West[68] who investigated the Ni-rich portion of the diagram. As with the case of the Al-Hf-Ni system, these experiments contained ~3 at.% Zr.

A eutectic reaction was observed by Khorunov et al.[48] when studying the system at 1227 °C. The liquid formation was extensive in the Ni-rich portion of the phase diagram with a reported Hf purity of 99.9%. Supposedly, Khorunov et al. also performed thermal analysis to obtain a verticle section of the system at 5 at.% Cr. However, only the proposed diagram resulting from that work was presented; i.e. no actual data points. A newer study exists which investigated this eutectic formation by Feng et al.[105] who performed experiments on Ni-XCr-5Hf (wt.%)

samples to obtain liquidus and solidus temperatures between 0 and 30 wt.% Cr using Single Sensor Differential Thermal Analysis (SSDTA). Data by Feng does not report the purity of its initial metals and the melting temperature of their binary system disagrees appreciably with the present binary model. However, this data is to prefer over data by Khorunov et al. since the precise experimental liquidus is unclear in that work. Only the liquidus measured by Feng is used during modeling. This is to account for the disparity between the binary solidus observed in those experiments and the one modeled in the present binary.

4.3 Thermodynamic Models

In this work the Calculation of Phase Diagram (CALPHAD) method is applied to obtain a thermodynamic model of the present quaternary system[106]. What follows is a description of the models used to describe the experimentally observed phase behavior.

4.3.1 Solution Phases

In this work the fcc γ phase, the bcc α phase, and the liquid phase are treated as disordered solutions of each element on a single symmetrically equivalent site (sublattice) in the compound energy formalism (CEF) framework[38]. The molar Gibbs energy of a solution phase Θ is given as:

$$G_m^{\Theta} = \sum_i x_i \, {}^{\circ}G_i^{\Theta} + \sum_i x_i \ln x_i + \sum_i \sum_{j>i} x_i x_j \sum_{\nu} {}^{\nu}L_{i,j}^{\Theta} \left(x_i - x_j\right)^{\nu} + \sum_i \sum_{j>i} \sum_{k>j} x_i x_j x_k \left[\sum_{p=0,1,2} {}^{p}L_{i,j,k}^{\Theta} \left({}^{p}X + \frac{1 - x_i - x_j - x_k}{3} \right) \right] \quad \textbf{Eq. 4.1}$$

where first summation is the mechanical mixing of each ith species in the sublattice, x_i is the mole fraction of component i and ${}^{\circ}G_i^{\Theta}$ is the molar Gibbs energy of component i with respect to

the standard element reference (SER) taken from the SGTE database[107], the next summation is the ideal configurational mixing entropy of component i, followed by the non-ideal binary mixing summation between components i and j expanded as a Redlich-Kister polynomial[108] to the νth power, and finally the ternary mixing summation where ${}^{p}X$ refers to the pth term in the alphabetically ordered list of x_i, x_j, and x_k. The polynomial coefficients within the binary mixing summation are usually given as:

$$ {}^{\nu}L^{\Theta}_{i,j} = {}^{\nu}A + {}^{\nu}BT \qquad \textbf{Eq. 4.2} $$

where ${}^{\nu}A$ and ${}^{\nu}B$ are coefficients related to the mixing enthalpy and entropy, respectively. The ternary mixing coefficients, ${}^{p}L^{\Theta}_{i,j,k}$, are also typically represented this way.

4.3.2 Ordered Intermetallics: the β and γ′ Phases

Of particular importance to nickel-alloys for high temperature applications are the ordered γ' phase and the ordered β phase. Both the γ and γ' phases and the α and β phases in this system are modeled to be compatible with previous work in the Ni-Al-Cr system by Dupin et al.[72] where each set of phases are interconnected through an ordering contribution and the ordered phases are modeled using two sublattices (the 2SL model). Here the γ' phase sublattice model is given by $(Ni, Al, \mathrm{Cr}, \mathrm{Hf})_3(Ni, Al, \mathrm{Cr}, \mathrm{Hf})_1(Va)_1$ while the β phase sublattice model is given by $(Ni, Al, \mathrm{Cr}, \mathrm{Hf})_1(Ni, Al, \mathrm{Cr}, \mathrm{Hf})_1(Va)_3$. Given a disordered phase Θ and an ordered phase Θ′, the Gibbs energy of this phase is given by:

$$ G_m^{\Theta \; or \; \Theta'} = G_m^{\Theta} + \Delta G_m^{\Theta'} - \Delta G_m^{\Theta'}(y_i' = x_i, y_j'' = x_j) \qquad \textbf{Eq. 4.3} $$

where G_m^{Θ} is the molar Gibbs energy of the disordered phase, $\Delta G_m^{\Theta'}$ is the ordering contribution to the Gibbs energy as a function of site fraction of species i in the first sublattice, y_i', and species j in the second sublattice, y_j'', and $\Delta G_m^{\Theta'}(y_i' = x_i, y_j'' = x_j)$ is the ordering contribution when the site fraction of the species i or j is the same as the mole fraction of that species. It is important to note that $G_m^{\Theta \, or \, \Theta'} = G_m^{\Theta}$ when all sites are completely disordered. Within the 2SL model $\Delta G_m^{\Theta'}$ has the following form:

$$\Delta G_m^{\Theta'} = \sum_i \sum_j y_i' y_j'' \, \Delta \, G_{i:j}^{\Theta'}$$

$$+RT\left[\frac{a}{(a+b)}\sum_i y_i' \ln y_i' + \frac{b}{(a+b)}\sum_j y_j'' \ln y_j''\right]$$

$$+\sum_i \sum_{j>i} \sum_k y_i' y_j' y_k'' \sum_\nu {}^{\nu}L_{i,j:k}^{\Theta'} \left(y_i' - y_j'\right)^{\nu} \qquad \textbf{Eq. 4.4}$$

$$+\sum_i \sum_{j>i} \sum_k y_i'' y_j'' y_k' \sum_\nu {}^{\nu}L_{k:i,j}^{\Theta'} \left(y_i' - y_j'\right)^{\nu}$$

$$+\sum_i y_i' y_j' y_k' y_l'' L_{i,j,k:l}^{\Theta'} + \sum_i y_i'' y_j'' y_k'' y_l' L_{l:i,j,k}^{\Theta'}$$

where $\Delta G_{i:j}^{\Theta'}$ is the end-member ordering Gibbs energy related to the crystallographic bonding of the compound with i on the first sublattice and j on the second sublattice, the non-ideal mixing is again described using a Redlich-Kister-Muggianu polynomial[108] for binary mixing, ternary mixing is represented as a simple product of site-fractions and a and b are stoichiometric coefficients for the two sublattices of the Θ phase. For the 2SL γ' phase model $a = 3$ and $b = 1$ while for the 2SL β phase model $a = 1$ and $b = 1$. In the 2SL model for the β phase, elements can be interchanged between symmetrically distinct sites present in the structure. This site equivalence causes some end-members and interactions to be interchangeable, making $\Delta G_{i:j}^{\beta} = \Delta G_{j:i}^{\beta}$ and $L_{X:i}^{\beta'} = L_{i:X}^{\beta'}$ where X represents either binary or ternary mixing of components. A site equivalence is also present in the γ' phase but is only captured in the more complex model constructed by Ansara[109] and Dupin[72] using four sublattices (the 4SL model) since only this model can describe the ordered $L1_0$ ordering. To account for this in the 2SL model, the $L1_0$ phase must be modeled separately and relations must be made between binary and ternary interaction parameters in the 2SL model and the end-member ordering Gibbs energies from the 4SL model. In particular, these end-member ordering Gibbs energies are related to the bonding energies between elements in the γ' phase in the 4SL model. For an A-B system, the ordered compounds in the 4SL model would be AB_3 A_3B and A_2B_2. The Gibbs energies for each of these compounds can be related to the bonding energy between A and B, U_{AB}, as follows:

$$G_{\mathrm{AB_3}} = 3U_{AB} + \alpha_{\mathrm{AB_3}}$$

$$G_{\mathrm{A_2B_2}} = 4U_{AB} \qquad \textbf{Eq. 4.5}$$

$$G_{\mathrm{A_3B}} = 3U_{AB} + \alpha_{\mathrm{A_3B}}$$

Where α_{AB_3} and α_{A_3B} are factors to account for a change in bonding environment first introduced by Kusoffsky et al.[73] This permitted a relaxation of the relation between the end-members. Further parameters must be considered for the ternary case of an A-B-C system. These parameters and the other required relations between end-members and interactions can be found in the description of the Ni-Al-Cr system by Dupin et al[72]. In this work the stricter model by Dupin is used in all cases except for in the Al-Hf system. Only ternary and binary interactions are found to be necessary.

4.3.3 Compounds

The only other compounds treated in the ternary and quaternary systems in this work are the $L2_1$, Huesler phase (Fm-3m) with stoichiometry Ni_2AlHf, the λ phase ($P6_2m$) with stoichiometry NiAlHf, the η phase (C2/m) with stoichiometry Ni_7Hf_2 and the τ phase (R-3m) with stoichiometry Ni_3Hf. These phases are treated because of their proximity to the γ' and β phases and their prominence in the Ni-rich corner. All other ternary compounds are considered to have Hf concentrations which are too high to be relevant. The λ phase was reported by both Markiv et al[110] and Mudryi and Shved[101] without noticeable solubility and is therefore modeled only as a stoichiometric compound.

The $L2_1$ Huesler phase was reported by both Markiv et al[110] and Nash and West[68]. In the current model the sublattice model for this phase is given by $(Al,Hf,Ni)_{0.5}(Al,Hf,Ni)_{0.5}(Ni,Va)_1$ so as to adopt the description of this phase in the binary Ni-Al system[111]. No Cr additions are considered since the Huesler phase is not observed experimentally in the Ni-Cr-Hf system. The molar Gibbs energy of this phase is given as:

$$G_m^{\mathrm{L2_1}} = \sum_i \sum_j \sum_k y_i' y_j'' y_k''' \, {}^{\circ}G_{i:j:k}^{L2_1}$$

$$+ RT\left(\frac{1}{4}\sum_i y_i' \ln y_i' + \frac{1}{4}\sum_i y_i'' \ln y_i'' + \frac{2}{4}\sum_i y_i''' \ln y_i'''\right)$$

$$+ \sum_i \sum_{j>i} \sum_k \sum_l y_i' y_j' y_k'' y_l''' \sum_\nu {}^{\nu}L_{i,j:k:l}^{\mathrm{L2_1}} \left(y_i' - y_j'\right)^{\nu} \qquad \textbf{Eq. 4.6}$$

$$+ \sum_i \sum_{j>i} \sum_k \sum_l y_i'' y_j'' y_k' y_l''' \sum_\nu {}^{\nu}L_{k:i,j:l}^{\mathrm{L2_1}} \left(y_i'' - y_j''\right)^{\nu}$$

$$+ \sum_i \sum_{j>i} \sum_k \sum_l y_i''' y_j''' y_k' y_l'' \sum_\nu {}^{\nu}L_{k:l:i,j}^{\mathrm{L2_1}} \left(y_i''' - y_j'''\right)^{\nu}$$

Finally the η phase is modeled with the sublattice model: $(Hf,Ni)_2(Cr,Al,Ni)_7$ and the τ phase is modeled with the sublattice model $(Ni,Al,Cr)_3(Hf)_1$. Ni is dissolved on both sublattices of the τ phase to account for observations of a wide solubility range of this phase in the Ni-Al-Hf and Ni-Cr-Hf systems by Nash and West[67], [68] and Zhang[51]. Al and Cr are introduced onto only the Ni dominant sites of both the τ phase and the η phase to represent the strong preference of these elements for this site expected from the equilibria behavior observed by Nash and West. If θ is a given intermetallic phase with two sublattices with stoichiometric coefficients a and b for each sublattice, the molar Gibbs energy of this phase can be expressed as:

$$G_m^{\theta} = \sum_i \sum_j y_i' y_j'' \, {}^{\circ}G_{i:j}^{\theta} + RT\left(\frac{a}{(a+b)}\sum_i y_i' \ln y_i' + \frac{b}{(a+b)}\sum_k y_k'' \ln y_k''\right) + \sum_i \sum_{j>i} \sum_k y_i' y_j' y_k'' \sum_{\nu} {}^{\nu}L_{i,j:k}^{\theta}\left(y_i' - y_j'\right)^{\nu} + \sum_i \sum_{j>i} \sum_k y_i'' y_j'' y_k' \sum_{\nu} {}^{\nu}L_{k:i,j}^{\theta}\left(y_i' - y_j'\right)^{\nu} + \sum_i \sum_{j>i} \sum_k \sum_{k>l} y_i'' y_j'' y_k' y_l' \; L_{i,j:k,l}^{\theta} \quad \textbf{Eq. 4.7}$$

Here $L_{i,j:k,l}$ is an interaction parameters representing short range ordering within the CEF[112]. This term is needed only in the η phase to replicate the observed solubility in the ternary systems.

In the Ni-Hf-X system (X=Al or Cr) if $X_aHf_bNi_c$ represents an end-member compound in this system, then the Gibbs energies of this compound in this work is described as:

$$G_m^{X_aHf_bNi_c} = a\,{}^{\circ}G_X^{SER} + b\,{}^{\circ}G_{Hf}^{hcp} + c\,{}^{\circ}G_{Ni}^{fcc} + \Delta_f H^{X_aHf_bNi_c} - T\Delta_f S^{X_aHf_bNi_c} \quad \textbf{Eq. 4.8}$$

where SER is the standard element reference for X (fcc for Al and bcc for Cr), $\Delta_f H^{X_aHf_bNi_c}$ is the formation enthalpy of the compound and $\Delta_f S^{X_aHf_bNi_c}$ is the formation entropy of the compound. Data from first-principles calculations are used to find values for the formation

enthalpies and entropies of some of the compounds in this work. Details for these calculations are given in the following section. Calculated data and relevant experiments are used to model the interactions and formation enthalpies and entropies of the phases listed. This is done using the PARROT module in Thermo-Calc[113].

4.4 First-Principles Methodologies

Finite temperature properties for condensed phases can be calculated by calculating the Helmholtz energy as a function of temperature and volume, F(V,T). In terms of the quasiharmonic approach this can be given as[75], [114]:

$$F(V,T) = E_{0K}(V) + F_{vib}(V,T) + F_{T-el}(V,T) \qquad \textbf{Eq. 4.9}$$

where $E(V,T)$ is the ground state energy, $F_{vib}(V,T)$ is the vibrational contribution to the Helmholtz energy, and $F_{T-el}(V,T)$ is the thermal-electronic contribution to the Helmholtz energy. It is important to CALPHAD modeling to note that the Helmholtz energy can be converted to the Gibbs energy when there is no apparent pressure[26]. In this work $E_{0K}(V)$ is the ground state energy at 0K determined either through a specific relaxation scheme or through a four parameter Birch-Murnaghan equation of state fitting of energy vs volume (E-V) calculations for a particular crystal structure[114]. The equations governing these fits can be found in the work by Shang et al[114].

$F_{vib}(V,T)$ is calculated using the quasiharmonic Debye-Grüneisen model instead of the phonon method for purposes of efficiency. In this method the Debye temperature is obtained from E-V calculations and modified by a scaling factor based on the anharmonicity of the crystal structure the details of which are addressed in a separate paper by Shang et al.[46]. Enthalpies of mixing are calculated in this work using special quasirandom structures (SQS). These structures mimic

random alloys which permits the calculation of mixing enthalpies through DFT calculations. Mixing enthalpy calculations in the α phase are calculated using 16 atom cells developed by Jiang for binary calculations[115] and 32 atom cells developed by Jiang for ternary calculations in the ternary structures developed by Jiang[116]. Mixing enthalpy calculations in the β phase are also calculated using 32 atoms cells developed by Jiang[79]. For the γ phase, binary mixing enthalpy calculations used 16 atom SQS cells developed by Wolverton et al.[78] while ternary mixing enthalpy calculations used 16 atom and 24 atom SQS cells developed by Shin et al.[117]. Finally calculations in the γ' phase are carried out using 24 atom SQS structures developed by Liu et al.[118] Each SQS calculation is given the following relaxation scheme: 1st) a volume relaxation fixing shape and ionic positions relative to the volume, 2nd) a volume and shape relaxation fixing ionic position relative to the cell, and finally 3rd) a relaxation where every parameter is permitted to change[119]. Once this relaxation scheme is completed only calculations which have kept symmetry are used to obtain a value for the enthalpy of mixing. While this has sometimes been analyzed using a radial distribution function (RDF) this is instead tested using spglib[120] as implemented through Pymatgen[121] with a distance tolerance of 0.1 Å and an angle tolerance of 0.. Notably, calculations involving Cr in the γ' and β phase are not performed since these phases are unstable in the Ni-Cr-Hf system.

DFT calculations are carried out using the Vienna Ab-initio Simulation Package (vasp). The projector augmented wave (PAW) method is used for electron-ion interactions with the generalized gradient approximation (GGA) as parameterized by Perdew Burke and Ernzerhof (PBE) used for electronic exchange and correlation. The pseudopotentials used for Al, Cr, Hf, and Ni are those recommended by vasp[74]. The plane wave basis cut-off is chosen to be 400 eV

for all cases for consistency and to ensure accuracy. For all calculations, a low accuracy step is performed where the precision in vasp is set to normal and the k-points per reciprocal atom (kppra) is set to 1000 per atom. If symmetry is not broken after this calculation another calculation is performed where the precision is set to high and the kppra is set to atleast 1000. If either of these calculations break symmetry a high accuracy calculation with fixed volume is used in place of a full relaxation. A final static relaxation step for each calculation is performed regardless of the required relaxation scheme. In this calculation the precision in vasp is set to high, the KPOINT mesh is set to at-least 5000 per reciprocal atom, and only a single ionic step is performed.

4.5 Experimental Methodologies

Alloys of nominal compositions given in Table 4.2 are used for the experimental study of phase equilibria in the Ni-rich Al-Hf-Ni and Cr-Hf-Ni systems. The compositions are chosen so as to fall into three different suspected three-phase regions of the Al-Hf-Ni system, and two two-phase regions of the Cr-Hf-Ni system, based on the pre-existing literature. Ingots are made by argon arc melting, drop cast into 10 mm diameter rods, and homogenized for 6 h at 1200 °C plus 48 h at 1150 °C in vacuum. Alloy processing was conducted at the Materials Preparation Center of Ames Laboratory[80]. Specimens approximately 1 mm thick are then vacuum-encapsulated in quartz capsules and annealed in tube furnaces at 900, 1000, 1100 and 1200 °C for 636, 206, 100 and 50 h, respectively. The heat treatments are terminated by water quenching to retain the equilibrium microstructures. Alloy HQ5 (Ni-3Cr-7Hf) is observed to partially melt at 1150 °C; due to difficulties in handling molten specimen in our current experimental setup, this alloy is not included in the 1200 °C run.

Polished sections of the heat-treated alloys are prepared by standard metallographic procedures. Phase compositions are determined by electron probe micro-analysis (EPMA) using a JEOL JXA-8530F field emission gun instrument. The measured intensities are converted to concentrations via a built-in ZAF calibration procedure, using pure metals as standards. The probe size was about 1 μm, and the alloy microstructures are in general coarse enough for each phase to be analyzed individually – cases where a phase was observed but its composition could not be determined reliably will be indicated.

4.6 Results and Discussion

4.6.1 Results from Experiments

Alloy phase constitutions are determined from microstructure examination, phase composition analysis, and pre-existing knowledge of the systems topology. The Al-Hf-Ni alloys provide equilibrium compositions in the following three-phase regions: γ-γ'-Ni_7Hf_2, γ'-β-Ni_7Hf_2 and β-$HL2_1$-Ni_7Hf_2 (see selected micrographs in Figure 3.1 and EPMA results in Table 4.3). One exception is noted: after annealing at 900 °C, alloy HQ2 presents both Ni_5Hf and Ni_7Hf_2 in addition to γ and γ'. As shown in Figure 4.2, Ni_7Hf_2 is present in small quantities, and forms a morphological complement to Ni_5Hf. The presence of four phases in this ternary system necessarily reflects a non-equilibrium situation. After casting, the alloy is first annealed at 1200 and then 1150 °C, where the Ni_7Hf_2 phase would have been stable; we conclude that the 900 °C heat treatment is not long enough for the $Ni_7Hf_2 \rightarrow Ni_5Hf$ conversion to be completed. Likewise, small Hf-rich precipitates are sometimes observed in the other AlHfNi alloys (see bright spots in Figure 3.1). The CrHfNi alloys provide terminal compositions for γ-Ni_5Hf and γ-Ni_7Hf_2 tie-lines (see Figure 4.3 and Table 4.4).

4.6.2 Results from First-Principles

The results for first-principles end-member calculations for the binary systems Ni-Hf, Al-Hf and Cr-Hf and the ternary systems Ni-Al-Hf and Ni-Cr-Hf are shown in Table 4.5 listing values for $\Delta_f H^{298.15K}$. This includes all end-member compounds in the γ' and β phases, all end-members for the given sublattice models of the η, τ, and the stoichiometric $L2_1$ and λ phases. Finite temperature information is only calculated for the $L2_1$ phase. This phase has an entropy of 31.92 J/mole-atom-K.

No experimental values are available in the literature to compare the present theoretical enthalpies of formation to. This is partly due to the stability of the γ' phase and the β phase which do not appear in any of the X-Hf binary systems. Hu and Nash[98] report enthalpies of formation for several alloys in the Ni-Al-Hf system but since the heat treatment of these alloys was not specified, it is difficult to say what phases these enthalpies of formation correspond to. The β phase appears to be stable in the Ni-Hf system at high temperatures as also noted in previous work and a discussion of these calculation results can be found in that study.

The formation energies of the η phase has also been covered in a previous study by Guo and Kleppa[60] where the enthalpy of formation of the compound is measured to be -44.1 ± 1.5 by high-temperature calorimetry. This is in good agreement with our calculated results from DFT which have been included in Table 4.5. No experimental information is available on the thermodynamics of mixing additional elements in this phase.

4.6.3 Results from CALPHAD Optimization

Equilibria results in Table 4.3 along with information by Zhang is used to construct a thermodynamic model in both the Al-Hf-Ni system and the Cr-Hf-Ni system using the PARROT module of Thermo-Calc. The results of this modeling is given below.

4.6.3.1 Al-Hf-Ni

The present description of the Al-Hf-Ni system includes new parameters for the γ phase to better describe the solubility of Hf in Ni. This is not just important from an alloy design standpoint but also from the standpoint of high temperature reactions and diffusion where the underlying activities play an important role in how Hf and Al are depleted during alloy service. Of particular importance is having a well described γ' phase and β phase since these will play a large role in oxidation resistance.

Given the lack of thermochemical information in this system, the underlying Gibbs energies for the γ'phase rely heavily on calculated values from first principles in this study. In particular, enthalpis of formation for the Ni_3Hf, $NiHf_3$, Al_3Hf, and $AlHf_3$ compounds are taken directly from first-principles. Entropies are modified for these end-member compounds to fit available experimental equilibria data with the exception of the Ni_3Hf phase which is fixed to previous calculations in the Hf-Ni system. As with the γ' phase, the β phase relies on first-principles calculations in the Al-Hf system since the β phase is not stable in this system and hence no experimental data is available to modify parameters with. In previous modeling of the Ni-Hf system, first principles information was also used to assess the parameters of the β phase. However, the β phase was shown to be stable in that case.

Results for the calculated enthalpies of mixing obtained from SQS calculations in the Ni-Al-Hf system and are given in Table 4.6 for the α, β, γ and γ' phases. Enthalpies of formation with

respect to the pure elements are given in this table for the first constrained symmetry calculation from DFT, the final, unconstrained relaxation from DFT, and the calculated value used in the current thermodynamic CALPHAD model. It has been postulated that the true lattice stability of a random alloy calculated by first-principles should fall somewhere between these two states[122]. Unfortunately, this calculation would be expensive to do and was not performed in this study. Notably, all calculations broke symmetry during unconstrained relaxation and only calculations which only permitted the volume to relax were used. However, it was found that all of the parameters involved in this paper relaxed away from these values and enthalpies of formation from the modeled system fall between the symmetry constrained and symmetry broken systems. However, the α and β mixing enthalpies calculated using the CALPHAD description are lower in every case than the DFT calculated mixing enthalpies. This disparity is partly due to a difference between the formation enthalpy calculated using DFT for β-NiAl (-63.583 kJ/mol-atom from the materials project[123] vs. -59.203 kJ/mol-atom from SGTE[41])

Isothermal sections at temperatures from 1000 °C to 1200 °C calculated using the present Ni-Al-Hf CALPHAD description are presented in Figure 4.4 for all available experimental equilibrium studies with the exception of work by Shved[101] which is out of the scope of this study. The current experiments at 900 °C apparently did not reach equilibrium as evidenced by one of the nominal alloy compositions being outside of the observed tie-triangle despite the long annealing time (636 h).The diffusion of Hf in Ni has been calculated to be relative fast[124] but it has been shown experimentally that the Hf diffusion in the γ' phase of the Ni-Al system at high temperatures is much slower[125]. Hence, it is possible that Hf diffusion in the current case may

have been obstructed by the γ' phase , preventing the alloy heat treated at 900 °C from reaching their equilibrium state.

It was found during optimization that the disordered phase needed to be decoupled from the ordered phase to obtain a satisfactory fit to experiments. This is unlike the optimization by Zhang et al.[51], where the γ and γ' interaction parameters are coupled through a bonding term. Furthermore, the present thermodynamic model describes a larger region around the Ni-rich corner compared to the work by Zhang et al. All observed tie-lines and tie-triangle sides involved in the described equilibria are well reproduced in the temperature range in focus here; i.e. from 1000 ° C to 1200 ° C.

Due to the strong mixing of Hf in the Al sites of Ni_3Al, the maximum solubility in the γ' phase is most strongly affected by the equilibrium with the η phase – although the direction of the tie-lines between the γ and γ' phase regions will not be as strongly affected. The model developed by Zhang has no solubility for Al in the η phase modeled but it does have solubility for Ni. This is introduced to match experimental observations in the ternary system. Indeed, Ni solubility in the Hf sublattice is also needed in this work to match experimental observations by Nash and West, Nagarajan, Zhang, and those in this work, all of which observed η phase compositions corresponding to a Ni rich η phase in the Ni-Hf system at high temperatures. A short range order term is used to fit interaction parameters in the η phase to experimental data. The Al solubility in this phase decreases as the solubility of Ni in the binary Ni-Hf system decreases. Since Ni solubility decreases with decreasing temperature no Al solubility is expected at low temperatures. Indeed Markiv[102] observed no Al solubility at 800 °C. Excellent agreement is

found between the modeled solubility in the η phase and the solubility measured in this work and in the work by Nash and West[68] at 1000 and 1200 ° C. Good agreement is also found in the measured solubility of Hf in the γ' phase available in the literature. Single phase γ' measurements from Nagrajan and Ochiai et al[99] at 1000 °C fall within the calculated region in this study.

Those phases not modeled in work by Zhang are the L21 Huesler phase, the τ-Ni_3Hf phase and the λ-NiAlCr phase. The Huessler phase is found to have substantial solubility for Ni with increasing temperatures. The current model shows excellent reproduction of the solubility measured in this study from observed tie-triangles. Agreement is also good with observations by Nash and West at 1200 ° C where both the observed tie-triangle between β, γ' and $L2_1$ and the observed tie-line between the η phase and the L21 phase are in agreement with the current model. However, a higher Ni solubility in the L21 phase was observed at 1000 ° C by Nash and West than at 1200 °C in disagreement with the current experimental data.

Some disagreement between this model and observations by Nash and West[68] can also be found in the observed equilibria between the τ-Ni_3Hf phase and the η phase at 1000 and 1200 °C. These reported equilibria would suggest that τ-Ni_3Hf has some solubility for Al as well. This is based on the position of measured values using EPMA. Al placed in the expected sublattice of the Ni3Hf phase, however, did not produce the expected results. While it is possible that Al and Ni mixing produces conditions permitting greater solubility in this phase, more experiments are first needed to justify these calculations.

Perhaps the largest discrepancy in previous experiments is the four phase equilibria observed by Nagarajan et al. Zhang asserted that the observed four phase equilibria by Nagarajan et al. was caused by an invariant reaction. However such a reaction would violate mass conservation given the nominal composition of the alloy used by Nagarajan et al. An alternative hypothesis would be that the alloy compositions were very close to two tie-triangles. This might result in the observed behavior. However the alloy composition resulting in the four phase equilibria by Nagarajan et al. is well within the expected γ, γ', η tie-traingle. Another explanation might be that the Ni_5Hf phase has a remarkably large barrier for dissolution. Indeed, in alloys annealed at 900 °C for 636 hours, the Ni_5Hf phase is observed where the γ phase is expected. However for a temperature of 1130 °C and an annealing time of 168 hours, the experiments by Nagarajan et al. should have readily reached equilibrium. This suggests that the resulting equilibria is actually due to the Zr present in the system. Hence, it would appear that Zr has a stabilizing effect on the Ni_5Hf phase in the alloy annealed by Nagarajan et al. Indeed, another large source of disagreement between Nash and West and the current model and experiments is the presence of a tie-triangle between Ni_5Hf, γ and γ' at 1000 °C. This equilibria does not appear in the current model until much lower temperatures for the alloy composition used by Nash and West for this equilibria – Ni-8Hf-9Al (at.%) and is also observed by Nagarajan at 1130 °C.

In addition, annealing times between experiments in this study at 1000 ° C and in the study by Nash and west are quite similar. This offers evidence that the presence of Ni_5Hf in that work was not due to a large barrier for dissolution.

The only solidus temperatures observed by Takeyama[126] between the Huessler phase and the β -NiAl phase are optimized to in this study. A vertical section between the Huessler phase and

the β-NiAl phase from 800 to 1400 °C is plotted in Figure 4.5 with observations by Takeyama[126]. This verticle section was called a pseudobinary by Takeyama[126]. In the current description the tie-lines do not fall in the same plane as the section between the Huesler phase the β-NiAl phase. Hence, there is no direct eutectic reaction in this calculated vertical section despite the assertion by Takeyama that the microstructure resembles a eutectic microstructure. In light of this, only the lowest melting point observed in these experiments is used to fit the ternary liquid parameters in this study. The current study find a greater solubility for Al in the Huessler phase than that observed or calculated by Takeyama. Calculated vertical sections between 0 and 30 at.% Al and between 1400 and 1750 K for 0, 0.5, 1 and 1.5 at.% Hf are given in Figure 4.6 and compared to experiments by Miura[95]. The liquidus observed by Miura is in good agreement with the current calculated liquidus at each Hf concentration. The corresponding solidus data shows a large degree of scatter and may actually represent the formation of other solid phases. Nash and West also measured the solidus temperature in the Ni-Al-Hf system. A comparison between these values and the calculated ones in this study are given in Table 4.7. Agreement is generally good given the low number of measured datapoints used to fit the liquid parameters. Disagreement is largest for samples with higher Al and higher Hf where the present model is less valid.

4.6.3.2 Cr-Hf-Ni

Aside from work by Kaufmam[87] no other work could be found in the literature attempting to model the Ni-Cr-Hf ternary system. This system is of large importance to MCRALY bond-coats and it is therefore vital to take careful consideration of the equilibria present in this system. The

only equilibria observed in this work is between γ and Ni_5Hf and between γ and η and hence these are the only phases modified during optimization. Similar to the Ni-Al-Hf system, the calculated mixing enthalpy from first principles and from the current model for the α and γ phases in the Ni-Cr-Hf system is given in Table 4.8.

No parameter could be justified to fit the α phase given the lack of experimental information in this system and thus this phase was left to be constructed from the binaries. Modeled enthalpies of formation for mixing in the α phase fall between symmetry constrained and symmetry broken calculations in all but the Cr-rich SQS composition. This may indicate that a positive ternary interaction should be present in the Cr-rich corner of the system. Future modeling in the Cr-rich corner should consider this. The phase equilibria between the η phase and the γ phase is fit exclusively using experiments. The resulting phase equilibria falls between the symmetry constrained and fully relaxed SQS calculations for all modeled values in the γ phase.

Isothermal sections of the Ni-Cr-Hf system are plotted in Figure 4.7 with experimental data from this work and work by Nash and West[70] between 900 and 1200 °C. Since there is no γ' phase present in these samples there should be no reason to suspect that equilibrium might not have been achieved for all samples involved in this study. On the nickel rich portion of the diagram, agreement is good between experiments in this work and those performed by Nash and West[70] for both 1000 and 1200 °C. This is especially true of the solubility of Cr in the η phase. Here, as in the Ni-Al-Hf system, a short range order term is needed to replicate the observed solubility from experiments.

Experiments by Nash and West disagree to a greater degree for those tie-traingles involving the η phase. Since there is little experimental data in this portion of the diagram the observed three phase equilibria between η, Ni_3Hf, and α is not modeled for either temperature. If this was to be modeled the, Cr solubility would probably be as small as the one suggested by Nash and West[70] in their work. The Ni_3Hf phase also seems to have some solubility for Cr much like the η phase. This would explain the large differences between the calculated phase regions and those observed by Nash and West. Here, as with the Al-Hf-Ni system, the calculated end-member enthalpy from DFT did not result in the expected solubility behavior. Furthermore, the tie-triangles involving γ, η and Ni_5Hf observed in work by Nash and West are not replicated in this model. This disagreement could be due to the aforementioned stabilization of Ni_5Hf due to Zr.

A plot of thermal analysis data by Feng et al.[127] and the calculated liquidus is given in Figure 4.8. Only partial agreement is found possible to this data since this data interferes somewhat with the stability of other phases in the system and since the binary Ni-Hf system model disagrees with the observed solidus from these experiments. However, the agreement in the observed trend of both the liquidus and solidus is quite good.

4.6.3.3 Ni-Al-Cr-Hf

With the Ni-rich corners of the Al-Ni-Hf, Cr-Hf-Ni, and Al-Cr-Ni systems well described it is possible to construct a model of the quaternary Ni-Al-Cr-Hf system. This is done using extrapolation methods not just from the CALPHAD method but also from the 2SL models for the both the β and γ phases where ternary and quaternary interactions have distinct correlations to the bonding between elements. Ternary extrapolations come from Dupin et al.[72] while

quaternary extrapolation terms come from[128]. Only ternary terms from the Al-Cr-Hf system are unavailable. This is not expected to have a significant effect on the Ni-rich quaternary system. Although the majority of experiments performed in the Ni-Al-Cr-Hf system are oxidation experiments, one recent experiment by Gheno et al. measured the element concentrations of γ and γ' from 900 to 1200 °C for an alloy with composition Ni-16.8Al-13Cr-0.1Hf[42]. These experiments are compared to calculated values using the present thermodynamic model in Figure 4.9. The calculations are found to be in excellent agreement with experiments.

4.7 Conclusions

A first-principles based CALPHAD model has been developed for the Ni-rich portions of the Ni-Al-Hf and Ni-Cr-Hf systems. This was further combined to create a model of the Ni-rich Al-Cr-Hf-Ni system. Modeling was based on newly performed experiments in each of the ternary systems from 900 to 1200 °C. High purity Hf was used in these experiments to avoid contamination by Zr. First-principles calculations based on density functional theory were carried out to obtain enthalpies of formation of compounds in the binary and ternary systems to obtain solubility information in the η phase (Ni_7Hf_2), to obtain solubility information in the τ phase (Ni_3Hf), and to calculate the enthalpy of mixing for the disordered and ordered solution phases. Special quasi-random structures were used to obtain mixing enthalpies for the disordered and ordered solution phases. However, no structure was able to retain symmetry after relaxation calculations. Hence, these values were only used initially as a starting point for optimization and only compared to later.

Phase compositions for equilibrated samples were measured using electron probe microscopy. Experiments agreed well with most other experiments in the Ni-rich corner. An increasing solubility for Ni in the $AlHfNi_2$ Huessler phase with increasing temperature was found in the present experiments from 1000 to 1200 °C. This was reproduced well in the model. Solubility in the γ' and β phases measured in the present experiments agrees with previous experimental measurements. Alloys at 900 °C in the Ni-rich Al-Hf-Ni system did not reach equilibrium and one alloy composition fell outside of the observed tie-triangle. It is hypothesized that this is either because of a large barrier for Ni_5Hf dissolution or because Hf diffuses more sluggishly in γ'.

Solubility for both Cr and Al was needed in the η phase to reproduce experiments. The τ phase also has some experimental evidence for Al and Cr solubility but not enough data was available to use during modeling. Density functional theory calculationsof the Ni_3Hf phase wasunable to reproduce the observed solubility in experiments. The η-Ni_7Hf_2 phase was also modeled with solubility for Ni in the binary to match experimental observations of a Ni-rich η-Ni_7Hf_2 phase in this work and in previous experiments in the ternary systems. A short range order term was used in this phase in both the Al-Hf-Ni system and the Cr-Hf-Ni system to match experimental observations. This results in good agreement with the present experiments and with previous experiments in both ternary systems.

Finally, experimental observations of the solidus in the Al-Hf-Ni system in the Ni-rich corner and experimental observations of the solidus in the Cr-Hf-Ni system in the Ni-rich corner were used to obtain an estimate of the liquid Gibbs energy in these systems.

The present modeling for both ternary systems in the Ni-rich corner is in good agreement with most experiments at high temperatures with the exception of disagreement with previous experiments believed to be caused by the stabilization of the Ni_5Hf phase by Zr in those experiments. A Ni-rich model of the Al-Cr-Hf-Ni system was constructed from the present ternary models and models available in the literature. Calculations in this quaternary system compare well to available experiments from 900 to 1200 °C. The present model will prove useful for the design of oxidation resistant alloys in the future.

Table 4.1. Summary of experiments used to model the Al-Hf-Ni and Cr-Hf-Ni systems.

References	Exp. method	Exp. data
Al-Hf-Ni		
This work	XRD, EPMA	Isothermal sections at 1000,1100 and 1200 °C
Zhang et al.[129]	XRD, EPMA	Isothermal section at 1160 °C
Takeyama and Liu[126]	Pyrometer with "± 10° accuracy"	Melting temperatures for alloys between NiAl and Ni2AlHf
Cr-Hf-Ni		
This work	XRD, EPMA	Isothermal sections at 900, 1000, 1100 and 1200 °C
Feng[105]	SSDTA	Observed transformation lines for solidifying alloys for Ni-5Hf-xCr (at.%) where x=0 to 30

Table 4.2. Nominal compositions (at. %) of the AlHfNi and CrHfNi alloys used for the experimental study.

#	Al	Cr	Hf	Ni
HQ2	10		9	81
HQ3	19		11	70
HQ4	19		18	63
HQ5		3	7	90
HQ6		15	11	74

Table 4.3. Phase compositions of the Al-Hf-Ni alloys measured by EPMA (at. %). "?" indicates that a phase was observed but was too finely dispersed to be analyzed.

alloy #		900 °C			1000 °C			1100 °C			1200 °C		
		Al	Hf	Ni	Al	Hf	Ni	Al	Hf	Ni	Al	Hf	Ni
HQ2	Ni_7Hf_2	0.1	21.4	78.5	0.2	21.1	78.7	0.3	21.2	78.6	0.4	20.8	78.7
	γ'	18.4	6.2	75.4	17.9	6.2	75.9	17.3	6.2	76.5	16.9	6.0	77.1
	γ	?	?	?	12.7	0.8	86.5	13.3	1.1	85.6	13.9	1.6	84.5
	Ni_5Hf	0.5	16.2	83.3									
HQ3	Ni_7Hf_2	3.9	20.8	75.3	4.8	20.1	75.0	5.3	21.2	73.4	5.2	21.1	73.7
	γ'	19.8	8.1	72.1	19.8	8.2	72.0	19.5	8.4	72.1	19.8	8.0	72.2
	β	42.6	0.5	57.0	41.2	0.8	58.0	39.6	1.3	59.1	37.3	2.0	60.7
HQ4	Ni_7Hf_2	11.5	21.5	67.0	11.7	21.5	66.8	12.0	21.6	66.4	11.9	21.6	66.6
	$HL2_1$	?	?	?	25.9	22.6	51.5	25.4	21.5	53.1	25.4	18.7	55.9
	β	48.4	0.8	50.8	47.0	1.3	51.7	44.8	2.3	52.9	41.2	4.2	54.6

Table 4.4. Phase compositions of the Cr-Hf-Ni alloys measured by EPMA (at. %). "?" indicates that a phase was observed but was too finely dispersed to be analyzed. Alloy HQ5 was not studied at 1200 °C.

alloy #		900 °C			1000 °C			1100 °C			1200 °C		
		Cr	Hf	Ni	Cr	Hf	Ni	Cr	Hf	Ni	Cr	Hf	Ni
HQ5	Ni_5Hf	0.2	16.4	83.4	0.2	16.3	83.5	0.2	16.4	83.4			
	γ	5.3	0.4	94.4	5.1	0.6	94.3	5.0	1.0	94.0			
HQ6	Ni_7Hf_2	1.5	21.1	77.3	1.4	21.2	77.4	2.0	20.9	77.1	2.4	20.6	76.9
	γ	30.4	0.3	69.3	30.2	0.4	69.4	30.0	0.5	69.5	29.6	0.7	69.7

Table 4.5. Summary of binary compound formation enthalpies and entropies.

End-member	Phase	$\Delta_f H^{298.15K}$ (kJ/mole-atom)	End-member	Phase	$\Delta_f H^{298.15K}$ (kJ/mole-atom)
Al_3Hf	γ'	-35.389	$(Al)_1(Hf)_1(Ni)_2$	$L2_1$	-62.343
$AlHf_3$	γ'	-22.570	$(Al)_1(Hf)_1(Ni)_1$	λ	-62.738
Al_2Hf_2	γ'	-19.318	$(Hf)_2(Al)_7$	η	-22.558
AlHf	β	-19.325	$(Hf)_2(Cr)_7$	η	9.433
Cr_3Hf	γ'	53.783	$(Hf)_2(Ni)_7$	η	-44.646
$CrHf_3$	γ'	35.275	$(Ni)_2(Al)_7$	η	10.542
Cr_2Hf_2	γ'	14.072	$(Ni)_2(Cr)_7$	η	
CrHf	β	20.777	$(Ni)_2(Ni)_7$	η	18.867
$HfNi_3$	γ'	-49.680	$(Hf)_1(Al)_3$	τ	-31.915
Hf_3Ni	γ'	3.589	$(Hf)_1(Cr)_3$	τ	38.438
Hf_2Ni_2	γ'	-41.766	$(Hf)_1(Ni)_3$	τ	-52.208
HfNi	β	-41.769			

Table 4.6. Comparison of SQS calculations and calculated values in the Ni-Al-Hf system

Configuration	Phase	$\Delta_f^{Sym} H^{298.15K}$ (kJ/mole-atom)	$\Delta_f^{ISIF3} H^{298.15K}$ (kJ/mole-atom)	$\Delta_f H^{298.15K}$ (kJ/mole-atom)
$(Al_{0.5}Hf_{0.25}Ni_{0.25})_1$	α	-28.01	-33.30	-44.91
$(Al_{0.25}Hf_{0.5}Ni_{0.25})_1$	α	-16.82	-24.98	-31.92
$(Al_{0.25}Hf_{0.25}Ni_{0.5})_1$	α	-22.12	-36.39	-43.01
$(Al)_1(Hf_{0.5}Ni_{0.5})_1$	β	-28.01	-37.19	-59.26
$(Hf)_1(Al_{.5}Ni_{0.5})_1$	β	-16.82	-30.95	-48.60
$(Ni)_1(Al_{0.5}Hf_{0.5})_1$	β	-22.12	-51.47	-44.40
$(Al_{0.5}Hf_{0.25}Ni_{0.25})_1$	γ	-12.910	-35.06	-29.53
$(Al_{0.25}Hf_{0.5}Ni_{0.25})_1$	γ	-4.14	-22.50	-19.04
$(Al_{0.25}Hf_{0.25}Ni_{0.5})_1$	γ	-12.149	-40.59	-35.77
$(Hf_{0.5}Ni_{0.5})_3(Al)_1$	γ'	-9.81	-35.20	-31.62
$(Al_{0.5}Ni_{0.5})_3(Hf)_1$	γ'	-32.40	-37.99	-43.08
$(Al_{0.5}Hf_{0.5})_3(Ni)_1$	γ'	-15.63	-26.20	-31.76

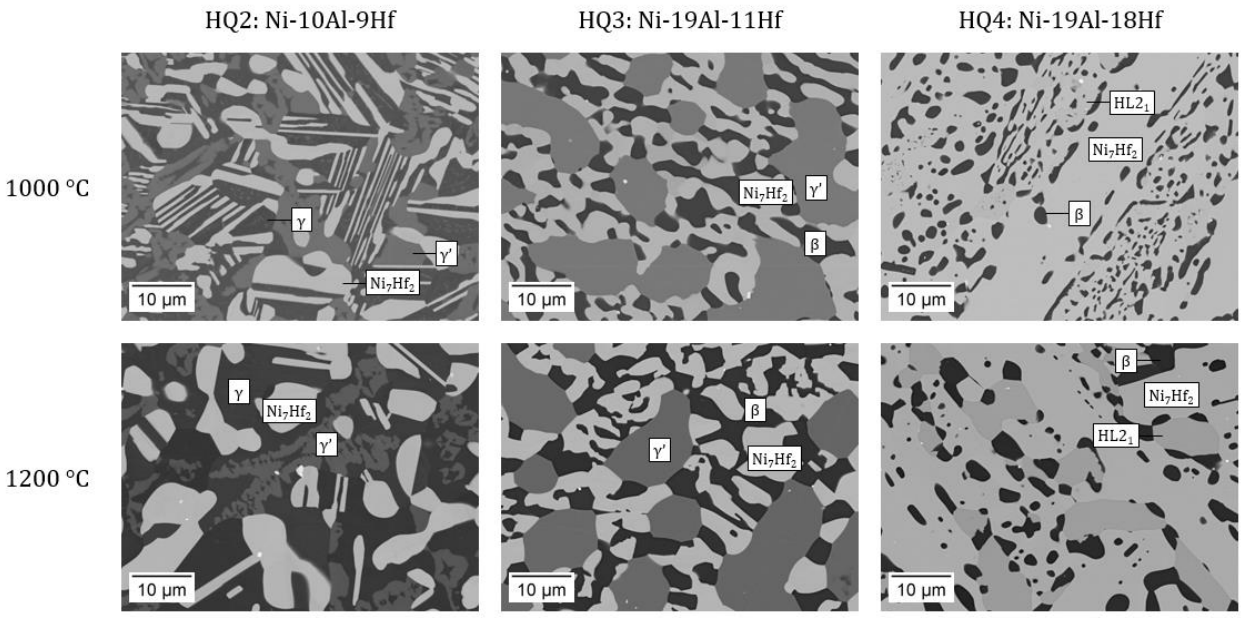

Figure 4.1. Microstructure of the Al-Hf-Ni alloys equilibrated at 1000 and 1200 °C.

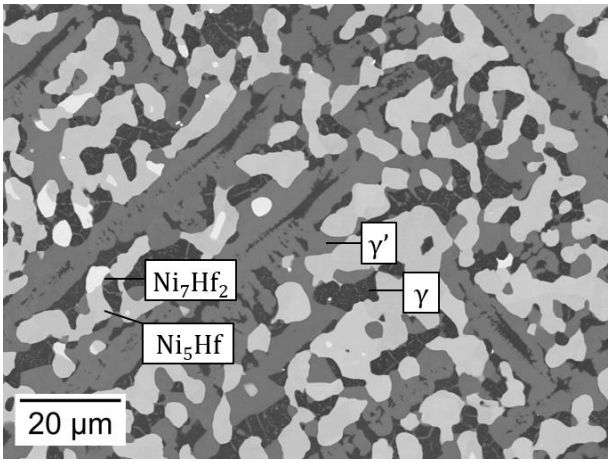

Figure 4.2. Microstructure of the HQ2 alloy (Ni-10Al-9Hf) after annealing at 900 °C. The Ni_7Hf_2 phase, stabilized during prior heat treatment at 1150 °C, has not fully transformed to Ni_5Hf.

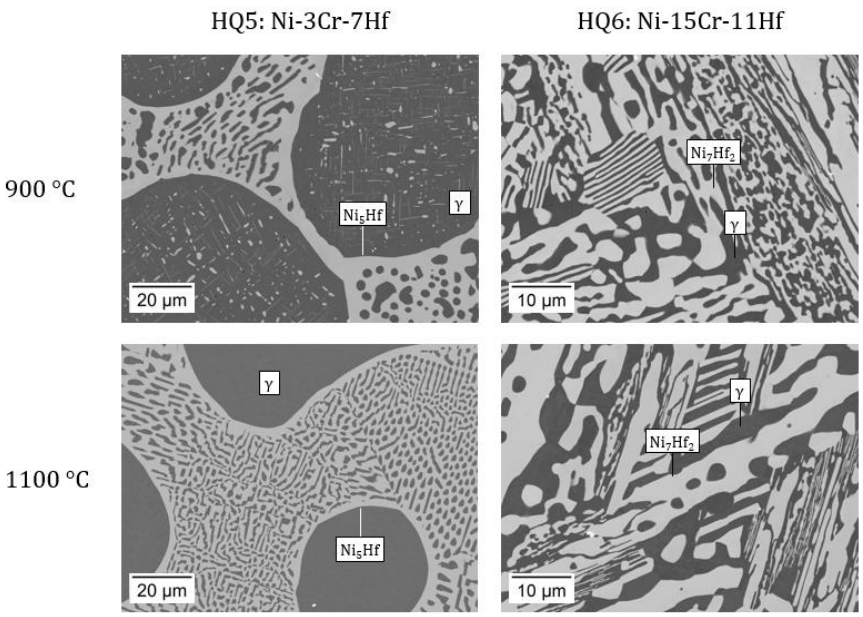

Figure 4.3. Microstructure of the Cr-Hf-Ni alloys equilibrated at 900 and 1100 °C.

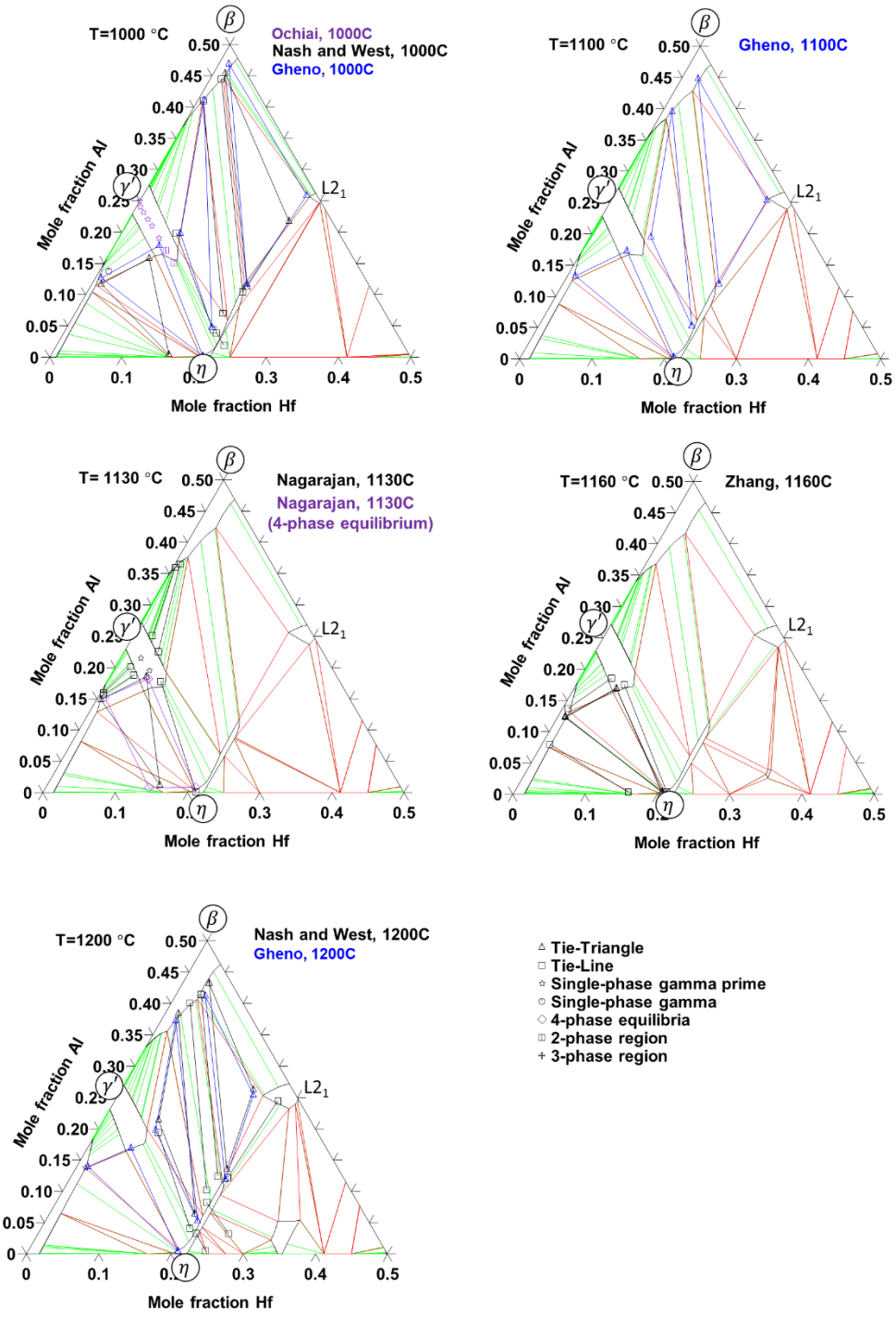

Figure 4.4. Isothermal sections in the Ni-rich portion of the Ni-Al-Hf system compared to experimental data in the literature.

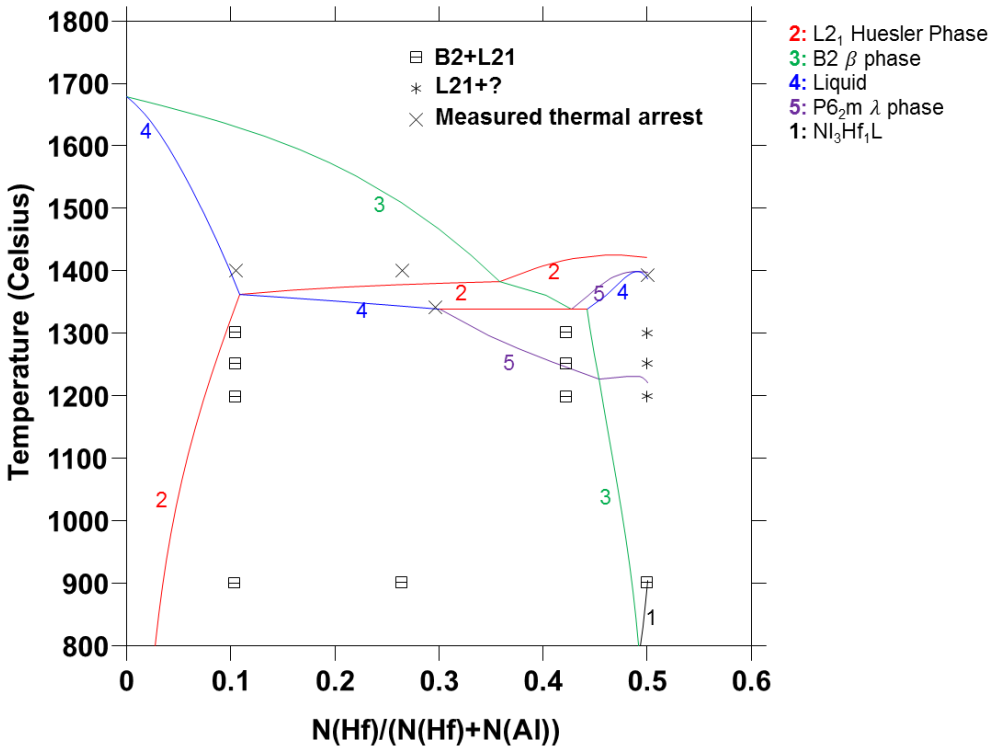

Figure 4.5. A vertical section between the Huessler phase and the NiAl β phase from 800 to 1400 °C

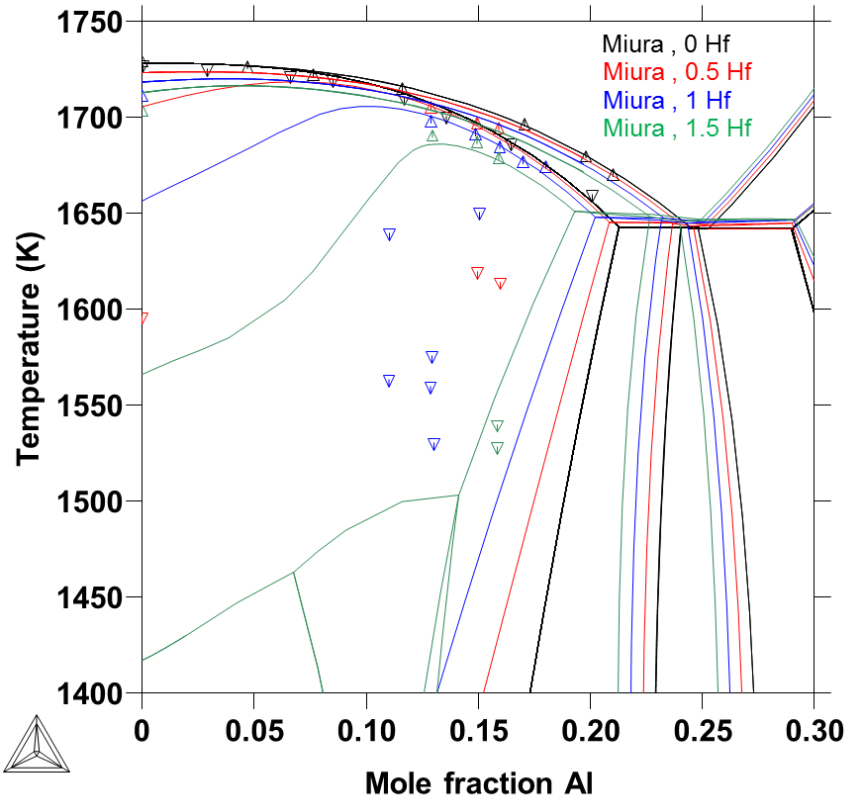

Figure 4.6. Calculated vertical sections between 0 and 30 at.% Al and between 1400 and 1750 K for 0, 0.5, 1 and 1.5 at.% Hf

Table 4.7. Solidus temperatures

Composition	Nash and West T(K)	This work T(K)
Ni-8Al-9Hf	1510	1599
Ni-15Al-25Hf	1506	1294
Ni-13Al-13Hf	1535	1635
Ni-23Al-15Hf	1500	1201
Ni-20Al-5Hf	1535	1645
Ni-16Al-20Hf	1510	1609
Ni-25Al-5Hf	1506	1268
Ni-18.4Al-20.3Hf	1506	1512

Table 4.8. Comparison of SQS calculations and calculated values in the Ni-Cr-Hf system

Configuration	Phase	$\Delta_f^{Sym} H^{298.15K}$ (kJ/mole-atom)	$\Delta_f^{ISIF3} H^{298.15K}$ (kJ/mole-atom)	$\Delta_f H^{298.15K}$ (kJ/mole-atom)
$(Cr_{0.5}Hf_{0.25}Ni_{0.25})_1$	α	30.34	12.71	0.81
$(Cr_{0.25}Hf_{0.5}Ni_{0.25})_1$	α	31.08	-0.15	0.52
$(Cr_{0.25}Hf_{0.25}Ni_{0.5})_1$	α	19.87	-7.05	-0.48
$(Cr_{0.5}Hf_{0.25}Ni_{0.25})_1$	γ		8.17	21.67
$(Cr_{0.25}Hf_{0.5}Ni_{0.25})_1$	γ	33.66	2.25	21.30
$(Cr_{0.25}Hf_{0.25}Ni_{0.5})_1$	γ	16.10	-5.70	0.44

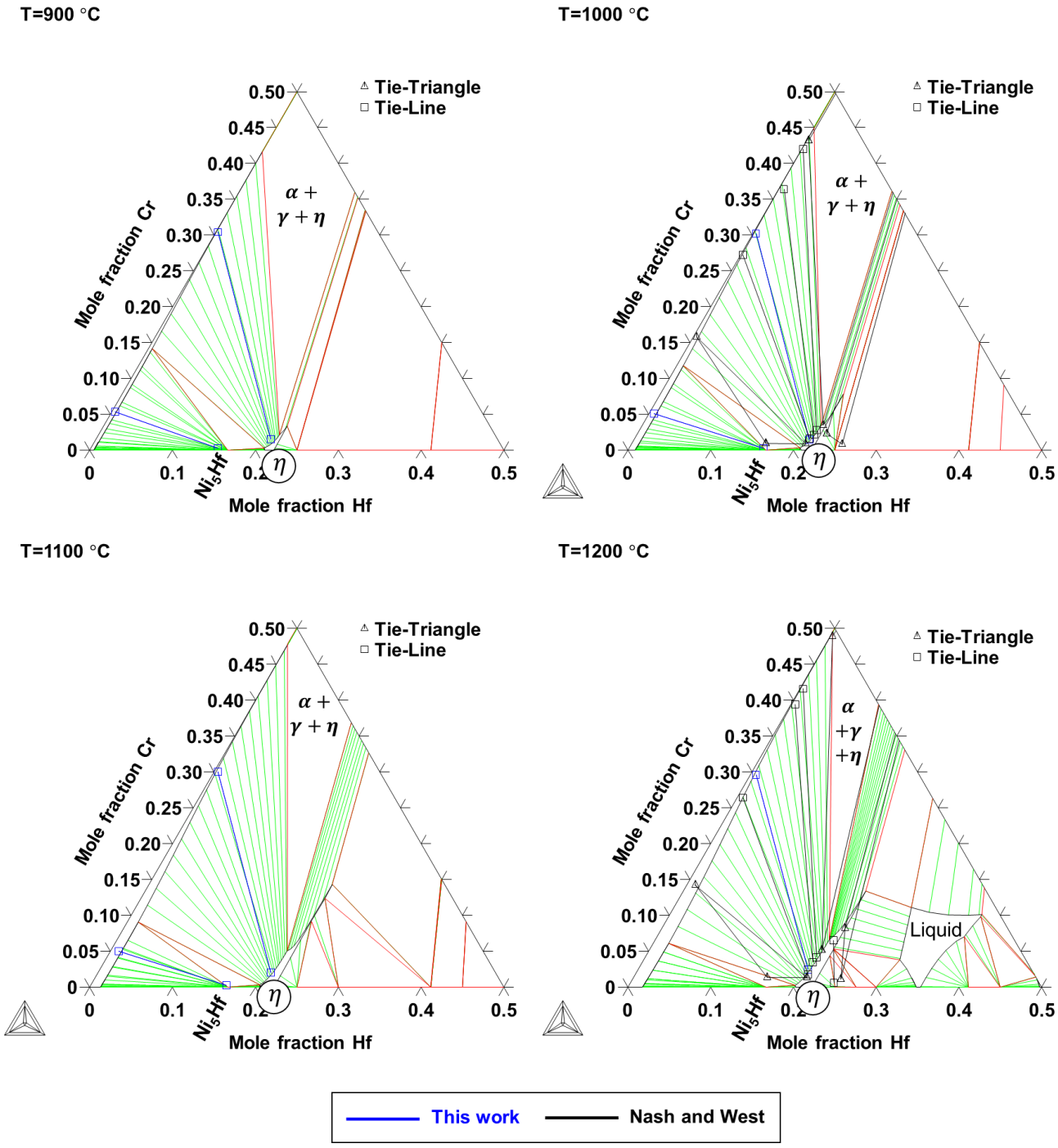

Figure 4.7. Isothermal sections in the Ni-rich portion of the Ni-Cr-Hf system compared to experimental data in the literature.

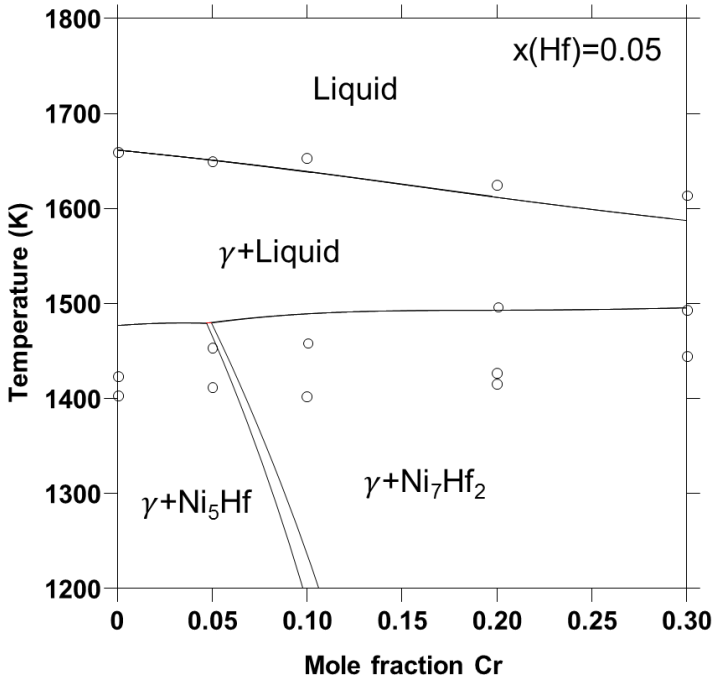

Figure 4.8. A plot of thermal analysis data by Feng et al. and the calculated liquidus

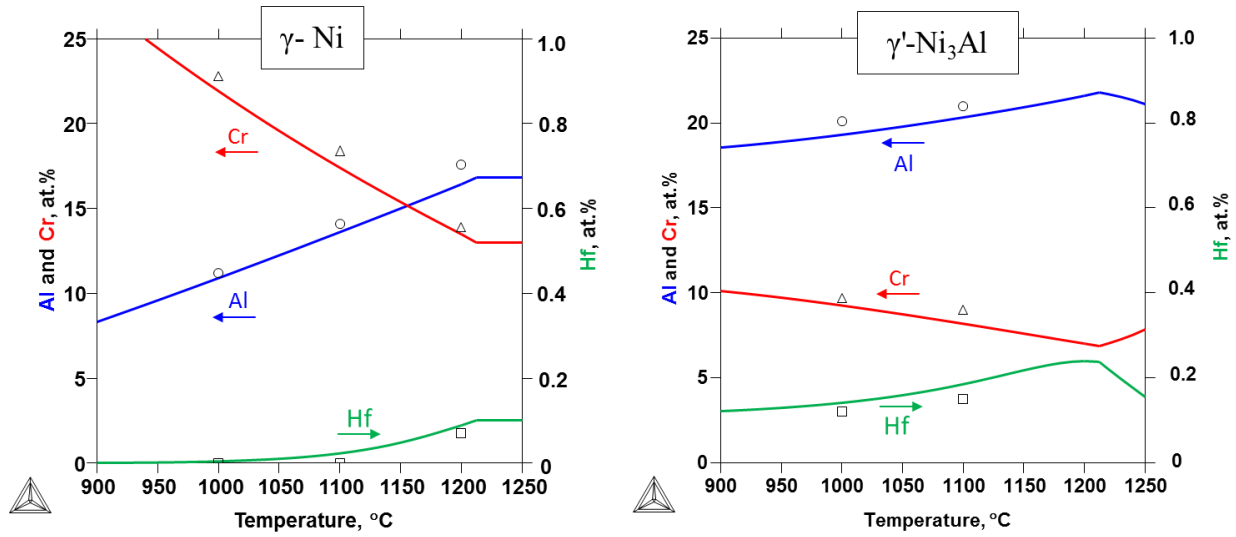

Figure 4.9. Measured the concentrations of γ and γ' from 900 to 1200 °C for an alloy with composition Ni-16.8Al-13Cr-0.1Hf

5 Calculating the Hf-tolerance: a thermodynamic model for predicting the limit of Hf concentration in NiCrAl alloys before over-doping occurs

5.1 Introduction

Nickel-based superalloys must sustain their excellent mechanical properties in oxidizing environments for long periods at high temperatures. To this end, they must develop external scales of slow-growing oxides like α-Al_2O_3 or Cr_2O_3, which are obtained through selective oxidation of Al or Cr in the alloy, respectively[2]. The growth rate of these thermally grown oxides (TGOs) can be reduced further by the addition of reactive elements like Y, Hf and Zr for Al_2O_3 forming alloys, or Ce and La for Cr_2O_3 forming alloys[16], [86]. These additions can also improve the adhesion of the TGO appreciably.

While small concentrations of these reactive elements have proven beneficial, too great a concentration can result in detrimental effects such as increased growth rates and decreased adhesion during cyclic oxidation[18]. This phenomenon is known as over-doping. Over-doping is typically correlated with the appearance of large oxide precipitates at the interface between the TGO and the alloy. Assuming that this interface is at local equilibrium at steady-state, an equilibrium condition for the precipitation of this oxide can be derived from the alloy composition and appropriate thermodynamic data, which defines a threshold concentration of the reactive element.

This concept was tested by the authors in a recent experimental study of the Ni-rich Al-Cr-Hf-Ni alloy system[42]. Alloys in the γ, γ-γ’ and γ’ regions were oxidized at 1000-1200 °C, after equilibrium heat treatments at the same temperatures. The samples were examined for Hf

oxidation beneath the external Al_2O_3; these observations were compared with the predictions made by a thermodynamic model of the equilibrium between HfO_2, Al_2O_3 and the base alloy. This equilibrium determines the amount of Hf which can be added to the alloy system; the corresponding Hf concentration was therefore termed the "Hf tolerance". Some deviation from this model occurred but the results were generally favorable in predicting the onset of over-doping.

This paper seeks to present this thermodynamic model and practical calculation in greater detail. First the model and its motivation are discussed conceptually. Following this, the Calculation of Phase Diagrams (CALPHAD) method[19] and its application to modeling the Ni-Al-Cr-Hf-O system are discussed. Equilibrium calculations in the Ni-rich Al-Cr-Hf-Ni system are performed followed by calculations of the Hf tolerance in the Ni-Al-Cr-Hf-O system. The Hf tolerance is sensitive to the underlying thermodynamics and the shapes of the equilibrium boundaries are related directly to the activities of Al and Hf in the base alloy and the associated O activity at the interface. Calculations are made to compare the calculated Hf tolerance to experimental observations of NiAl-Hf and NiCrAl-Hf alloys oxidation. These results confirm that the most important factor governing to the Hf tolerance is the phase fraction of the γ' phase, which modifies the Hf activity greatly compared to the Al activity. Finally limitations of this model are discussed and suggestions for future improvements and directions are made.

5.2 The Hf-Tolerance Model

For the sake of simplicity, we consider the case of alloys which form an external Al_2O_3 scale. Once a steady-state is reached, the oxygen partial pressure (P_{O_2}) at the alloy/scale interface is determined by the $\underline{Al}$-Al_2O_3 equilibrium ($\underline{Al}$ denotes Al in solution in the alloy). Precipitation of

HfO_2 beneath the Al_2O_3 scale will be determined by the activity of Hf at this interface. This can be understood from the schematic in Figure 5.1. For a Ni-rich Al-Hf-Ni alloy, if the concentration of Al is high and kept constant, the equilibrium between the alloy and Al_2O_3 will take a nearly constant P_{O_2} value with changing Hf activity. This is represented by the pink, verticle line in Figure 5.1. However, the equilibrium P_{O_2} between the alloy and HfO_2 will decrease with increasing Hf activities. This is represented by the blue line in Figure 5.1. At a given Hf activity the P_{O_2} required to form HfO_2 and the P_{O_2} required to form Al_2O_3 will become equal, represented by the intersection of the blue and pink lines, and the alloy will be in equilibrium with each of these phases. Hence, there is a maximum Hf activity at the interface for which HfO_2 precipitation at the interface is expected if this activity in the alloy is exceeded. This activity can easily be converted back to a concentration once determined giving us the Hf tolerance.

Finally it should be pointed out that a simple way of understanding this model is to consider the displacement reaction between HfO_2 and Al_2O_3 at the alloy/scale interface:

$$3Hf + 2Al_2O_3 \rightarrow 4Al + 3HfO_2 \qquad \textbf{Eq. 5.1}$$

Infact, this concept was already eluded to by Mu et al[130] while studying the oxidation of alloys in the Ni-Al-Pt-Hf system. In this study it was pointed out that this reaction could be used to understand the effect of Pt on the associated activities and conditions under which internal oxidation of HfO_2 occurred. For this reaction the criteria for HfO_2 precipitation is given by:

$$RT \ln\left(\frac{K}{K_{eq}}\right) < 0 \qquad \textbf{Eq. 5.2}$$

Where R is the gas constant, K is the reaction quotient given by the ratio of activities, $\frac{a_{Al}^4}{a_{Hf}^3}$, and K_{eq} is the equilibrium constant of this reaction. The current model allows the alloy composition and phase constitution to vary, and automatizes the search for the equilibrium condition based on appropriate thermodynamic data. This equation will become useful later when discussing the shapes the Hf-tolerance boundary takes on and the importance of the γ' phase.

5.2.1 Calculation Methodology

The software Thermo-Calc[131] was used for calculations in the Ni-Al-Cr-Hf-O system using the database constructed in this work. This database can be found in the supplementary section along with example macro files for calculating and plotting the Hf tolerance. For this calculation it was important to obtain values corresponding to the equilibria where HfO_2 and Al_2O_3 are in contact with the alloy system. To achieve this, a starting condition which has a low P_{O_2} is used and following this HfO_2 and Al_2O_3 are given zero-phase fractions. Without this starting condition the equilibria will sometimes be found with other oxides instead of the metal system.

5.3 Thermodynamic Models

To design alloys resistant to oxidation it is of the utmost importance to understand the activity of those elements which will be oxidized. These activities can be measured directly through careful experimental techniques. However, this method is costly and becomes more difficult with increasing alloy complexity. The CALPHAD method provides the means for calculating the alloy-oxide thermodynamics by building the Gibbs energy description of phases in higher order systems through extrapolation methods from the Gibbs energies of phases in lower order systems. These extrapolations are carried out using the compound energy formalism (CEF)

where the Gibbs energy of a solution phase is described by mixing between symmetrically distinct positions (sublattices) in a given phase.

The system of interest in this work is the Ni-Al-Cr-Hf-O system. In the Ni-rich Al-Cr-Hf-Nisystem only the ternary Ni-Al-Cr had been modeled previously[72]. To account for this, experiments were performed in the Ni-rich Al-Hf-Ni and the Ni-Cr-Hf systems and thermodynamic models were constructed to capture these experiments. This is detailed in previous work. The Al-Cr-Hf system was considered too far from the region of interest to model and was, therefore, neglected. In addition to these ternaries the Ni-Hf system was also remodeled to account for an experimentally observed solubility which was greater than the solubility fit to previously by Wang et al.[50] The solubility of Hf in Ni plays a large role in the resulting Hf activity in the alloy, making these experiments important to consider when modeling the Gibbs energy of the disordered fcc phase.

The Hf-tolerance model looks only at the equilibrium between Al_2O_3, HfO_2 and the alloy. These will be the only oxides present at low partial pressures of oxygen beneath the alloy surface. Furthermore, at temperatures below 1600 °C these oxides are not expected to have significant solubility[132]. Hence, these oxides were modeled to be stoichiometric and taken from the SGTE description available in Thermo-Calc[107]. There is a possibility that Cr will be incorporated into the oxide scale during establishment. For temperatures greater than 1000 °C a solid solution would be expected between Al_2O_3 and Cr_2O_3[133]. However, Cr diffuses much less quickly than Al. Hence the Al concentration in the Al_2O_3 is expected to be much greater than the Cr concentration and its effects have been neglected here for simplicity – though there is no

reason one could not capture this effect with a good estimate of the Cr concentration in the external oxide. No other oxides were used during modeling. However, fcc Ni-O[134] and fcc Cr-O[135] descriptions were taken to capture any effect oxygen might have on the activity of other elements in the fcc matrix.

5.4 Results and Discussion

5.4.1 Calculated Thermodynamics

A plot of the Ni-rich corner of the Al-Hf-Ni system is given in Figure 5.2. Although this work is interested in the Ni-rich Al-Cr-Hf-Ni system, this ternary plot is representative of systems of interest for small Cr concentrations. An important aspect of this system is the large solubility of Hf in the γ' phase compared to the relatively small solubilities of Hf in the γ and β phases. The solubility decreases with increasing Cr content since the γ' phase is not stable in the Ni-Cr-Hf system and because Cr also has a positive interaction with Hf in both the γ phase and γ' phase.

Figure 5.3a shows the calculated activity of Hf and Al from Ni-5Cr-0.1Hf to Ni-30Al-5Cr-0.1Hf. In the single phase regions the activity of Hf always increases while the Hf activity decreases in the $\gamma' + \gamma$ two phase-region and increases in the $\gamma' + \beta$ two-phase region. The decrease and increase in the two-phase regions is a consequence of the direction of tie-lines crossed in the system as composition is changed. To understand this, it is instructive to again consider Figure 5.2. In the $\gamma' + \gamma$ two-phase region, tie-lines corresponding to low Hf concentrations in the γ region correspond to high Hf concentrations in the γ' region. However, increasing only Al concentration in the two-phase region will move the system to tie-lines corresponding to lower Hf concentrations in both the γ and γ' region and, consequently, a lower Hf activity for the system. The same concept is at play when the Al concentration is increased in the $\gamma' + \beta$ two-

phase region: the system moves from tie-lines connecting lower Hf-concentrations in each phase, to higher Hf-concentrations in each phase. In the single-phase regions the Hf concentration is fixed and the resulting Hf activity has more to do with the thermodynamic interactions of Hf with the given phase. The Al activity increases in all phase regions due to the increasing Al concentrations. In two-phase regions the Al activity only increases slightly due to relatively constant Al concentration in the phase boundary between γ' and γ and between γ' and for low Hf concentrations.

Figure 5.3b shows the Hf and Al activity as a function of Cr concentration from Ni-23Al-0.1Hf to Ni-23Al-10Cr-0.1Hf. In this example the alloy passes first through the single phase γ' region and then through the two phase $\gamma + \beta$ region. There is a slight inflection of Hf activity in the single phase γ' region before 2 at.% Cr after which the Hf activity rises linearly with Cr concentration. This change in behavior is caused by competition between a negative ternary mixing interaction in the Ni-Cr-Hf system and positive mixing interaction in the Cr-Hf system. When the system reaches higher Cr concentrations the later term dominates in both the γ and γ' phases. Cr also increases the Al activity due to positive mixing between Al and Cr. The activity of Hf increases with increasing Cr concentrations in the two phase $\gamma + \beta$ region because the associated activity is higher in the β phase region. The Al activity increases, albeit with a much slighter slope, for the same reason.

One final factor to consider is how the Hf activity changes with temperature. This effect can be understood by considering the alloy Ni-13Cr-16.8Al-0.1Hf studied in Ref. 5 as an example. The calculated Hf and Al activity and calculated fraction of γ' are given in Figure 5.3c for this alloy

from 950 to 1250 °C. In the $\gamma + \gamma'$ region, the Hf activity increases as the γ' phase fraction decreases and temperature increases. These changes can be seen, once again, as an average of behaviors between each phase region. The Hf activity increases in the single phase γ region due to an increase in solubility with increasing temperature.

5.4.2 Features of the Calculated Hf Tolerance

Figure 5.4 shows the calculated P_{O_2} diagram at 1150 °C for the Ni-20Al-5Cr-xHf system. The pink line is the boundary between the metal system and the metal+ Al_2O_3 system while the blue line is the boundary corresponding to the precipitation of HfO_2. As stated before, the intersection between these lines should correspond to the point where the alloy and the oxides are in equilibrium. For an increase in Hf activity at low values of P_{O_2}, the alloy undergoes a transition from the $\gamma + \gamma'$ region to the γ' region since an increase in Hf concentration in this system will result in the system moving into the γ' phase region. For low activities of Hf, increasing the P_{O_2} will move the system from the $\gamma + \gamma' + \alpha$-$Al_2O_3$ region to the $\gamma + \alpha$-Al_2O_3. This is a consequence of the Ni-Al-O where increasing O concentration will move the system into this two phase region. The intersection found in this diagram results in the aforementioned maximum Hf activity and corresponds to a Hf concentration of ~0.14 at.%.

It is often more convenient from a design aspect to work in concentration space. Figure 5.5a shows the calculated Hf concentration corresponding to this maximum Hf activity as a function of changing Al concentration in the Ni-xAl-5Cr-yHf system. This maximum Hf concentration is the Hf tolerance in the alloy. Two experimental alloy concentrations are included in this plot: Ni-

20Al-5Cr-0.1 Hf and Ni-15Al-5Cr-0.1 Hf. Both alloys are sufficiently high in Al concentration to be able to establish an external Al_2O_3 scale. The latter alloy is above the Hf tolerance line and thus expected to precipitate HfO_2 beneath the Al_2O_3 surface during oxidation while the former is below the Hf tolerance line and hence no HfO_2 at the oxide-alloy interface is expected. Cross sections of these alloys post oxidation are shown below Figure 5.5a. Both alloys underwent isothermal oxidation for 100 hours at 1150 °C and displayed the expected behavior with internal precipitation of HfO_2 in the Ni-15Al-5Cr-0.1Hf alloy and no observed internal precipitation in the Ni-20Al-5Cr-0.1Hf alloy. The Hf tolerance is calculated as a function of Cr concentration from Ni-23Al-0.1Hf to Ni-23Al-10Cr-0.1Hf at 1000 °C and as a function of temperature for the Ni-16.8Al-13Cr-0.1Hf system from 950 °C to 1250 °C in Figure 5.5b and c, respectively. Experimental observations and corresponding cross sections from Ref.[42] agree reasonably well with the model predictions in each case – although some HfO_2 was observed locally in portions of the Al_2O_3 scale for the alloy below Figure 5.5b.

In Figure 5.5a the Hf tolerance is largest in the γ' region and smallest in the γ region. The shape of the tolerance varies with Al composition in all regions – though it is slightly straighter in the two phase regions. The Hf tolerance is once again largest in the γ' region in Figure 5.5b but in this case the tolerance increases until ~2 at.% Cr and then begins to decrease again while in the single phase region. The Hf tolerance in Figure 5.5c most closely resembles the observed behavior of the calculated tolerance in Figure 5.5a considering since the γ' phase fraction decreases with increasing temperature. However, unlike in that system, there is an increase in the Hf tolerance in single phase γ region.

The reason for this variation in shape is a result of the competition between Hf and Al for any given condition. Although not a perfect analogue, it becomes useful to consider the ratio $\frac{a_{Al}^4}{a_{Hf}^3}$ obtained from the reaction in **Error! Reference source not found.** since this ratio represents the boundary between precipitation and no precipitation much as the calculated Hf tolerance does. A plot of $\frac{a_{Al}^4}{a_{Hf}^3}$ for each plotted system in Figure 5.5 with 0.1 at.% Hf included is given in Figure 5.6. The variation in shape of the calculated Hf tolerance follows the approximate shape of these curves in each case. Looking back at Figure 5.3 it becomes apparent that the Hf tolerance in Figure 5.5a is largest in the γ' region due to the dip in Hf activity relative to Al activity in this phase region. Likewise, the Hf tolerance increases and then subsequently decreases in the Ni-23Al-xCr-0.1Hf alloy system due to the inflection in the Hf activity mentioned previously. Finally, in the Ni-16.8Al-13Cr-0.1Hf system the Hf and Al solubility increase in the γ region with increasing temperature. The associated drop in Hf activity with temperature relative to the Al activity results in the increased Hf tolerance. Another way of looking at this, from an oxidation standpoint, is that when the Al activity increases the equilibrium p_{O_2} at the alloy/scale interface decreases. This will correspond to an increase in the Hf activity required to precipitate HfO_2 at the interface.

5.4.3 Calculated Hf Tolerance in Ni-rich Al-Hf-Ni and Ni-Al-Cr-Hf

In addition to the experiments reported in Ref. 5, there exists other experiments in the literature measuring oxidation in the Ni-rich Al-Cr-Hf-Ni system by Mu et al.[130]. It is desirable to compare all of the available data in a qualitative way. One way to assess the current model is to consider the difference between the calculated Hf tolerance and the Hf concentration in the This

difference is plotted against the Al concentration in the experimental alloy in Figure 5.7a for the two available sources in the literature for the Ni-Al-Hf[130] alloy system and the Ni-Al-Cr-Hf[42], [130] alloy system. The temperature range for these experiments fell between 1000 and 1200 °C. In Ref. 5, we considered three distinct behaviors relative to Hf oxidation: i) observations of internal HfO_2 precipitation, ii) observations where HfO_2 only precipitated locally and other portions of the scale were clear of HfO_2 and iii) observations where very little to no HfO_2 precipitated. These categories were adopted for the available cross sections by Mu et al.[130] for the present analysis. Below the black dotted line in Figure 5.7a $x_{Hf}^{tolerance} < x_{Hf}^{nominal}$ and HfO_2 precipitation is expected while above the line $x_{Hf}^{tolerance} > x_{Hf}^{nominal}$ and no HfO_2 precipitation is expected according to the model. Generally, alloys with higher $x_{Hf}^{tolerance}$ had higher Al concentrations and lower Cr concentrations while most alloys with a lower $x_{Hf}^{tolerance}$ had lower Al and higher Cr concentrations. All data points in the Ni-rich Al-Cr-Hf-Nialloy system which underwent internal HfO_2 precipitation fell within the region where $x_{Hf}^{tolerance} < x_{Hf}^{nominal}$, while all experiments which underwent very little to no HfO_2 precipitation fell within the region where $x_{Hf}^{tolerance} > x_{Hf}^{nominal}$. Only in cases where local oxidation was observed is the agreement less systematic. Generally these points are closer to the transition line. The points in this category with values of $x_{Hf}^{tolerance} > 0.15$ correspond to alloys with 23 at.% Al, 5 at% Cr and $x_{Hf}^{nominal}$=0.1 at.%. Only in the Ni-rich Al-Hf-Ni alloy system was there an alloy where HfO_2 precipitation was observed under the surface when $x_{Hf}^{tolerance} > x_{Hf}^{nominal}$. However, this alloy underwent cyclic oxidation as opposed to isothermal oxidation. Cyclic oxidation can lead to several complicating factors which could lead to greater precipitation of HfO_2.

As stated before, the Hf alloy activity and tolerance will depend strongly on the fraction of γ' in the alloy. $x_{Hf}^{tolerance} - x_{Hf}^{nominal}$ is plotted against γ' fraction in Figure 5.7b. This graph yields a similar picture to Figure 5.7a because the fraction of γ' depends strongly on the Al concentration for alloys in the $\gamma + \gamma'$ region. The difference comes from the fact that these alloys are at different temperatures and the temperature will control the equilibrium fraction of γ' for alloys in the $\gamma + \gamma'$ region.

5.4.4 Model Limitations

There are two main limitations with the current model. These were partially addressed in Ref.[42] but will be discussed here again from a modeling perspective. The first limitation is that kinetics have not been factored into the present model. Hence, the present model cannot capture Al depletion from the alloy surface during oxidation. This means that once the oxidation has reached a steady-state reaction, the Al concentration at the alloy/scale interface is lower than the nominal Al concentration. This was pointed out by Gheno et al. where it was found that shifts in the Cr and Al concentrations at the scale/alloy interface yielded lower Hf tolerances which subsequently was used to explain local HfO_2 precipitation in alloys where no HfO_2 was expected at the nominal alloy composition. The degree of this shift in Al concentration will depend not just on the initial Al concentration but also on the initial Cr concentration since Cr will have some effect on the diffusion of Al once the Al_2O_3 has been established.

The second limitation is that at the transient stage of oxidation, the underlying alloy is not yet at equilibrium with the scale. Since the alloy region below the scale will be depleted of Al when

Al_2O_3 is formed, this will lead to non-equilibrium alloy compositions which could affect the Hf activity at the scale/alloy interface. Indeed, a three minute oxidation study performed on a Ni-13Cr-17Al-0.1Hf alloy at 1100 °C found that Cr and Hf concentrations were supersaturated in the γ phase in what appeared to be prior γ' regions[42]. Thermodynamic calculations showed that this would have a large effect on the driving force for HfO_2 nucleation – although the investigation yielded no direct evidence of this at that time.

5.4.5 Extensions of this Model in the Ni-Rich Al-Cr-Hf-Ni Alloy System

The current model was applied only to alloys in the γ, $\gamma + \gamma'$ and γ' phase regions. This is due to a lack of equilibrium information in more Al rich portions of the Al-Cr-Hf-Ni system. Such information would permit the extension of this model to alloys with appreciable amounts of the β phase. This is important since the majority of alloys used as coatings in high-temperature systems are alloys in the $\beta + \gamma$ phase region[7]. Some information was obtained in the study by Zhao et al.[ref for Bi-Cheng] but no intensive study was made into the equilibrium with the β phase. In the current system Hf solubility in the β phase is small when β is low in Al. This is why the Hf tolerance decreases in the $\beta + \gamma'$ region. This can be seen in Figure 5.2. The Hf tolerance will increase with increasing Al concentration in the β phase due to a subsequent increase in Hf solubility.

5.5 Conclusions

The effects of alloy phase, composition and temperature on the activity of Hf and Al were discussed in regards to the most current Ni-rich Al-Cr-Hf-Ni thermodynamic description. It was shown that the Hf activity decreases appreciably compared to Al activity for compositions tending towards the single phase γ' region. This is due to a high solubility of Hf in the γ' phase.

However, increasing Cr concentration in any phase or phase region will usually increase the Hf activity due to the positive interactions between Cr and Hf in Ni.

A thermodynamic model was developed to predict the formation of HfO2 at the alloy/scale interface of Al2O3-forming alloys. This model calculates the Hf tolerance - the maximum Hf concentration which can be added to a Ni-Al-Cr alloys before HfO_2 can be expected during oxidation. This was discussed with respect to the underlying thermodynamics in the Ni-rich Al-Cr-Hf-Ni system. Due to the low Hf activity with respect to Al activity, the γ' phase region shows the highest Hf tolerance. The shape of the boundary between HfO_2 precipitation at the interface and no HfO_2 precipitation can be most closely related to a simple ratio of $\frac{a_{Al}^4}{a_{Hf}^3}$ at a fixed Hf concentration.

Calculated values for the Hf-tolerance were compared to alloy compositions in the literature in the Ni-rich Al-Cr-Hf-Ni system and the Ni-rich Al-Hf-Ni systems. The model agreed well with experimental observations for isothermal oxidation and cyclic oxidation with agreement being worse in the latter case. A collective study of these alloys found that γ' fraction played a dominant role in determining whether an alloy would precipitate HfO_2 at the interface which was expected from calculated Hf activity trends. These successes come despite a lack of kinetic considerations within the model.

Finally, there is no reason why this model cannot be extended to alloys containing higher fractions of the β phase, but a more extensive thermodynamic study of the Ni-rich Al-Hf-Ni

system is recommended beforehand. The current model shows a poor Hf tolerance in the Al poor portion of the pure β phase region. The Hf tolerance in the β phase will improve for higher Al concentrations.

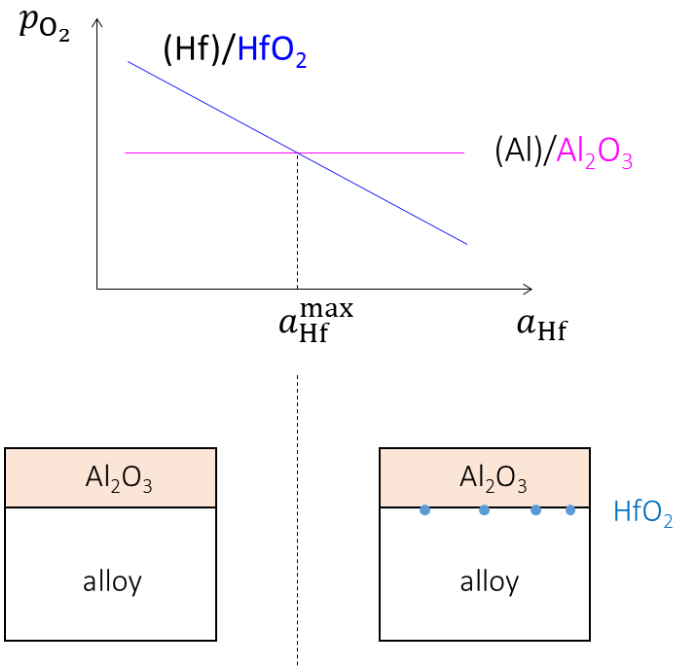

Figure 5.1. Schematic of the interfacial reaction of Hf at the alloy/Al_2O_3 interface. Above a given Hf activity, HfO_2 will form at the interface.

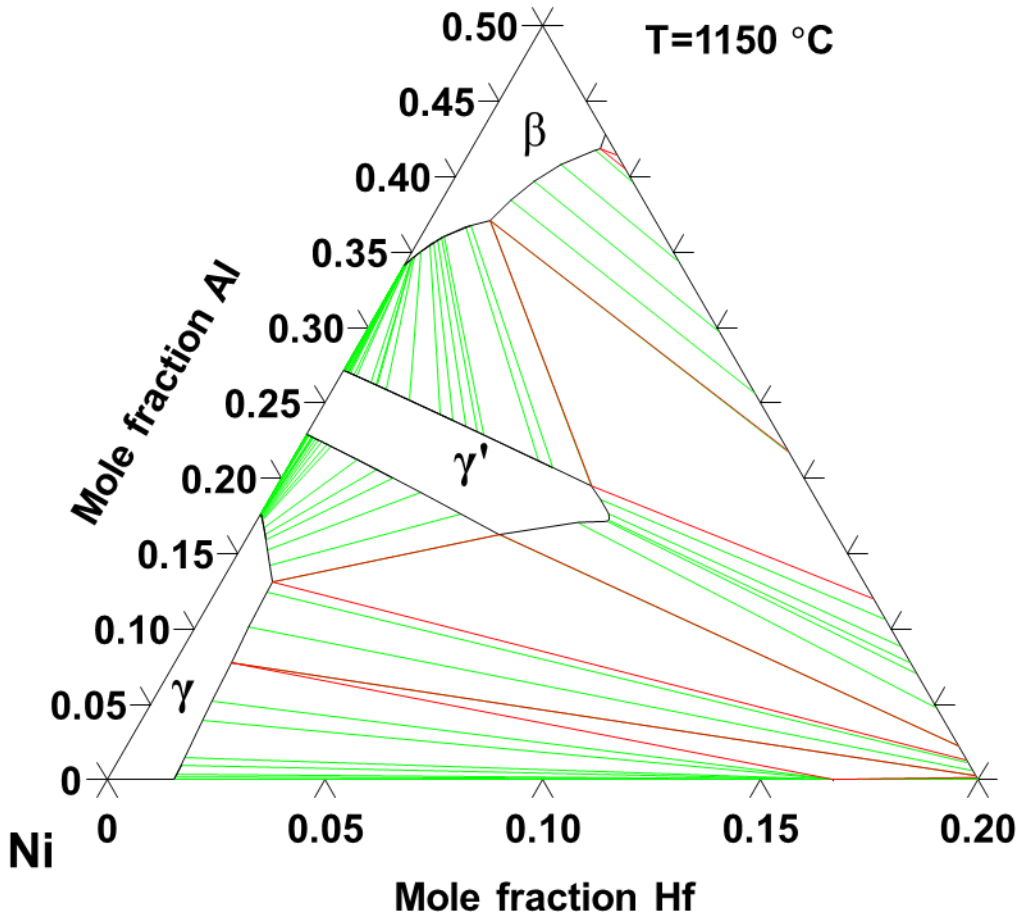

Figure 5.2. Isothermal section in the quaternary Ni-rich Al-Hf-Ni system at 1150 °C calculated using a thermodynamic model from previous work[ref of assessment]. Only the single phase regions are marked. Tie-lines are shown in green.

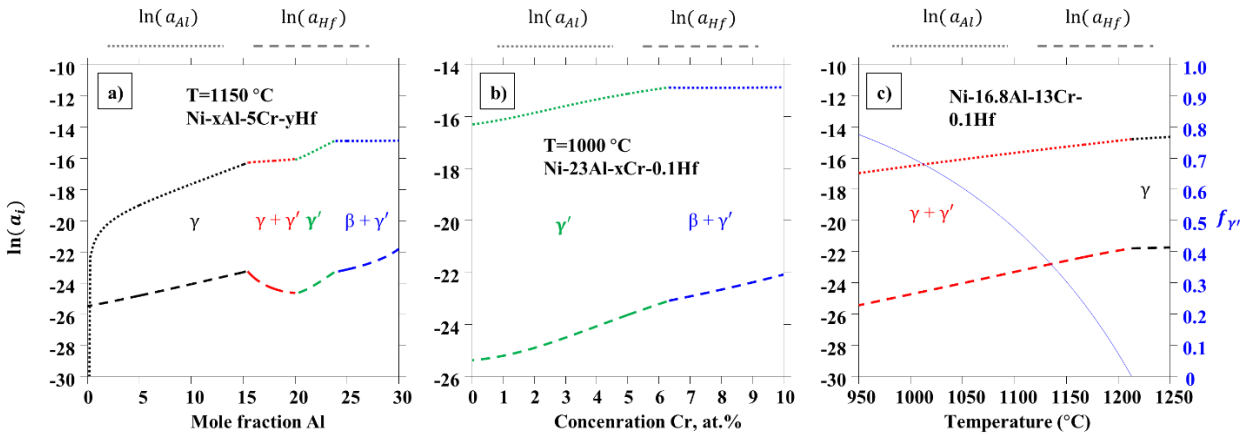

Figure 5.3. Calculated Al and Hf activity for the Ni-xAl-5Cr-0.1Hf system at 1150 °C for x=0 to 30 (a), the Ni-23Al-xCr-0.1Hf system at 1000 °C for x=0 to 10 (b), and the Ni-16.8Al-13Cr-0.1Hf system from 950 °C to 1250 °C.

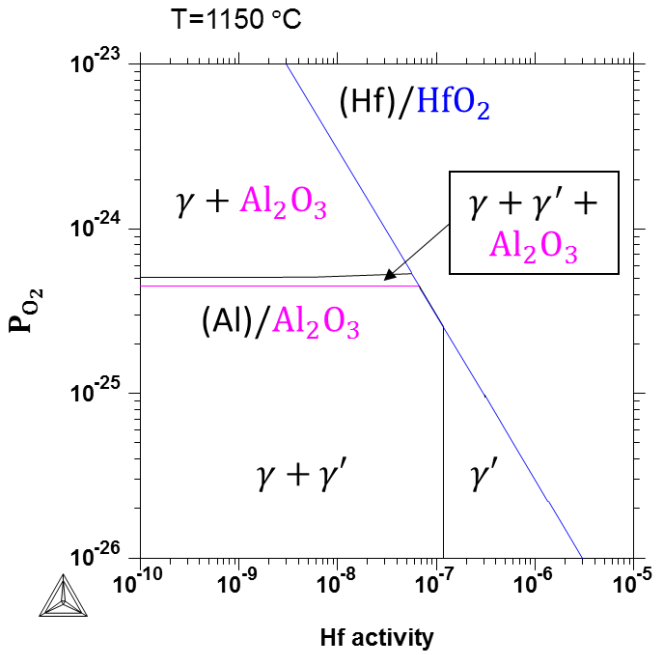

Figure 5.4. Calculated O_2 partial pressure diagram for the Ni-20Al-5Cr-xHf system at 1150 °C.

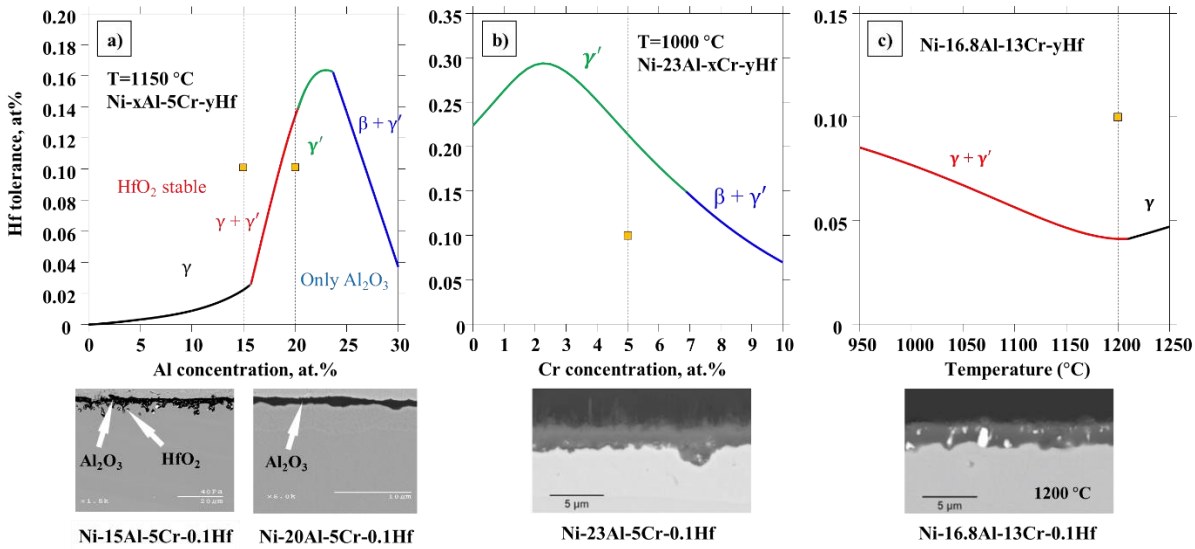

Figure 5.5. Calculated Hf tolerance for the Ni-xAl-5Cr-0.1Hf system at 1150 °C for x=0 to 30 (a), the Ni-23Al-xCr-0.1Hf system at 1000 °C for x=0 to 10 (b), and the Ni-16.8Al-13Cr-0.1Hf system from 950 °C to 1250 °C. Cross sections of alloys oxidized for 100 hours at 1150 °C are included beneath (a), for 20 hours at 1000 °C beneath (b), and for 20 hours at 1200 °C beneath (c).

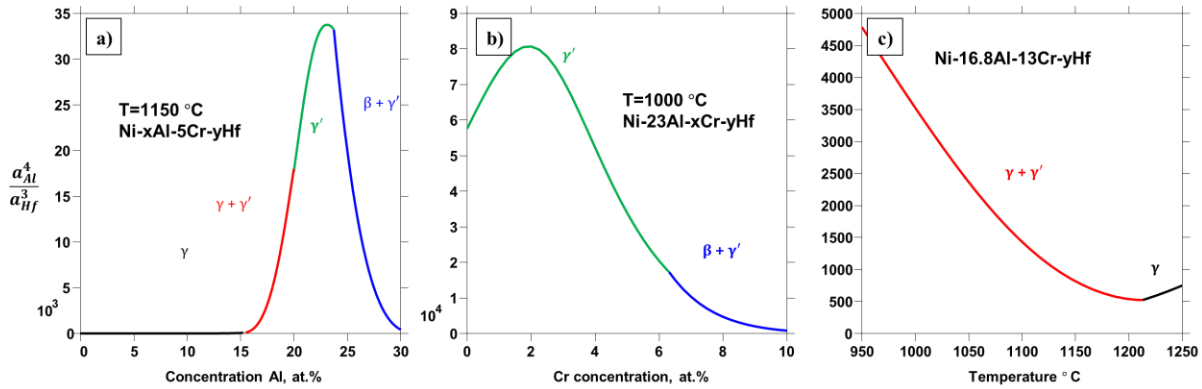

Figure 5.6. Plot of $\frac{a_{Al}^4}{a_{Hf}^3}$ for each system in Figure 5.5 with 0.1 at.% Hf.

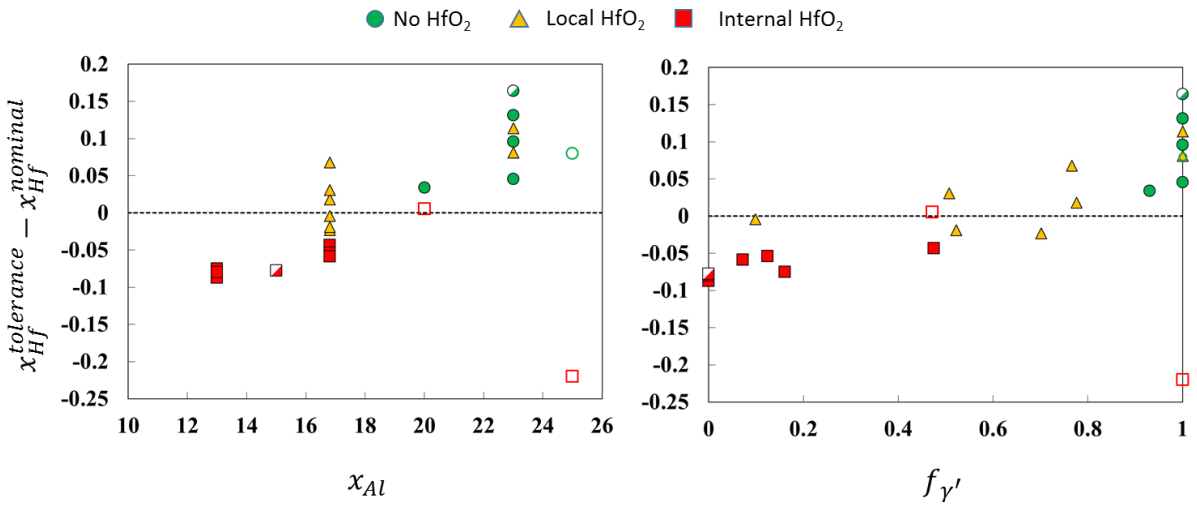

Figure 5.7. Collected values of $x_{Hf}^{tolerance} - x_{Hf}^{nominal}$ plotted against the concentration of Al (a) and the calculated fraction of γ' (b) in the oxidized alloy for cases where little to no oxidation of HfO_2 was observed (●), when HfO_2 oxidation occurred locally (▲) and when this oxidation occurred everywhere internally (■). Closed symbols were oxidized isothermally in the quaternary Ni-rich Al-Cr-Hf-Ni system by Gheno et al[42], half open and open symbols were oxidized cyclically by Mu et al.[130] in the quaternary Ni-rich Al-Cr-Hf-Ni system and in the ternary Ni-rich Al-Hf-Ni system, respectively.

6 Calculating a Design Space for Hf Doping and Hf co-doping in High Temperature Ni-Alloys

6.1 Introduction

The performance of reactive elements in MCrAlYs can often be improved by the addition of other elements in the alloy such as Si, Pt, or Pd. However, the exact mechanism of the improvement in performance is unclear. Si has been shown to be beneficial to oxide growth rates in Cr_2O_3 forming alloys by forming a continueous layer of SiO2 beneath the scale[136]. For Al_2O_3 forming alloys, small concentrations (~2at.%) have been proven to have little effect on oxidation properties[137] but at larger concentrations (~6at.%) Si has been proven useful in reducing the amount of Al required to form Al2O3[138]. Pt to have proven to have a plethora of beneficial effects for the oxidation[130]. This is not for alloys containing reactive elements but also for Ni-Al alloys where Pt has been shown to reduce the amount of Al required to form Al2O3 by promoting uphill diffusion of Al during oxidation[139]. This shows that Pt has the ability to modify and reduce the activity of Al in the alloy. Pd has been shown to have similar benefits to Pt when added to Al-rich alloys[140].

Previous work has shown that thermodynamic considerations of the underlying alloy and oxide can be used to model the interface reaction between Al_2O_3 and the alloy to form HfO_2[42]. The onset of HfO_2 is typically referred to as over-doping and results in increased oxide growth rates and decreased oxide adhesion during cylclic oxidation[18]. The thermodynamic boundary for this behavior in composition space has been termed the Hf-tolerance and this value has been used to predict the onset of HfO2 precipitation in several NiAlCrHf alloys[42].

The most important contribution to the Hf tolerance is the activity of Hf relative to the activity of Al. When the Hf activity is below a certain threshold level at the interface between Al_2O_3 and the alloy, HfO_2 is unlikely to precipitate. The ordered intermetallic γ' phase has a much larger solubility for Hf relative to the disordered fcc phase (γ). Given the Al concentrations needed to form γ', this means that the Hf activity relative to the Al activity will drop appreciably when the γ' phase is present in the alloy. Hence, the two most important factors to consider when designing a Hf containing alloy is the phase fraction of the γ' phase and how the Hf activity is affected relative to the Al activity in all phases.

The concept of Hf-tolerance has already been applied to alloys in the Ni-rich Al-Cr-Hf-Ni system. The present work seeks to search for other beneficial elements to add to the system to increase the Hf-tolerance through an extensive computational and thermodynamic search. Given the importance of the γ' phase, an initial selection process is established by searching for elements a large solubility in the γ' phase. These elements will have the most prominent interactions with Hf for alloys with appreciable equilibrium fractions of γ'. Once these elements are selected, a computational search is performed to calculate the mixing enthalpies of these phases in the γ phase and the formation enthalpies of the $L1_2$-Hf_3X and L12-HfX_3 in the Hf-X system. This not only provides valuable thermodynamic information for each Hf-X system but also highlights which element will have the strongest effect on the activity of Hf since the mixing enthalpy will play a significant role in the partial molar quantities, and hence on the activity. In all, this will amount to a study of the Hf interactions with the elements Al, Co, Cr, Cu, Fe, Ga, Ge, Hf, Mn, Nb, Ni, Pd, Pt, Sc, Si, Ta, Ti, V, and Zn. Of these elements Pt, Pd, Rh and Si were found to have the strongest interaction with Hf.

As an example, the interactions of Hf with Pt are considered in more detail given the wealth of oxidation experiments already available for the Ni-rich Al-Cr-Hf-Ni-Pt alloy system. To properly describe this system it is important not just to capture the binary thermodynamic interactions for the γ and γ' phases but also the ternary interactions in these phases. Binary descriptions are modified in the literature based on present DFT calculations and new ternary calculations are carried out for the Ni-Pt-Hf, Cr-Pt-Hf and Al-Hf-Pt systems to adequately describe the γ and γ' phases in these systems. O is further added to the system to calculate the Hf-tolerance for a variety of conditions observed in the literature. The described thermodynamics, in combination with the calculated interactions from DFT produces excellent results when compared to these experiments.

6.2 Search Criteria

For an alloying element to play a beneficial role in the Hf-tolerance it must have the chance to mix appreciably with Hf in the γ' phase. Therefore, a search criteria for beneficial element additions with Hf to improve oxidation resistance must focus on those elements having an appreciable solubility of this element in the Ni_3Al, γ' phase. The solubility of alloying additions into the , γ'-Ni_3Al phase has been regularly studied throughout the years[1], [141]. This is a prominent design criteria because the γ' phase is a strengthening precipitate and the partition of elements into γ' and the disordered γ phase plays an important role in a superalloy's mechanical properties and processing[1].

A chart of elements investigated for their solubility in the γ' phase at 1000 ° C is given in Figure 6.1. This work comes from an initial investigation by Ochial et al. with some information

available from other investigations[141]. Elements with a solubility between 0 and 5 at.% are considered to have poor solubility, elements with a measured solubility between 5 and 10 at.% are considered to have moderate solubility and with a solubility exceeding 10 at.% are considered to have a high solubility. Y, Re and Zr had the lowest solubility of these transition elements at 1000 °C. From this chart only those 17 elements with either moderate or high solubility in the γ' phase were chosen with the addition of Ag, Au, Ir and Rh where no solubility data could be found but which are of interest due to their proximity to, or position in, the Pt group. Os is excluded from investigation due to the toxicity of its oxide.

In order for one of these elements to be incorporated into a thermodynamic model meant to design alloys, a reasonable description of the Ni-rich corner of a system is desirable for a given system. In this case, it would be desirable to have all the Ni-rich ternaries of the Ni-Al-Cr-X-Hf system well described before a thermodynamic model is implemented for designing alloys. Hence, the simplest scenario is for three ternaries and one binary to be added to the Ni-Al-Cr-Hf system for any given element added.

In this case, it is most important that the γ and γ' phases are well described even if complete binary and ternary thermodynamic models cannot be achieved. To ease the number of calculations only mixing and formation enthalpies of the γ' phase compounds Hf_3X and HfX_3 in the Hf-X systems are tested between Hf and the added element X. Only elements with large, negative enthalpies of formation are selected from this pool since only these elements are likely to decrease the Hf activity and improve the Hf-tolerance in a given alloy system.

6.3 First-Principles Methodology

The brunt of the work performed in this work focuses on the calculation of mixing enthalpies from density functional theory (DFT). The formation enthalpy of a structure $A_aB_bC_c$ at 0K, $\Delta^f H^{0K}_{A_aB_bC_c}$ can be calculated with respect to A, B and C at their standard element reference structure. In this work the assumption is made that $\Delta^f H^{0K}_{A_aB_bC_c} \approx \Delta^f H^{298K}_{A_aB_bC_c}$ so as to adopt calculated values from DFT into thermodynamic modeling where 298.15 is the cut-off temperature for functions[41].

Finite temperature properties are calculated using the quasiharmonic approach[27], [75] for some select structures to obtain a more complete description of the Ni-rich portion for a given system of interest. In this approach $F(V,T)$ is calculated from the summation of the ground state energy, the thermal electronic and vibrational contributions of the Helmholtz energy, E^{0K}, $F_{ele-T}(V,T)$ and $F_{vib}(V,T)$, using a 4-parameter Birch–Murnaghan equation of state (EOS) fitting to calculations at different volumes[27]. $F_{vib}(V,T)$ is calculated using the Debye-Gruneisen model with a scaling factor calculated from the elastic stiffness constants of a given structure and $F_{ele-T}(V,T)$ calculated using from the electronic density of states[27].

All calculations of E^{0K} were carried out using a two-step relaxation scheme: first the structures were only allowed to change volume, then structures were allowed to relax along all degrees of freedom. If the later calculation broke symmetry then the only the energy of the former calculation was used. DFT calculations are carried out using the Vienna Ab-initio Simulation Package (vasp). Calculations in vasp are carried out using projector augmented wave (PAW)

potentials where electron-ion interactions are treated using the generalized gradient approximation (GGA) parameterized by Perdew Burke and Ernzerhof (PBE)[24]. The specific potentials used were those recommended by vasp[74] with a plane wave cut-off of 400 eV.

Relaxation calculations are carried out using a multi-step relaxation method where the structure i) volume is relaxed, ii) followed by the volume and shape and then finally the volume, shape, and iii) ionic positions. Symmetry of these structures is analyzed after steps (ii) and (iii) using spglib[120] which is implemented through Pymatgen[121]. An angle tolerance of 0.1 and a distance tolerance of 0.1 Å is used for this analysis. Energies of structures which loose symmetry are not considered in this work except for comparison in some cases.

For binary Hf-X calculations, multi-step relaxations are carried out starting with a low accuracy calculation and ending with a higher accuracy static calculation. Brilloin zone integration is carried out using the Methfessel-Paxton method[142]. Reciprocal k-meshes are set such that the k-points per reciprocal atom (kppra) are at-least 1000 initially for low accuracy calculations, with a convergence of 10^{-4} eV for electronic degrees of freedom. High accuracy calculations are carried out using a kppra of at-least 5000 and a convergence of 10^{-8} eV for electronic degrees of freedom. A final static calculation is carried out for calculations using the tetrahedron-bloch correction.

Mixing enthalpies are calculated out using special quasirandom structures (SQS)[143]. These structures mimic the random structure of alloys for a given repeat-cell size. Binary mixing enthalpies were calculated using 16 atom structures developed by Wolverton et al.[78] Ternary

mixing enthalpies were calculated for the γ phase using 32 atom structures developed Shin et al.[117] and for the γ' phase using 24 atom structures developed by Liu et al [118]. Note that computational restrictions restricted these calculations to only 1000 kppra.

Note that to save resources ternary calculations in the γ phase were carried out using a plane wave cut-off of 360 eV and these calculations were relaxed with only volume as a degree of freedom. In addition, to save resources for ternary calculations in the γ' phase, these calculations were not given a volume and shape relaxation step – only a volume relaxation step and a full relaxation step.

6.4 The CALPHAD Method

The main body of thermodynamic modeling carried out in this work comes from the work by previous work in the Ni-Al-Cr-Hf system. Descriptions of sub systems can be found in this work. The addition of O to systems in this work is done in the same way that it is added to the Ni-Al-Cr-Hf system in previous work. Additional work is carried out on the alloying element with the most beneficial mixing with Hf here referred to temporarily as X.

Thermodynamic modeling in the present work is carried out using the calculation of phase diagram (CALPHAD) method[106]. Within the CALPHAD method the Gibbs energy of solution phases can be constructed for higher order systems from lower order systems using the compound energy formalism (CEF)[144]. This is done primarily between extrapolation formalisms between compounds representing extremes in composition space (end-members).

6.4.1 Thermodynamic Models

6.4.1.1 The Disordered γ Phase

As in the previous work, the disordered fcc γ phase is treated as a disordered solution on a single symmetrically distinct site. In the CEF this symmetrically distinct site is called a sublattice. The sublattice model for this phase is given as $(Al,Cr,Hf,Ni,X)_1(Va)_1$ which has been adopted from previous work[ref]. The Gibbs energy of this phase is given with respect to end-members representing extremes in composition (e.g. fcc Cr and fcc Hf), configurational mixing entropy, and non-ideal mixing terms. The exact expression for this Gibbs energy is given in previous work for the Ni-Al-Cr-Hf system and will not be addressed here. It is, however, important to note that the binary, non-ideal mixing contribution to the Gibbs energy, G_m^{EX}, is given as:

$$G_m^{EX} = \sum_i \sum_{j>i} x_i x_j \sum_\nu {}^\nu L_{i,j}^\gamma \left(x_i - x_j\right)^\nu \qquad \textbf{Eq. 6.1}$$

$$+ \sum_i \sum_{j>i} \sum_{k>j} x_i x_j x_k \left[\sum_{p=0,1,2} {}^p L_{i,j,k}^\gamma \left({}^p X + \frac{1 - x_i - x_j - x_k}{3} \right) \right]$$

Here the binary terms are described using a Redlich-Kister polynomial[108] of the mole fraction, x, of species i and j, expanded out to the νth order in terms of coefficients ${}^\nu L_{i,j}^\gamma$ representing mixing between species i and j. The ternary mixing between species i, j, and k is given by a simpler expression with coefficients ${}^p L_{i,j,k}^\gamma$, where ${}^p X$ is the pth term within the list of x_i, x_j, and x_k, ordered alphabetically. The coefficients for both the binary and ternary mixing summation in this work are given as:

$$L = A + BT \qquad \textbf{Eq. 6.2}$$

A and B are here used to fit to the excess enthalpy and entropy. These terms will be used to fit first-principles calculations in this work.

6.4.1.2 The Ordered γ' Phase

The ordered γ' phase in this work has the sublattice model is modeled by the two sublattice (2SL) model formulated by Ansara[145] and Dupin[72]. In this model the γ' is connected to the γ phase through an ordering contribution to the Gibbs energy expression of the γ' phase. The sublattice model in this work is given as (Al,Ni,Cr,Hf,X)3(Al,Ni,Cr,Hf,X)1. The generalized Gibbs energy expression of this phase is, once again, given elsewhere. Since the 2SL model is a simplification of a more complex model which accounts for mixing on four distinct sites, there exists relations between interactions and end-members. The interactions go up to quaternary terms and are also given elsewhere. The end-members, however, are important to consider. For an A-B system the end-member compounds for the $L1_2$ phase are A_3B, A_2B_2 and AB_3. The Gibbs energies of the end-member compounds for the $L1_2$ model are as follows:

$$G_{\mathrm{AB_3}} = 3U_{AB} + \alpha_{\mathrm{AB_3}}$$

$$G_{\mathrm{A_2B_2}} = 4U_{AB} \qquad \textbf{Eq. 6.3}$$

$$G_{\mathrm{A_3B}} = 3U_{AB} + \alpha_{\mathrm{A_3B}}$$

where $U_{AB}$is the bond energy between A and B and α_i is a factor to account for changes in the bonding environment of the structure i. The energy of these structures not only plays an important role in the binary system but also in the ternary and quaternary systems where

interactions are a function of end-member compound energies in the 2SL model[72]. In general, the Gibbs energy for an $L1_2$ end-member compound $A_aB_bC_c$ is given as:

$$G_{\mathrm{A_aB_bC_c}} = abU_{AB} + acU_{AC} + bcU_{BC} + \alpha_{\mathrm{A_aB_bC_c}} \quad \textbf{Eq. 6.4}$$

The expression for quaternary terms and interactions in the 2SL can be found in work by Dupin[72]. Each bond energy term U_{ij} is modeled in a similar manor to the interaction coefficients:

$$U_{ij} = a_{ij} + b_{ij}T \quad \textbf{Eq. 6.5}$$

In this work these terms are used to model the Enthalpies of formation and entropies of the binary L12 end-member compounds. After this ternary formation enthalpy terms calculated using SQS structures are fit using compounds described by Eq. 6.4.

6.5 Results and Discussion

6.5.1 Ordering Enthalpies in the $L1_2$ Phase and Mixing Enthalpies in the fcc Phase

Results obtained from DFT calculations of $L1_2$ unit cells are given in Figure 6.2 as ordering enthalpies with respect to the calculated fcc structure of each element. Ordering calculation results of Hf-X compounds are segmented into five groups: i) first row transition metals, ii) Pt group metals, iii) Refractory metals, iv) metalloids and post-transition metals and v) ordering with Ni and Al. This last group is important as both usually represent the major elements in each MCRALY bond-coats. Information on the relaxation progress of each element can be found in the supplemental spreadsheet. In general, most compounds broke symmetry when both shape and

volume were allowed to relax. In these cases only results from those compounds which underwent a volume relaxation were taken.

6.5.1.1 First Row Transition Metals

From the first row transition metals, Fe, Co, Ni, and Zn all have negative ordering enthalpies with Hf for the X_3Hf compound but a much more positive ordering enthalpy for the XHf_3 compounds with the exception of Zn. The other first-row transition metals have positive ordering enthalpies for each compound. Of these compounds Ni_3Hf is calculated to have the most negative ordering enthalpy of -51.35 kJ/mole-atom. Cr_3Hf is calculated to have the most positive ordering enthalpy of 24.71 kJ/mole-atom.

Mixing enthalpies in the fcc phase were more symmetric for all cases with the exception of Mn which showed a positive mixing enthalpy towards the Mn rich side and Ni which was the only first row transition element which showed a negative mixing towards the Ni rich side. Ni and Zn were the only elements which showed a negative mixing enthalpy. The ordering enthalpies at 0.25 mole fraction Hf were much more negative compared to the mixing enthalpies for Fe, Co, Ni, and Zn and comparable or higher for the other elements.

6.5.1.2 The Pt Group Elements

The Pt-group all form X3Hf compounds with large negative ordering enthalpies with the exception of Ag3Hf. As with the first row transition metals those compounds which had large negative ordering enthalpies for X3Hf had much higher ordering enthalpies for XHf3. Pt3Hf by far had the most negative formation enthalpy of -106.86 kJ/mole-atom followed closely by

Pd3Hf, Ir3Hf and Rh3Hf with values of -84.95, -79.30, and -73.67 kJ/mole-atom respectively. Ag3Hf had the largest formation enthalpy at 18.62 kJ/mole atom.

Mixing enthalpies in the fcc phase of the Pt-group show a similar trend as for the ordering enthalpies in all cases. The ordering enthalpies at 0.25 mole fraction Hf were much more negative compared to the mixing enthalpies for Pt, Pd, Ir, and Rh, and comparable or higher for the other elements.

6.5.1.3 The Refractory Elements

All compounds of XHf_3 and X_3Hf with Nb and Ta have a small ordering enthalpy of less than 5 kJ/mole-atom. Mixing enthalpies in the fcc phase were comparable to these energies.

6.5.1.4 Post-Transition Metals and Metalloids

As opposed to other groups, the ordering enthalpy for the X_3Hf and XHf_3 compounds were generally close for each case. Si_3Hf and $SiHf_3$ had the most negative ordering enthalpies of -45.65 and -46.01 kJ/mole-atom respectively.

Ordering enthalpies were lower than mixing enthalpies in the fcc phase in all cases for the post-transition metals and metalloids but did not show as dramatic a difference as compared to ordering at 0.25 mole fraction Hf for Pt, Pd, Ir, and Rh in the Pt group and Fe, Co, Ni, and Zn in the first row transition metals.

6.5.1.5 Discussion and Selection Process

While Fe, Co, Ni, and Zn in the first row transition metals each had negative ordering enthalpies at 0.25 mole fraction Hf, their positive mixing enthalpies in the fcc phase make them less than

ideal choices. Hence, no element in the first-row transition elements was considered a candidate for investigation. The refractory metals are also not considered since their mixing and ordering enthalpies were small. It is interesting to note that of the first-row transition metals Cr had the most positive mixing enthalpy and ordering enthalpy. Cr is a common alloying element in MCRALY systems and appears to have a detrimental effect on the Hf-tolerance. This contribution has already been noted in a previous investigation into the Hf-tolerance and was offset by a negative contribution in the ternary mixing between Hf, Ni and Cr required to match experimental solubility observations.

The most promising results of the current calculated elements are Pt, Pd, Ir, and Rh in the Pt group and Si in the metalloids and post-transition metals. Each of these elements not only have negative mixing enthalpies in the fcc system but also extensive ordering enthalpies. Indeed, Pt and Pd have already been observed to have a beneficial effect on Hf additions during cyclic oxidation by Gleeson[130], [140], [146], [147].

Of these elements, Pt is not only the most promising due to its mixing and ordering enthalpies but also the element with the greatest number of thermodynamic experiments in the Ni-Al-Cr-Pt system and oxidation experiments in the Ni-Al-Cr-Hf-Pt alloy system[130], [146], [148]. This makes it a prime example in the present study.

6.5.2 Ni-Al-Cr-Hf-Pt Thermodynamic Assessment

For the test case of this work, Pt is used as an alloying addition to the Ni-rich Al-Cr-Hf-Ni system and the thermodynamics of this system are described using the CALPHAD method. Of

the three ternaries containing Ni and Pt in the five component system, only the Ni-Al-Pt system and its constituent binaries have already been addressed by Liu et al.[149]. Since Hf contents are expected to be low for those alloys of interest, only the γ and γ' phases are modeled for the binary Cr-Pt and Hf-Pt systems and for the ternary Ni-Cr-Pt, Ni-Hf-Pt and Al-Cr-Pt systems. While it is possible to model a system completely from first-principles, a combination of both CALPHAD models and first-principles calculations were used here[20]. This was done for two reasons: i) to obtain entropy related properties which are notoriously difficult to accurately model using first-principles calculations and ii) to obtain a thermodynamic model which better replicates any available phase boundaries of the complete 5-component system since these boundaries are of prime importance to the underlying activities.

6.5.2.1 Literature

6.5.2.1.1 The Cr-Pt System

The Cr-Pt system contains an extensive ordering range in composition space and an even more extensive composition range for the disordered fcc state at high temperatures. The ordering was observed by Waterstrat et al to go from 80 to 25 at.% Pt. at 900 °C[97]. The dataset by Waterstrat remains the most extensive to date. Additional data of relevance to this work is observations of ordering by Goto et al.[150], thin film experiments by Baglin[151], and transition temperatures for the order-disorder reaction by Kussmann et al.[152]

The Cr-Pt system was first modeled by Preuβner et al.[153] using the complex four sublattice (4SL) model for the ordering contribution of the γ' phase in this system. Preuβner et al. not only provided additional experiments to test the transition between the ordered and disordered states,

but also based the thermodynamic modeling on first principles data. Unfortunately the precise calculation details are not clear from this work. However, to avoid repeating calculations the SQS structures calculated by Preuβner will be kept for the fcc phase and an ordering term is taken from the Open Quantum Materials Database (OQMD)[81].

6.5.2.1.2 The Hf-Pt system

Five phases are modeled in the present system: the Liquid phase, the γ phase, the $D0_{24}$-Pt_3Hf phase, and the Pt_4Hf phase. This represents the Pt-rich portion of the diagram. Only two datasets were found with information on the equilibria in this system: an experimental investigation into the solid phase equilibria and into melting points for sever compositions in the Hf-Pt system performed by Stallick and Waterstrat[97] and an experimental investigation up to 0.25 Hf by Meschter and Worrell[154]. These two investigations disagree on the nature of the $L1_2$ phase equilibria. Stallick and Waterstrat observed a highly ordered version of this phase in the form of Pt_4Hf with where only Pt occupied the 3c site of the structure and the structure was postulated to be in equilibrium with the γ phase at 0.2 mole fraction Hf. Meschter and Worrell observed a wider solubility for the $L1_2$ phase but did this only with some XRD information. Stalick and Waterstrat's instruments were undoubtedly more accurate since they used neutron diffraction data for both room and high temperature measurements. However, these samples also contained a higher concentration of Zr (~3 wt.%) compared to samples by Meschter and Worrell who reported that their Hf samples contained less than 120 ppm Zr. Which dataset should be used over the other is debatable. For the present assessment Stalick and Waterstrat's measurements of the phase equilibria are used during optimization. These measurements represent the more extensive dataset and the measurements come from a more reliable instrument designed to

measure equilibria at high temperatures. It should also be noted that the present 2SL model is not capable of causing short range ordering so severe that Hf_4Pt could appear as a stoichiometric compound experimentally. Hence, this phase and the $L1_2$ phase are modeled seperately.

6.5.2.1.3 The Al-Cr-Pt, Ni-Cr-Pt, and the X-Hf-Pt (X=Al,Cr,Ni) systems

For the Ni-Cr-Pt and Al-Cr-Pt systems an experimental dataset from diffusion couple work at 1010 °C was available from a thesis by Eastman[155]. This represents a bulk of the data available in the literature. After this data, only data in the Pt-rich portion of the Al-Cr-Pt system was available from investigations by Kornienko et al.[156] was available. Some phase data in the Pt-rich corner of this system was also available from work by Hill et al.[157] but samples in this study were furnace cooled from 1350 °C unlike samples from Kornienko et al. where samples were quenched at a rate of 30-50 K per minute. No data could be found for the Al-Hf-Pt, Cr-Hf-Pt, or Ni-Hf-Pt systems and hence these will only be assessed using DFT data.

6.5.2.2 CALPHAD modeling

All CALPHAD modeling is carried out using the PARROT module of the software Thermo-Calc and using those models described in the methodology. The resulting database files and optimization files used can be found in the supplemental section. What follows is a brief description of the optimization of each system and the results of these optimizations.

6.5.2.2.1 The Cr-Pt system

Remodeling was performed with respect to observations of transition temperatures in the literature[152], [153] and to two-phase and single phase equilibria observations data by

Waterstrat[158]. The CALPHAD modeling performed by Preuβner et al. on the 4SL was used as a rough starting point for parameter optimization in the the current 2SL model and the models for the liquid, bcc and Cr_3Pt phases are kept from this model.

A combined plot of the mixing enthalpy and ordering enthalpy and formation enthalpy of compounds from first principles is given in Figure 6.4. This data is plotted with data from OQMD and from the original paper by Preuβner et al. Data was not fit to the ordering enthalpies by Preuβner et al. due to the lack of procedural details listed in this phase.

The resulting phase diagram from this optimization is given in Figure 6.5. Generally, the same transitions observed in the 4SL model between the $L1_2$ phase and γ were achieved in the present diagram. One place of disagreement, however, was found in the $L1_0$ equilibria. In the original model the transition to this behavior is smooth and only a thin region represents the $L1_0$ phase. In the current model this region is much more prominent. Although this was mostly due to modeling constraints, there are some places where the present model agrees with experimental observations better than the previous model. In thin film experiments performed at high temperatures by Baglin[151], a large two phase region between $L1_0$ and γ' at temperatures below 1000 K is reported and is reproduced by the present model. Furthermore, another large two phase region is also observed between Cr_3Pt and what was suggested to be the $L1_2$ phase by Waterstrat[158]. Because of this two phase region, Waterstrat asserted that the transition between L12 and the γ phase occurred near 1200 K. This is in disagreement with the experiments by Preuβner which found this transition to be at a much higher temperature. Hence, it seems reasonable that this equilibrium is actually between $L1_0$ and Cr3Pt. However, there is also some

experimental disagreement with the present assessment. Mostly, this falls in observations of single phase regions. One of these observations by Preuβner at 37 at.% Pt disagrees with experimental observations by Waterstrat at 1173 K. Annealing times by Waterstrat were by far longer than those annealing times by Preuβner and hence data by Waterstrat can be taken as more reliable in place of this value. For the time being the disagreement between observations by Waterstrat and this model must be attributed to limitations in the $L1_0$ model chosen.

6.5.2.2.2 The Hf-Pt system

SQS mixing information and $L1_2$ formation enthalpies are used from this work to model the mixing enthalpies and ordering enthalpies of the fcc and $L1_2$ phases. In addition, finite temperature properties are calculated both for the $L1_2$-Pt3Hf end-member and the $D0_{24}$-Pt_3Hf compound. The exact structure for Pt_4Hf is assumed not to be part of the $L1_2$ phase in this modeling since the short-range ordering required to obtain this composition could not be achieved in the 2SL model. For the present model the formation enthalpy of this phase is estimated by extrapolating the formation enthalpy between $L1_2$-Pt_3Hf calculated using DFT and a structure where a single Pt occupies the 1a site of the $L1_2$ structure with stoichiometry $Pt_{13}Hf_3$ calculated using DFT.

A plot of the enthalpies of formation thermodynamically modeled in this work, from first principles data in the literature, first-principles data calculated in this study and experimental measurements is given in Figure 6.6. Although available experiments are limited, the agreement between calculated first principles enthalpies of formation and experimental enthalpies of formation is good. This lends some confidence to the present calculated results. In addition,

agreement can be found between the calculated formation enthalpy of $L1_2$-Pt_3Hf from this work, OQMD and the Materials Project. Some disagreement occurs with thermochemical experiments from Meschter and Worrell for the formation enthalpy of the $D0_{24}$-Hf_3Pt phase. However, this formation enthalpy was actually estimated from Pt activities measured in the Zr-Pt system. Due to this disagreement, this enthalpy is only compared to.

CALPHAD optimization is carried out by first fitting an enthalpy of formation and entropy at 298.15 K for the $D0_{24}$-$HfPt_3$ phase from values calculated from first principles. At 300 K the entropy of this phase was calculated to be 33.32 J/mole-K from the Debye model. This information is subsequently used to model the 0^{th} mixing parameter in the liquid phase to match the expected melting observed by Stallick and Waterstrat. The entropy of the $HfPt_4$ phase is then modified to the observed melting temperature by Stallick and Waterstrat. In the current model the phase boundary observed by Stallick and Waterstrat is modeled not as the equilibria between the disordered phase and $HfPt_4$ but as the equilibria between $HfPt_4$ and the ordered $L1_2$-$HfPt_3$ phase. This was done because $HfPt_4$ is hypothesized to have strong short-range ordering. Furthermore, this is considered plausible since the XRD patterns between these two structures are quite similar and difficult to de-convolute. Finally, mixing entropy and mixing enthalpy of the fcc phase and the formation enthalpy and entropy of the $HfPt_4$ phase are fit to this phase boundary and the melting temperatures observed in the system. To properly fit the liquid phase, a stoichiometric HfPt phase was also added to the system with an enthalpy of formation from DFT and an entropy of formation of 10 J/mole-atom·K. This formation entropy is close to the formation entropy for the $D0_{24}$-$HfPt_3$ phase. 0^{th},1^{st} and 2^{nd} order interaction parameters were needed in the liquid to fit the observed phase boundaries.

Calculated finite temperature properties obtained using the quasiharmonic Debye model are given for the $L1_2$-$HfPt_3$ phase and $D0_{24}$-$HfPt_3$ phase in Figure 6.7. A poisson's ratio of 0.3 taken from the materials project for the $D0_{24}$-$HfPt_3$ phase[123] was used to determine the scaling factor using equations from Shang et al[76]. However, the $L1_2$-$HfPt_3$ phase was found to be mechanically unstable. To assign a scaling factor to this compound an average of the poisson ratios of chemically similar compounds with the same crystal structure was taken from the materials project using $TiPd_3$, $TiPt_3$, $ZrPd_3$ and $ZrPt_3$ with calculated poisson ratios of 0.3, 0.3, 0.29 and 0.29 respectively[123]. The resulting value of 0.295 was used to determine a scaling factor within the Debye model.

A plot of the representative phase diagram from 0 to 0.3 mole fraction Pt and the calculated mixing enthalpies of fcc and L12 at 298.15 K are given in Figure 6.8a and b. No modification to the mixing enthalpy of the $L1_2$-Pt_3Hf phase is made but some modifications to the calculated fcc SQS enthalpies are required to fit the observed melting temperatures. The calculated melting temperatures match well with the experimental melting temperatures observed by Stallick and Waterstrat. However, the present liquid description suffers from a lack of experimental data. It is likely that this liquid description will change in later models.

6.5.2.2.3 The Al-Cr-Pt system

Optimization of the Pt-rich corner of the Al-Cr-Pt system is carried out with respect to the two available datasets and the fixed-volume, ternary SQS calculations for the fcc phase. While there were observations of other phases near the Pt-rich corner these are largely ignored and only two ternary parameters in the ordered γ' phase are modified and only three ternary parameters in the γ phase are modified.

Isothermal sections at 1010, 1150 and 1350 °C from the resulting parameter optimization are shown in Figure 6.9a b and c respectively. Single-phase and tie-line data corresponding to the γ and γ' regions is in excellent agreement for both 1010 °C and 1350 °C. Not shown at 1150 °C are some tie-lines from this dataset which are suspected to correspond to equilibria with the (Al)Pt2 phase which is suggested to have some solubility for Cr by Kornienko et al[156]. A transition in equilibria behavior between the γ and γ' phase occurs between 1010 °C and 1350 °C due to the γ' solvus in the Cr-Pt system. Alloys cooled slowly from 1350 °C might display features of this transition. Hence, data from Hill is plotted at 1150 °C in Figure 6.9b. Single phase data and tie-line data observed by Hill agrees well with the interpretation that these alloys are in the transition in behavior between 1350 °C and lower temperatures.

6.5.2.2.4 The Ni-Cr-Pt system

Results for all ternary, fixed volume calculations are given in Table 6.1. To obtain a more accurate model of the fcc phase in this system, however, a fitting was also performed with respect to the available phase boundaries. One limitation in this system is that the $L1_2$ phase was

not observed in experiments by Eastman[155]. The presence of the $L1_2$ at 1473.15 K leads to a large solubility for Ni within the present model. This may signal that the $L1_2$ phase is too stable in Cr-Pt system. In place of changing the binary model $L1_2$ mixing terms were calculated using the 24 atom $L1_2$ SQS structures. The results for these calculations are given in Table 6.2. Considering the relative uncertainties in this system, only one ternary term was used to fit each ternary mixing parameter in Eq. 6.1. The subsequent isothermal section at 1200 °C plotted against data from C.M. Eastman is given in Figure 6.10.

.

6.5.2.2.5 The Al-Hf-Pt, Cr-Hf-Pt and Ni-Hf-Pt systems

SQS results for the fcc phase and the $L1_2$ phase of the X-Hf-Pt (X=Ni,Al, and Cr) systems are given in Table 6.2. With the exception of the $(Ni_{0.5}Pt_{0.5})_3Hf_1$ structure in the $L1_2$ phase, all calculations lost symmetry upon relaxation. Resulting formation enthalpies from calculations relaxing only volume were used to fit ternary interaction parameters in the fcc phase and ternary bonding parameters in the $L1_2$ phase except in the Hf-Pt-Ni system where only the $(Ni_{0.5}Pt_{0.5})_3Hf_1$ structure calculation was fit to. In each ternary system only one parameter was used in the fcc phase such that ${}^0L^{\gamma}_{i,j,k} = {}^1L^{\gamma}_{i,j,k} = {}^2L^{\gamma}_{i,j,k}$ and only one parameter was used for the $L1_2$ bonding parameters such that $\alpha_{A_2B_1C_1} = \alpha_{A_1B_2C_1} = \alpha_{A_1B_1C_2}$. This was done to avoid over fitting in the Al-Hf-Pt and Cr-Hf-Pt and the resulting formation enthalpies fit to these for gamma and $L1_2$ were well represented by this assumption. In the Hf-Pt-Ni resulting formation enthalpies in the fcc phase are well represented by this assumption but in the $L1_2$ phase formation enthalpies for the $(Hf_{0.5}Pt_{0.5})_3Ni_1$ and $(Hf_{0.5}Ni_{0.5})_3Pt_1$ configurations had formation enthalpies between cases between calculation which kept symmetry and calculations which broke

symmetry. However, since the calculation of the $(Ni_{0.5}Pt_{0.5})_3Hf_1$ structure represents the most accurate enthalpy the assumption that the bonding environment changes similarly between all cases, i.e. $\alpha_{Hf_2Ni_1Pt_1} = \alpha_{Hf_1Ni_2Pt_1} = \alpha_{Hf_1Ni_1Pt_2}$, is kept. In-fact, the concept that the actual enthalpy should be between the broken and restricted symmetry case has some backing from work by Van de Walle[159]. However the structure search proposed in that work was considered too expensive for this work. For the time being the present assumptions are kept.

For the Al-Hf-Pt system no interaction parameter was needed and $\alpha_{Hf_2Al_1Pt_1} = \alpha_{Hf_1Al_2Pt_1} = \alpha_{Hf_1Al_1Pt_2}$=0 appropriately reproduced the calculated enthalpies.

6.5.2.2.6 The Ni-Al-Cr-Hf-Pt system

With the ternaries of each system assessed it is possible to compare to experiments in the Ni-rich Al-Cr-Hf-Ni-Pt system. There was only one available experimental work on this system by Heidloff et al.[160] in which experiments on the alloy Ni-15Al-5Cr-2.5Pt-0.1Hf (at.%) were performed to determine the phase compositions at 1000°C after 850 hour heat treatments using electron probe microanalysis (EPMA), the γ' solvus using differential thermal analysis, and crystallographic behavior at high temperatures using high-temperature synchrotron analysis. Comparison of the phase compositions from the 1000 °C heat treatment with calculated equilibrium results for this alloy composition are given in Table 6.3. The agreement between the calculated equilibrium and the observed phase equilibrium is excellent except for the Al concentration which is roughly 0.6 at.% off from the observed value in the γ phase and the Cr concentration in the γ phase which is roughly 0.5 at.% off from the observed value in the γ phase. A plot of the γ' phase fraction with temperature for the Ni-15Al-5Cr-2.5Pt-0.1Hf (at.%)

alloy is given in Figure 6.11. The calculated γ' solvus is in excellent agreement with the experimentally observed solvus with a calculated γ' solvus of 1151.62 ° C compared to a measured solvus of 1153 °C from DTA. However, the phase fractions calculated here are higher than those observed experimentally. The calculated fraction at 1000 °C is 0.40 compared to an observed fraction of ~0.35. Notably, no time duration is listed past a 4 minute dwell time at each high-temperature measurement in these experiments. Samples were prepared by solution treating at high temperatures and then annealed for 4 hours at 1150 °C. This may have driven down the volume fraction of γ'. Notably, no entropic values were assessed for ternary parameters in the Cr-Ni-Pt system. This may be an additional source of error.

6.5.3 Hf Tolerance Calculation in a Ni-Al-Pt-Hf Alloy

6.5.3.1 Oxidation in the Ni-rich Ni-Al-Pt-Hf Alloy System

It has been suggested that an important aspect of Pt is its effect on the activity of oxidizing species[161]. Pt is suggested to lower both the Al[161] and Hf[130] activities in a Ni-matrix at high temperatures during oxidation. Both effects are important during oxidation but, as noted in previous work, the Hf-tolerance is actually a competition between Al activity and Hf activity. A plot of the Hf and Al activity for Ni-xAl-5Cr-XPt-0.1Hf (X=0,2.5 and 5 at.%) at 1150 °C from 0 to 20 at.% Al is given in Figure 6.12. In the two phase γ-γ' region Pt has the effect of lowering both the activity of Hf and Al. However, the effect is far stronger on Hf than on Al. This will result in an increase in the Hf tolerance in the two phase γ-γ' region with increasing Pt. In the single phase γ region the Hf activity shows a significant increase compared to Al activity with increasing Pt. Hence, the Hf tolerance will decrease with increasing Pt in the γ phase.

Data in the literature is scarce for oxidation of alloys only containing elements in the Al-Cr-Hf-Ni-Pt system. The majority of the work which could be found in this system was performed by Mu et al.[17], [130] Mu studied the cyclic and isothermal oxidation behavior of alloys containing up to 5 at.% Cr, up to 25 at.% Al, up to 20 at.%Pt and up to 0.5 at.%Hf. While this information is valuable to compare to, it should be noted that cyclic oxidation introduces further complications during oxidation since spallation of the external Al_2O_3 scale and crack grown in the scale is more likely to occur and equilibrium conditions are less likely to be reached for long times at the scale/alloy interface.

Oxidation of select alloys in the Ni-rich Al-Hf-Ni-Pt system was also studied in by Mu[17], [130]. A plot of the Hf-tolerance for a Ni-xAl-20Pt (at.%) alloy system compared to this data is given in Figure 6.13. The Hf-tolerance in the γ phase is nearly zero and the Hf-tolerance increases quickly with increasing Al concentration into the $\gamma - \gamma'$ and γ' zone. Note also that, as expected, the Hf-tolerance continues to increase with increasing Al concentration into the γ' zone. This was not the case for the Ni-Al-Hf system where the Hf-tolerance decreases with increasing Al concentration in the single phase γ' region.

Experimental oxidation behavior is plotted with this curve at 20 at.% Al for alloys having Hf concentrations ranging from 0.05 at.% to 0.94 at.% which have been oxidized isothermally at 1150 °C for 100 hours. The calculated Hf tolerance of 0.53 at.% is in excellent agreement with these experimental observations. There is some disagreement, however, between the expected behavior and the experimentally observed behavior for higher Al concentrations since some HfO_2 is seen within the scale at 25 at.% Al and 0.5 at.% Hf after 96 hours isothermal oxidation at 1150 °C. It is quite possible that this observed oxidation is actually due to local Hf concentration

fluctuations. Indeed, glow-discharge optical emission spectrometry (GD-OES) of this sample oxidized for short times by Mu showed only a mild alteration of the Hf concentration near and within the Al_2O_3 scale and did not show an increase in Hf concentration with increasing oxidation times[17]. This may indicate that the HfO_2 formed within this oxide is actually an artifact of the transient Al_2O_3 scale formation.

A plot of the Hf-tolerance for the Ni-20Al-xPt alloy system is given in Figure 6.14. Here was see the direct effect of Pt increasing the Hf-tolerance with increasing Pt concentrations. Notably Pt is not just improving the ratio of Al to Hf activities but also adjusting the phase equilibria between γ and γ' by decreasing the amount of Al required to form γ'. This was also evidenced in the earlier plot of Hf and Al activities in Figure 6.12 where the $\gamma - \gamma'$ phase region boundary could be seen moving towards lower Al contents with increasing Pt contents. Experimental observations in this plot come from isothermal oxidation experiments at 1150 ° C by Mu[17], cyclic oxidation experiments at 1150 ° C by Mu et al.[130] and isothermal oxidation experiments at 1150 ° C Izumi[148]. Despite the fact that the oxidation is cyclic, the results are still in good agreement with the present predictions with the exception of the Ni-20Al-0.1Hf alloy where cyclic oxidation is suspected to have caused enough strain to cause cracking and short-circuit O diffusion.

6.5.3.2 Oxidation in the Ni-rich Ni-Al-Cr-Pt-Hf alloy system

Oxidation in the Ni-Al-Cr-Pt-Hf system which reported HfO_2 precipitation behavior or showed micrographs of the scale cross-sections is available only from work by Mu et al.[130] where cyclic oxidation experiments were performed at 1150 °C on Ni-15Al-5Cr-xPt-0.1Hf alloys

(x=0,5, and 10) for 500 1 hour cycles, and 500 hour cyclic oxidation at 1150 °C of a Ni-20Al-5Cr-5Pt-0.1Hf alloy. A plot of the Hf tolerance in the Ni-15Al-xPt-yHf alloy system is given in Figure 6.15. In this alloy system the role of Pt in improving the Hf-tolerance by changing the equilibrium γ' fraction is apparent with an increase in Pt moving the system from the γ region to the two-phase γ-γ' region where the Hf-tolerance is much higher. This transition is visibly apparent for the Ni-15Al-10Pt-5Cr-0.1Hf alloy in the work by Mu et al.[130] which shows roughly 5% γ' in the micrograph. This experiment clearly undergoes far less HfO_2 precipitation than the 15Al-5Pt-5Cr-0.1Hf alloy. However, the resolution on the micrograph presented was far too low to actually resolve the scale make-up. Indeed, there are some internal precipitates clearly visible in this micrograph but these were not pointed to as HfO_2 by the authors. This observation is in disagreement with the present calculated results. A possible reason for this disagreement could be that the γ' phase is actually far more effective at interacting with Cr, Hf and Pt. Although no calculations in this system were made, adjusting ternary parameters in the Cr-Hf-Pt $L1_2$ phase did not significantly alter the present calculated result. Even a shift in the γ' phase fraction would not be likely to agree with experiments since the γ' fractions required to satisfy this observation are around 0.2 compared to the present value of ~0.05. Because there is clearly an internal precipitate in this micrograph for this alloy and because the resolution for this micrograph is about three times lower than others in the same work, an asterisk has been added to this data point.

A plot of the Hf tolerance in the Ni-xAl-5Cr-5Pt-yHf alloy system at 1150 ° C is given in Figure 6.16. This plot resembles Figure 6.13 but with a much diminished effect of Pt on the γ' phase. Experimental comparisons from Mu et al.[130] and Gleeson[162] are included in this plot. There are also alloys with higher concentrations of Hf reported to have oxidized at the interface, with

micrographs as evidence, by Hou et al.[163] for the alloys Ni-22Al-5Cr-0.3Hf (at.%) and Ni-22Al-5Cr-0.3Hf-5Pt (at.%). However, these Hf concentrations are much greater than the present Hf-tolerance for cases with and without 5 at.% Pt. While agreement with the present alloys is quite good, the Hf tolerances of these alloys without Pt are able to capture the observed effects. The calculated Hf tolerance has a maximum of 0.21 and 0.17 for 0 and 5 at.%, respectively. Despite the lack of experimental data this displays a significant improvement with just a small concentration of Pt added.

6.6 Conclusions

In this work a selection procedure of alloying additions to Ni-rich Al-Cr-Hf-Ni alloys was performed using first-principles to determine which additions are most likely to improve the oxidation resistance of these alloys. This selection procedure was performed using density functional (DFT) theory calculations on elements which have a solubility of greater than 5 at.% in γ'-Ni_3Al at 1000 °C and on select elements without reported solubility in the Pt group. Thermodynamically, the elements with the largest mixing enthalpies with Hf in the fcc phase and enthalpies of formation with Hf with respect to the fcc phase in the $L1_2$ phase are the most likely to reduce the Hf activity in either of these phases. This will result in a subsequent improvement of oxidation properties by decreasing the stability of HfO_2 at the interface between an external Al_2O_3 layer and the alloy. Hence, the mixing enthalpies in the fcc phase were calculated for X-Hf systems using special quasi-random structure (SQS) calculations and the enthalpies of formation of $L1_2$ structures with respect to the fcc phase for the X-Hf system. It was found that Pt, Pd, Ir, Rh and Si were the most promising candidates from this selection procedure.

Since Pt presented the most promising case, a first-principles based thermodynamic model of the Ni-rich Al-Cr-Hf-Ni-Pt-O alloy system was constructed to predict the Hf tolerance – i.e. the maximum amount of Hf which can be added to the alloy system before HfO_2 precipitates at the at the interface between an external Al_2O_3 layer and the alloy. This amounted to a remodeling of the Cr-Pt system, a new first-principles based model of the Pt-rich Pt-Hf system, and new models of the Al-Cr-Pt, Cr-Ni-Pt, Al-Hf-Pt, Ni-Hf-Pt, and Cr-Hf-Pt systems. Experiments were available in the Al-Cr-Pt system and Cr-Ni-Pt system but not for the X-Hf-Pt systems (X=Al,Cr,Ni). To compensate for this lack of data, ternary SQS calculations were carried out in the fcc system and the L12 system for the Cr-Ni-Pt, Al-Hf-Pt, Ni-Hf-Pt. No calculations were carried out for the Cr-Hf-Pt systems since its effect was considered unimportant. Simplified thermodynamic interactions were fit to this data to compensate for the fact that most SQS calculations were mechanically unstable and lost symmetry during structure relaxation. Using these models and models available in the literature, a full model of the Ni-rich Al-Cr-Hf-Ni-Pt system was constructed and thermodynamic calculations were compared with equilibria observed in the literature for this system. Results agreed well for γ-γ' equilibria data at 1000 °C and the experimentally observed solvus. However phase fractions calculated using this database were slightly higher than those measured using high-temperature synchrotron data.

The Hf-tolerance was calculated in the Ni-rich Al-Hf-Ni-Pt and Al-Cr-Hf-Ni-Pt alloy system at 1150 ° C and compared with oxidation observations in the literature. Calculations matched well with experimental oxidation results for most cases in this system with the exception of samples with high Al concentrations where experimental observations had HfO2 precipitates in the oxide scale. It is hypothesized that these formed as a consequence of the transient oxidation stage and did not represent the steady state oxidizing behavior.

Pt was shown to decrease the Hf activity relative to the Al activity as well as decreasing the amount of Al required to form γ' when substituting for Ni. The calculated Hf tolerance had a maximum of ~0.21 at.% Hf at 1150 ° C for the Ni-xAl-5Cr-5Pt-y Hf system compared to a maximum of 0.17 at.% Hf at 1150 ° C for the Ni-xAl-5Cr-y Hf system. This shows a clear demonstration of the ability of Pt to improve oxidation resistance in the Ni-rich Al-Cr-Hf-Ni-Pt alloy system.

The present culmination of work represents a bottom-up approach to designing oxidation resistant alloys. A similar first-principles based modeling procedure could be carried out for Pd, Ir, Rh, or Si additions which could yield similar models for the design space of oxidation resistant alloys.

Table 6.1. Calculated enthalpies of formation in the fixed volume ternary systems.

End-member	$\Delta_f H^{298.15K}$ **(kJ/mole-atom)**	**End-member**	$\Delta_f H^{298.15K}$ **(kJ/mole-atom)**
Al-Cr-Pt		**Cr-Hf-Pt**	
$(Al_{0.333}Cr_{0.333}Pt_{0.333})$	-28.21	$(Cr_{0.333}Hf_{0.333}Pt_{0.333})$	-10.57
$(Al_{0.5}Cr_{0.25}Pt_{0.25})$	-25.43	$(Cr_{0.5}Hf_{0.25}Pt_{0.25})$	13.64
$(Al_{0.25}Cr_{0.5}Pt_{0.25})$	-9.82	$(Cr_{0.25}Hf_{0.5}Pt_{0.25})$	0.17
$(Al_{0.25}Cr_{0.25}Pt_{0.5})$	-37.93	$(Cr_{0.25}Hf_{0.25}Pt_{0.5})$	-26.41
Al-Hf-Pt		**Cr-Ni-Pt**	
$(Al_{0.333}Hf_{0.333}Pt_{0.333})$	-49.94	$(Cr_{0.333}Ni_{0.333}Pt_{0.333})$	-3.13
$(Al_{0.5}Hf_{0.25}Pt_{0.25})$	-41.1	$(Cr_{0.5}Ni_{0.25}Pt_{0.25})$	3.39
$(Al_{0.25}Hf_{0.5}Pt_{0.25})$	-38.51	$(Cr_{0.25}Ni_{0.5}Pt_{0.25})$	-2.13
$(Al_{0.25}Hf_{0.25}Pt_{0.5})$	-59.23	$(Cr_{0.25}Ni_{0.25}Pt_{0.5})$	-2.51
Hf-Ni-Pt			
$(Hf_{0.333}Ni_{0.333}Pt_{0.333})$	-34.54		
$(Hf_{0.5}Ni_{0.25}Pt_{0.25})$	-29.51		
$(Hf_{0.25}Ni_{0.5}Pt_{0.25})$	-24.75		
$(Cf_{0.25}Ni_{0.25}Pt_{0.5})$	-42.07		

Table 6.2. Calculated enthalpies of formation in the Ni-Hf-Pt, Ni-Cr-Pt and Al-Hf-Pt systems

Configuration	$\Delta_f^{Sym} H^{298.15K}$ (kJ/mole-atom)	$\Delta_f^{ISIF3} H^{298.15K}$ (kJ/mole-atom)	$\Delta_f H^{298.15K}$ (kJ/mole-atom)
Al-Hf-Pt			
$(Hf_{0.5}Pt_{0.5})_3(Al)_1$	-53.03	-71.54	-55.92
$(Al_{0.5}Pt_{0.5})_3(Hf)_1$	-70.89	-73.29	-70.96
$(Al_{0.5}Hf_{0.5})_3(Pt)_1$	-51.16	-60.71	-50.97
Hf-Ni-Pt			
$(Hf_{0.5}Pt_{0.5})_3(Ni)_1$	-42.46	-66.34	-60.42
$(Ni_{0.5}Pt_{0.5})_3(Hf)_1$	-75.61	-77.41	-75.63
$(Ni_{0.5}Hf_{0.5})_3(Pt)_1$	-33.14	-61.83	-57.04
Ni-Cr-Pt			
$(Cr_{0.5}Pt_{0.5})_3(Ni)_1$	1.755	*	-1.98
$(Ni_{0.5}Pt_{0.5})_3(Cr)_1$	-11.18	*	-7.73
$(Ni_{0.5}Cr_{0.5})_3(Pt)_1$	-5.127	*	-5.16

* Calculations not considered necessary

Table 6.3. Calculated and experiment phase compositions of γ and γ' for Ni-15Al-5Cr-2.5Pt-0.1Hf (at.%) at 1000 °C

	Ni	Al	Cr	Hf	Pt
Experimental					
c_i^{γ} (at.%)	80.36 ± 0.32	11.79 ± 0.14	5.97 ± 0.1	0.05 ± 0.04	1.84 ± 0.22
$c_i^{\gamma'}$ (at.%)	74.03 ± 0.22	18.56 ± 0.04	4.15 ± 0.18	0.19 ± 0.02	3.07 ± 0.02
Calculated					
c_i^{γ} (at.%)	79.44	12.57	5.59	0.01	2.40
$c_i^{\gamma'}$ (at.%)	74.38	18.61	4.12	0.24	2.66

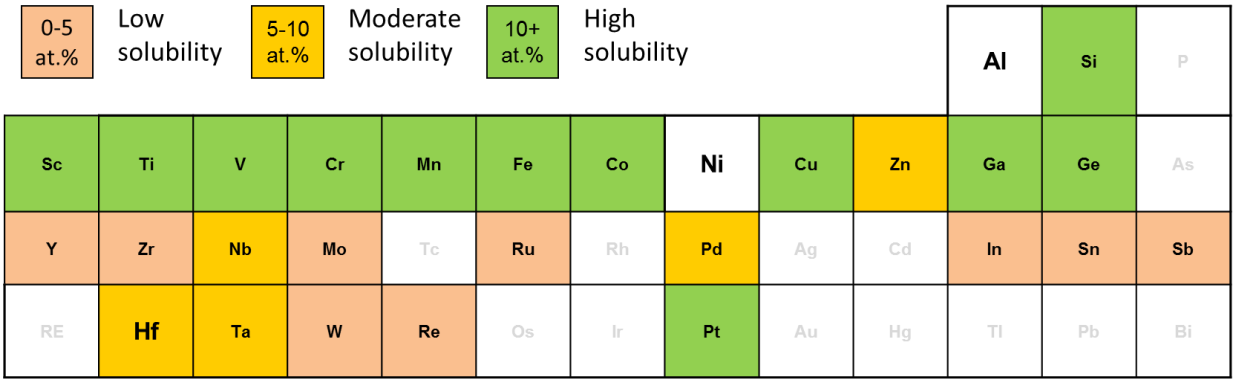

Figure 6.1. Chart of selected element's maximum solubility in the γ' phase at 1000°C by Ochial and other sources.

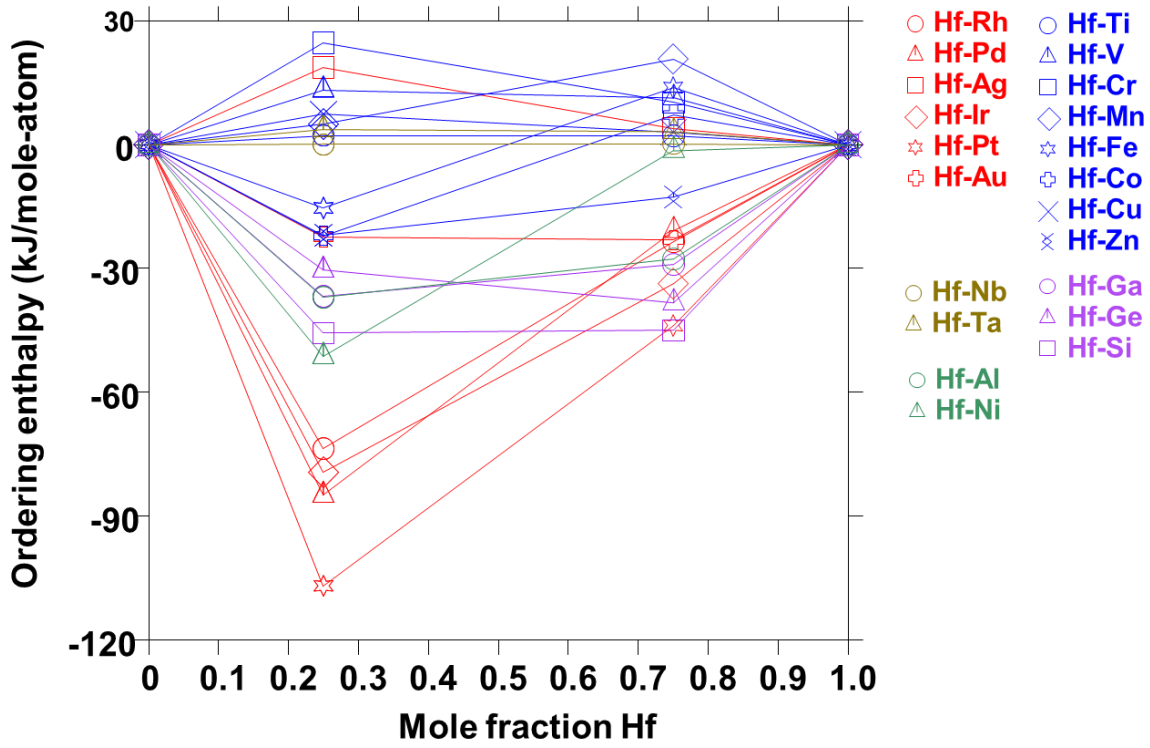

Figure 6.2. Enthalpies of formation with respect to the fcc phase for L12 structures in the X-Hf system.

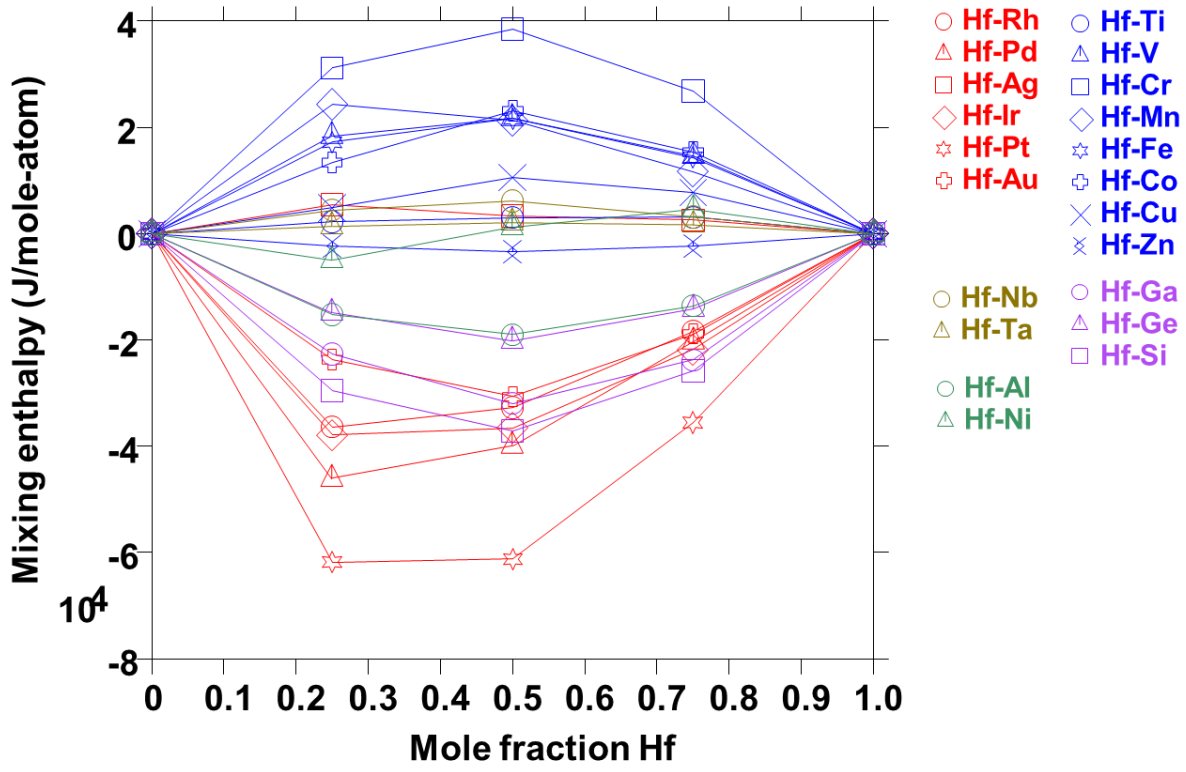

Figure 6.3. Enthalpies of formation with respect to the fcc phase for fcc structures in the X-Hf system.

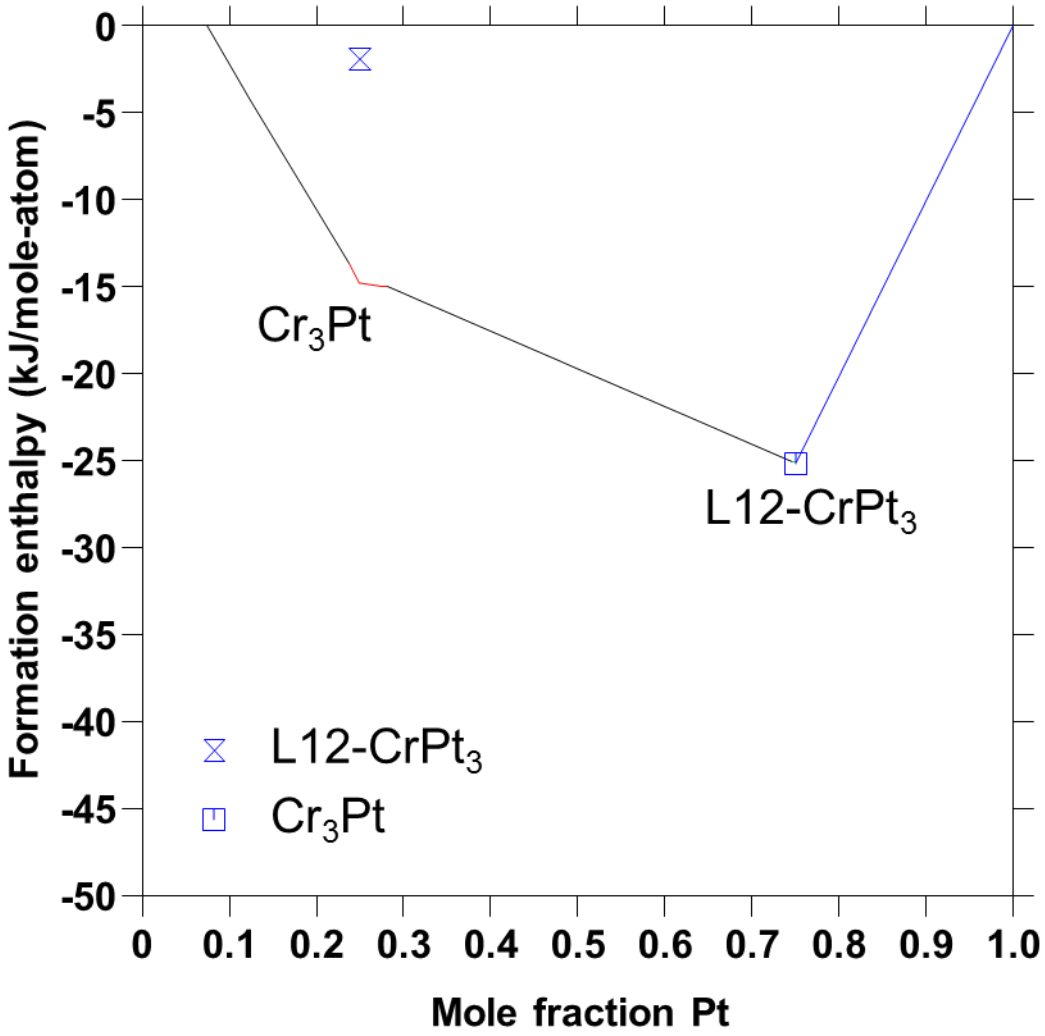

Figure 6.4. A combined plot of the mixing enthalpy and ordering enthalpy and formation enthalpy of compounds from first principles

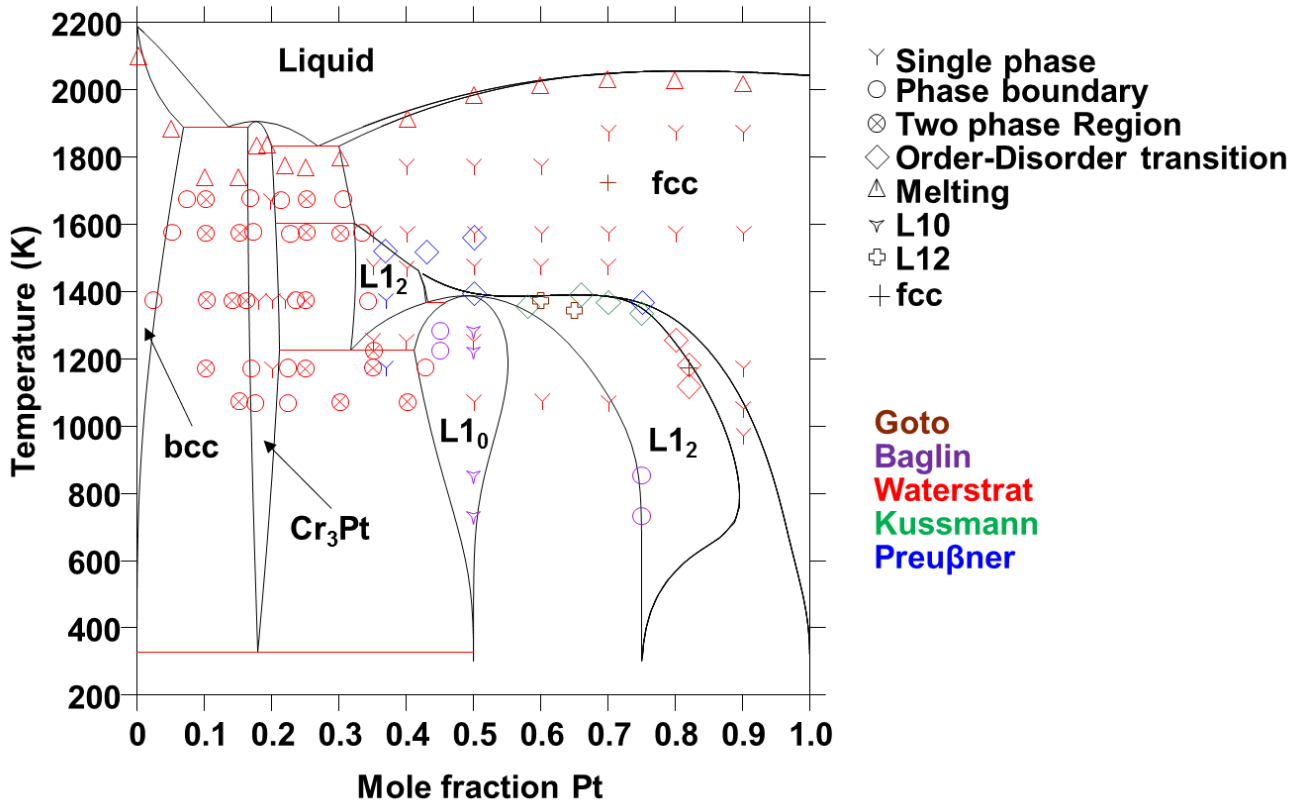

Figure 6.5. Cr-Hf Phase diagram comparing data from Goto et al.[150] (brown), Baglin et al.[151] (purple), Waterstrat[158](red), Kussmann et al.[152](green) and Preuβner et al.[153](blue).

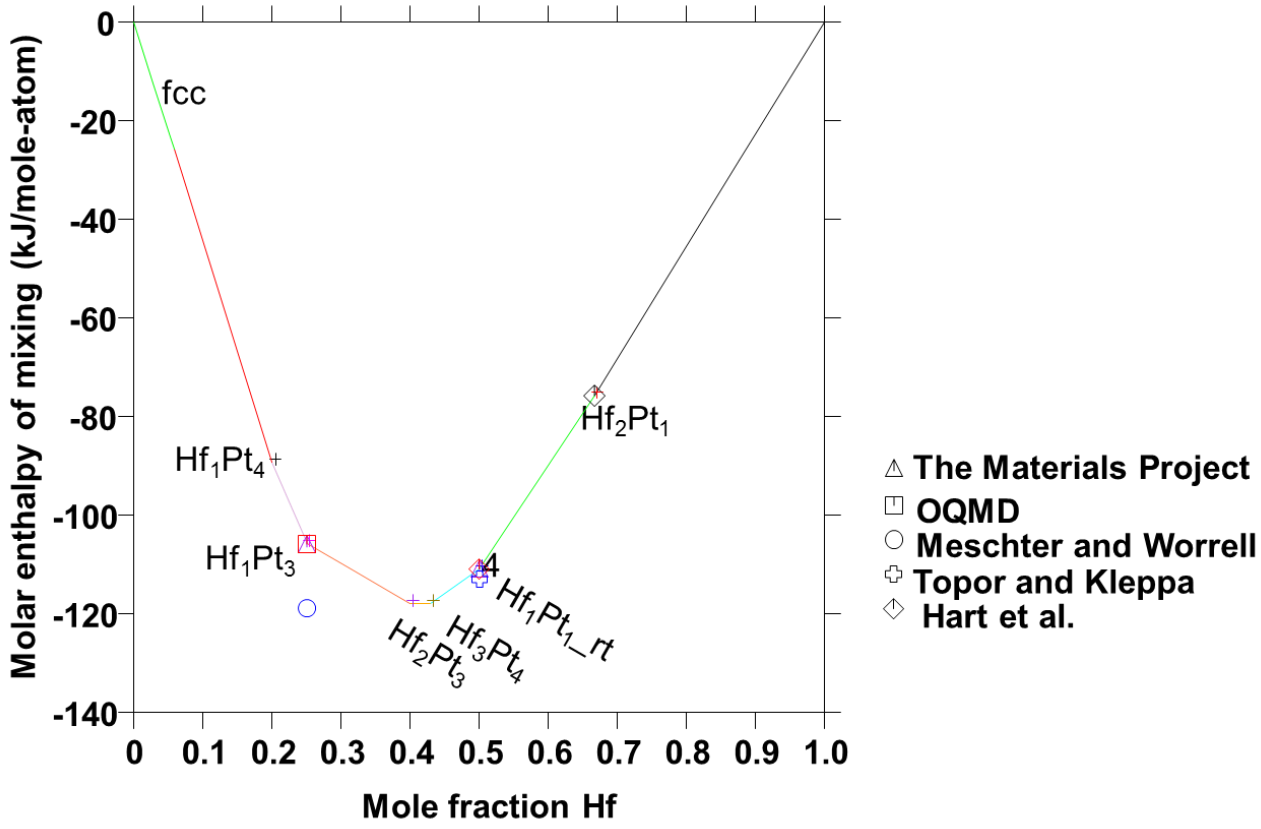

Figure 6.6. A plot of available first principles data in the literature[65], [81], [123] and available experimental observations in the Hf-Pt system[154], [164]

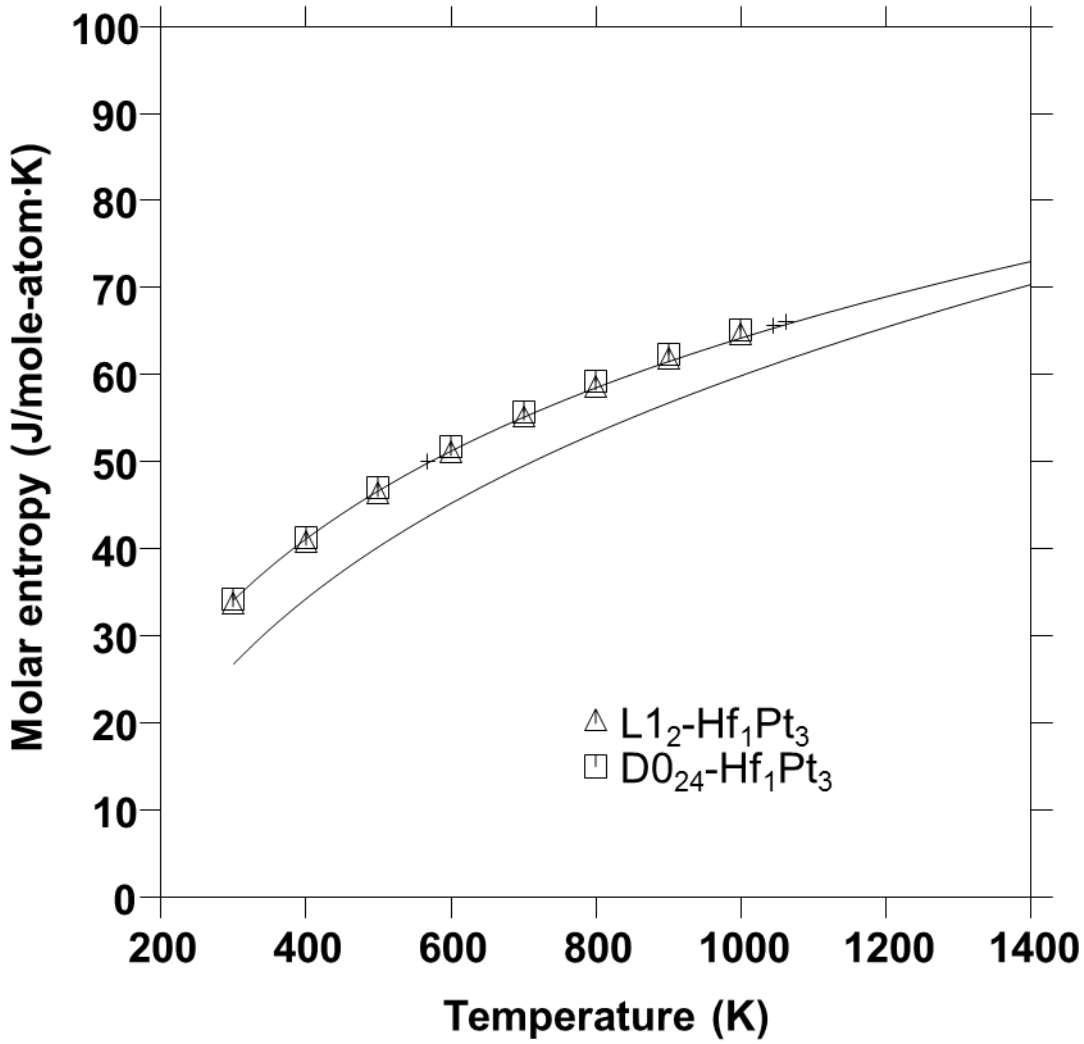

Figure 6.7. Molar entropy calculated for the $L1_2$-Hf_1Pt_3 and $D0_{24}$-Hf_1Pt_3 structures compared to entropies modeled in this work.

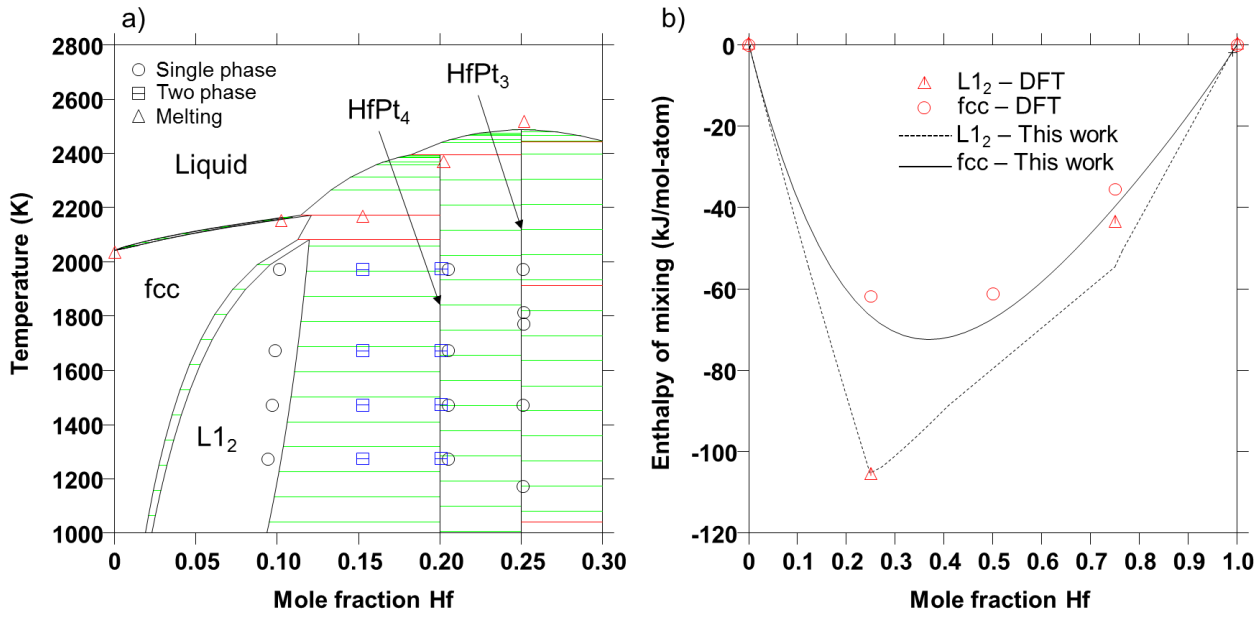

Figure 6.8. A plot of (a) phase diagram in the Pt rich corner of the Hf-Pt system compared to experiments by Stalick and Waterstrat[97] and (b) the enthalpy of mixing for the fcc phase and the $L1_2$ phase in the Hf-Pt system calculated from the present model and DFT calculations.

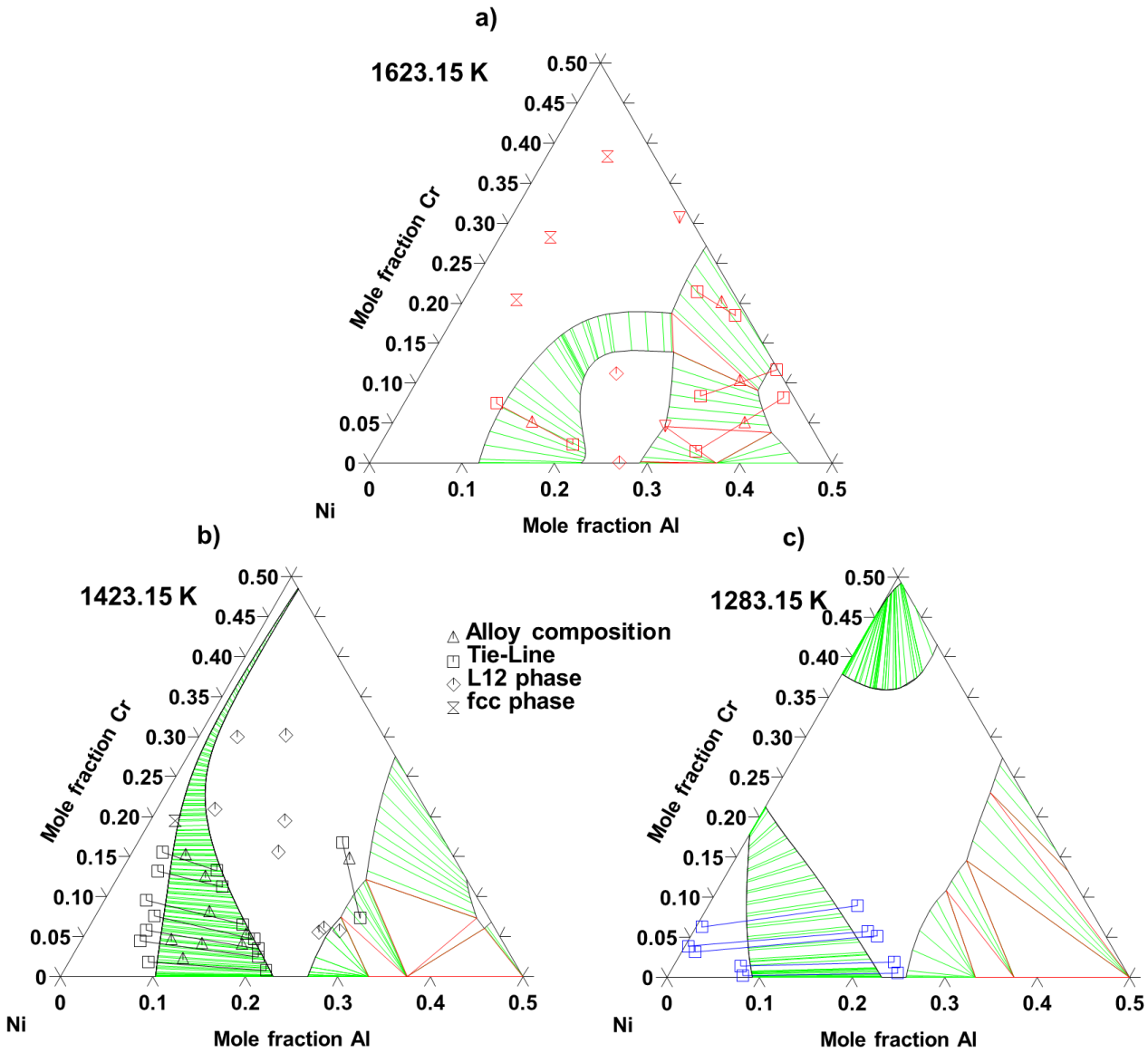

Figure 6.9. Isothermal sections in the Al-Cr-Pt system compared to data by Eastman[155] (blue), Kornienko et al.[156] (blue) and Hill et al.[157] (black)

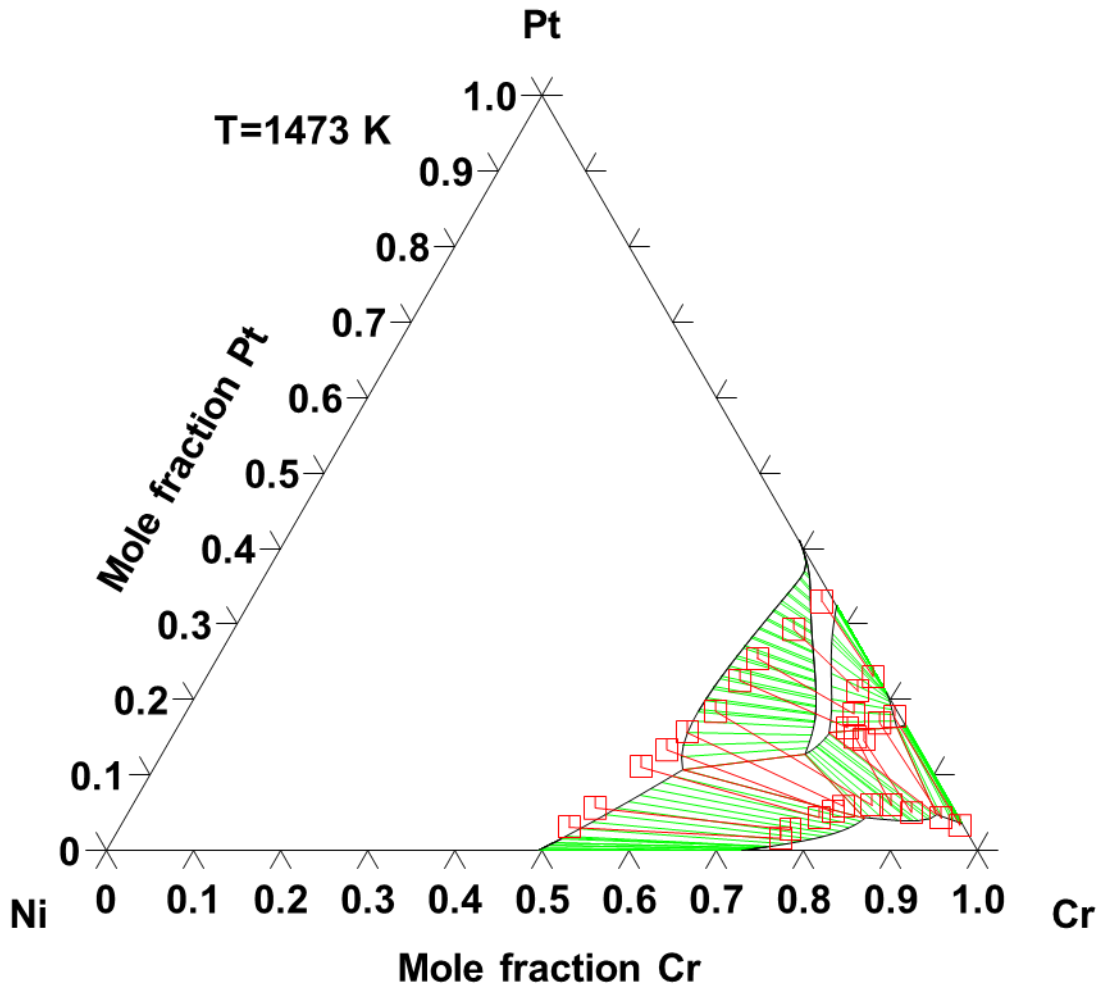

Figure 6.10. Isothermal section of the Ni-Cr-Pt system at 1473.15 K compared to data by Eastman[155] (red)

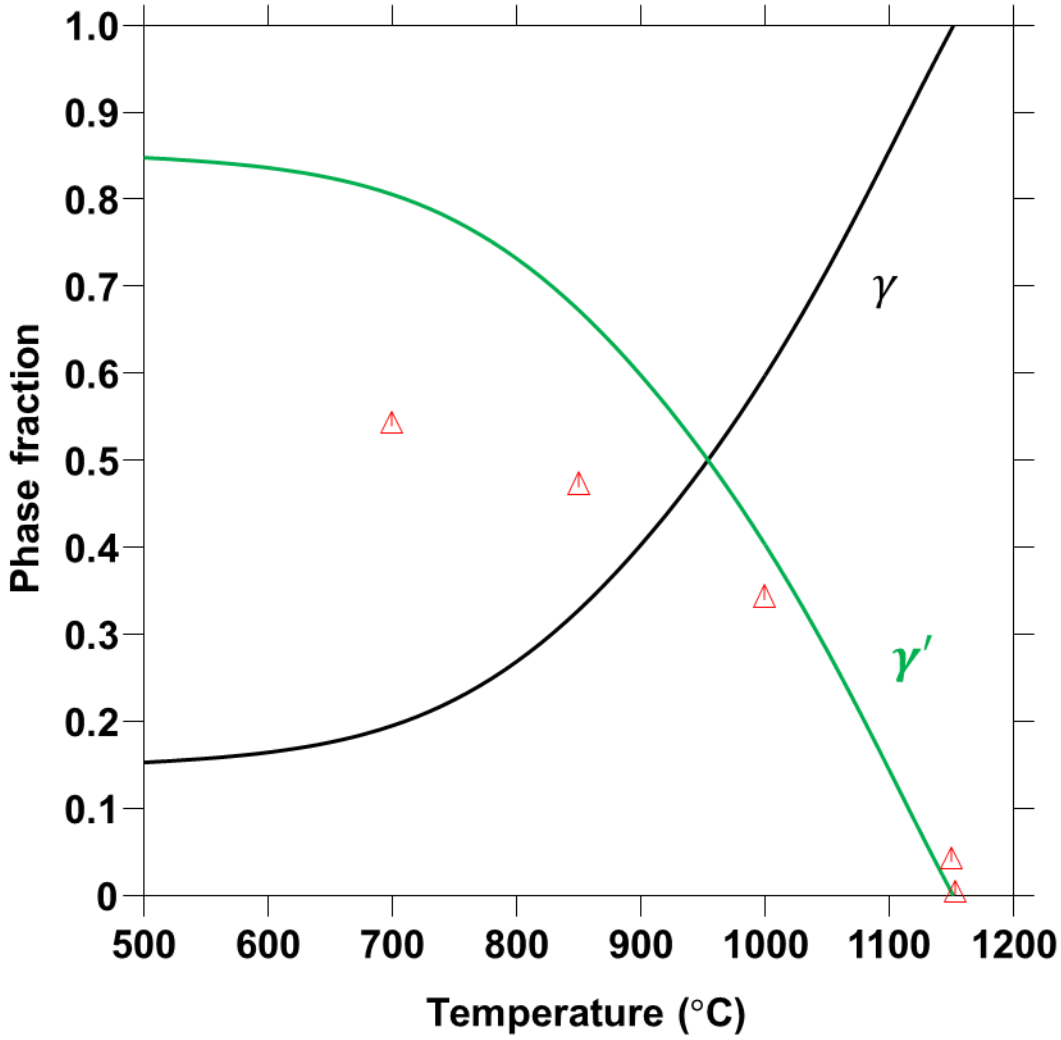

Figure 6.11. Fractions of γ and γ' for Ni-15Al-5Cr-2.5Pt-0.1Hf compared to experimental synchrotron data by Heidloff et al[160](⚠).

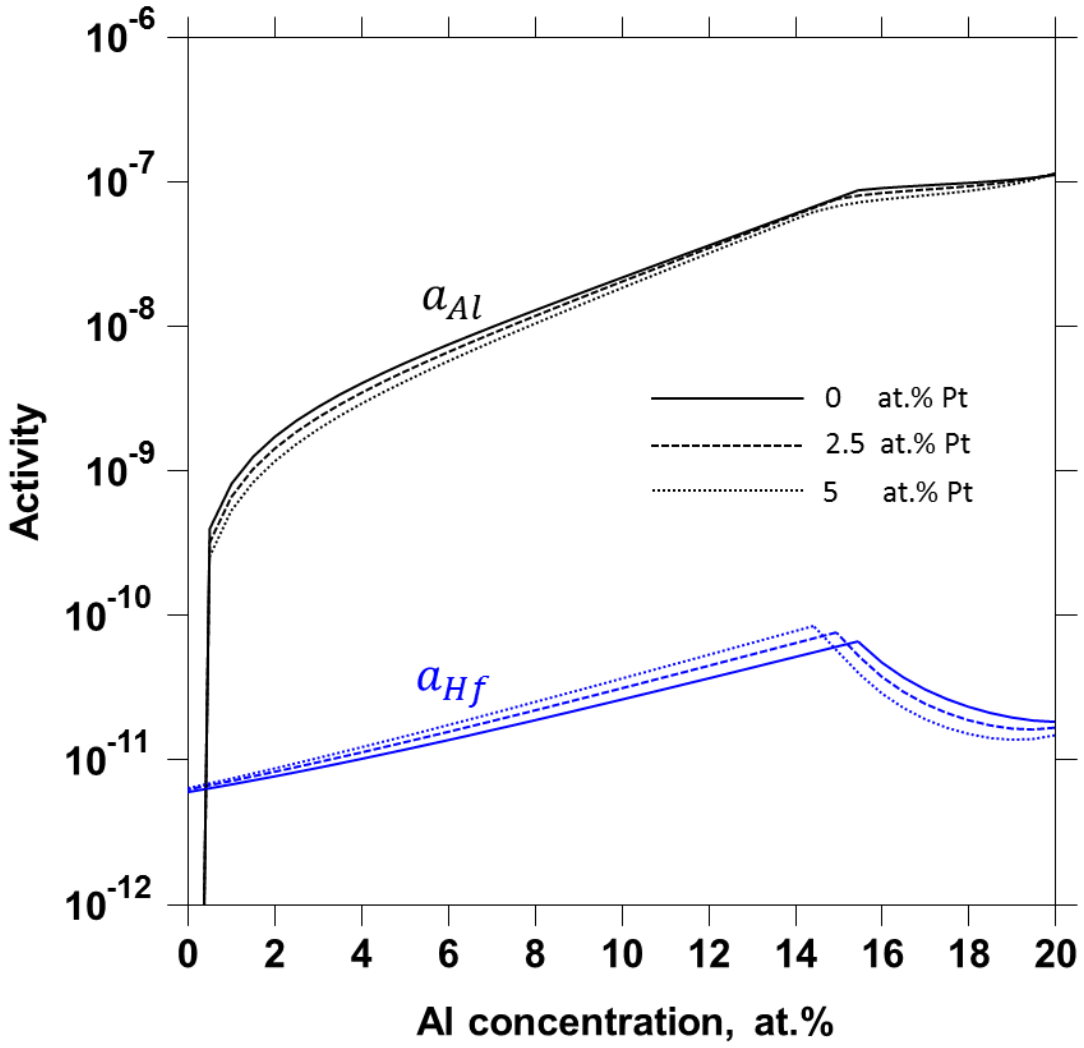

Figure 6.12. Hf (blue) and Al (black) activity for Ni-xAl-5Cr-XPt-0.1Hf (X=0,2.5 and 5 at.%) at 1150 °C from 0 to 20 at.% Al

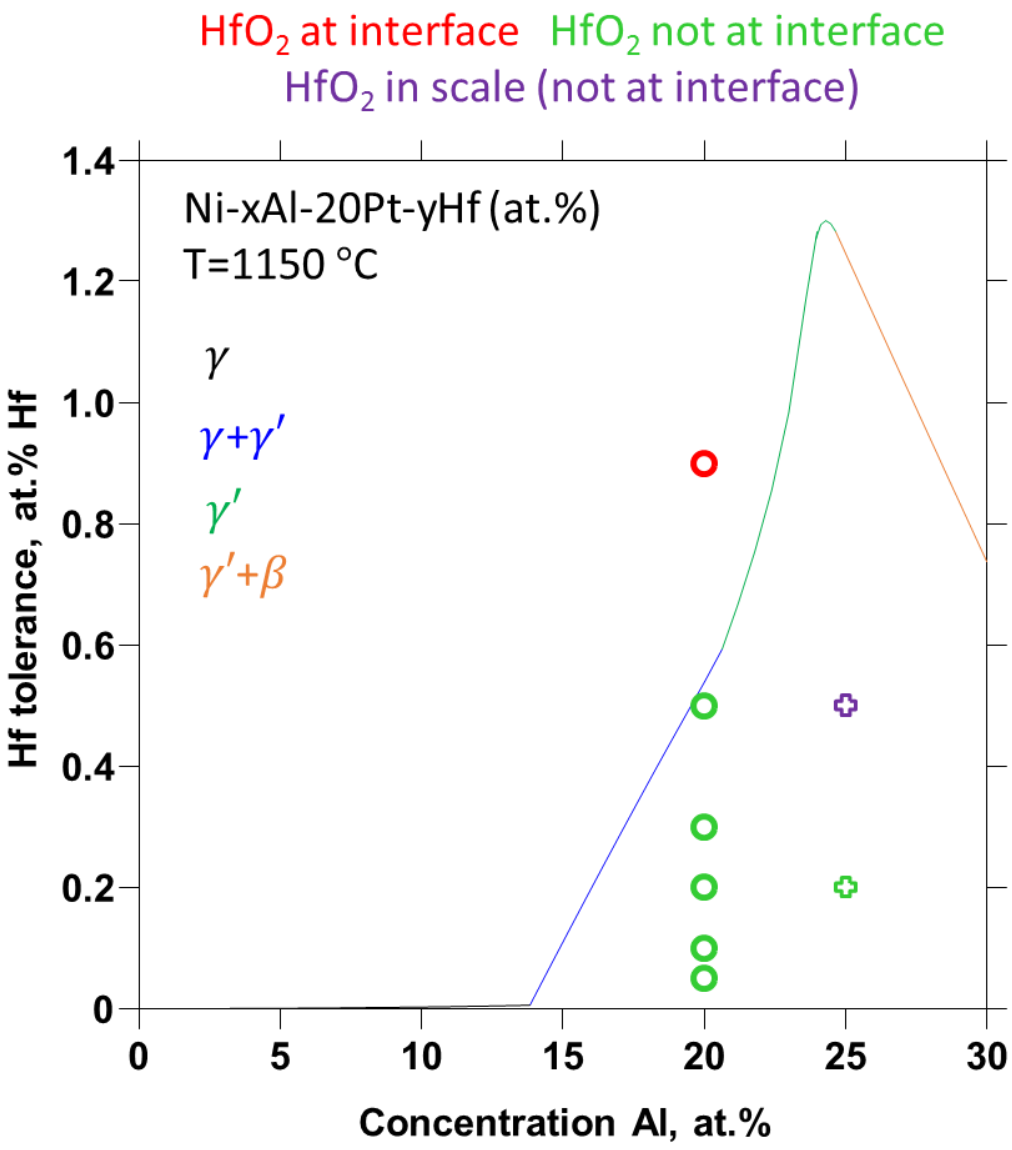

Figure 6.13. Hf tolerance in the Ni-20Pt-xAl-yHf system compared to cyclic oxidation experiments by Mu et al.[130] (✪) and isothermal oxidation experiments by Mu et al.[17] (○). Symbols indicate when HfO_2 was observed at the interface (green), when it was not observed at the interface (red), and when it was observed in the scale but not at the interface (purple).

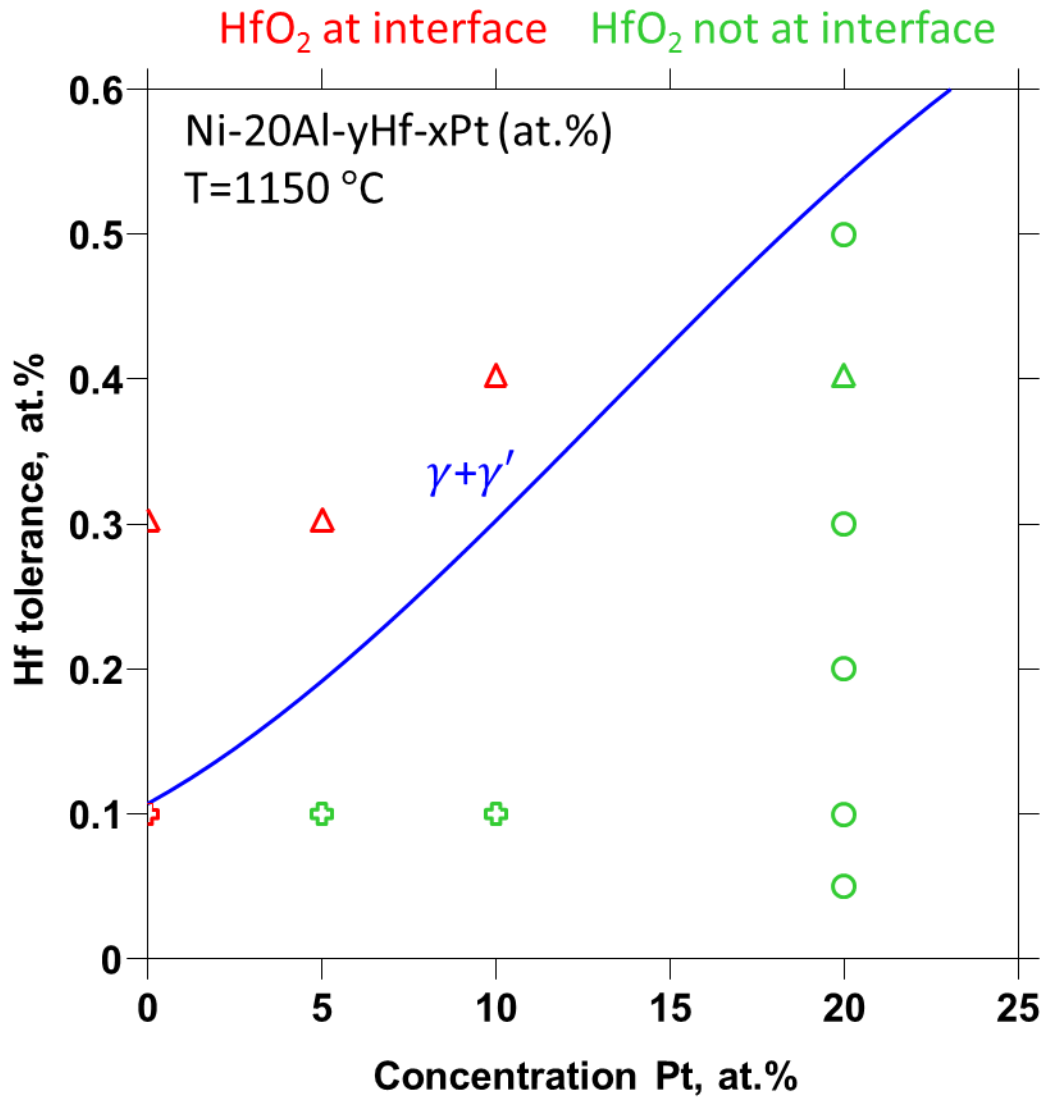

Figure 6.14. Hf tolerance in the Ni-20Pt-xAl-yHf system compared to cyclic oxidation experiments by Mu et al.[130] (✪), isothermal oxidation experiments by Mu et al.[17] (○), and cyclic oxidation experiments provided by Izumi et al[130](Δ). Symbols indicate when HfO_2 was observed at the interface (green) and when it was not observed at the interface (red).

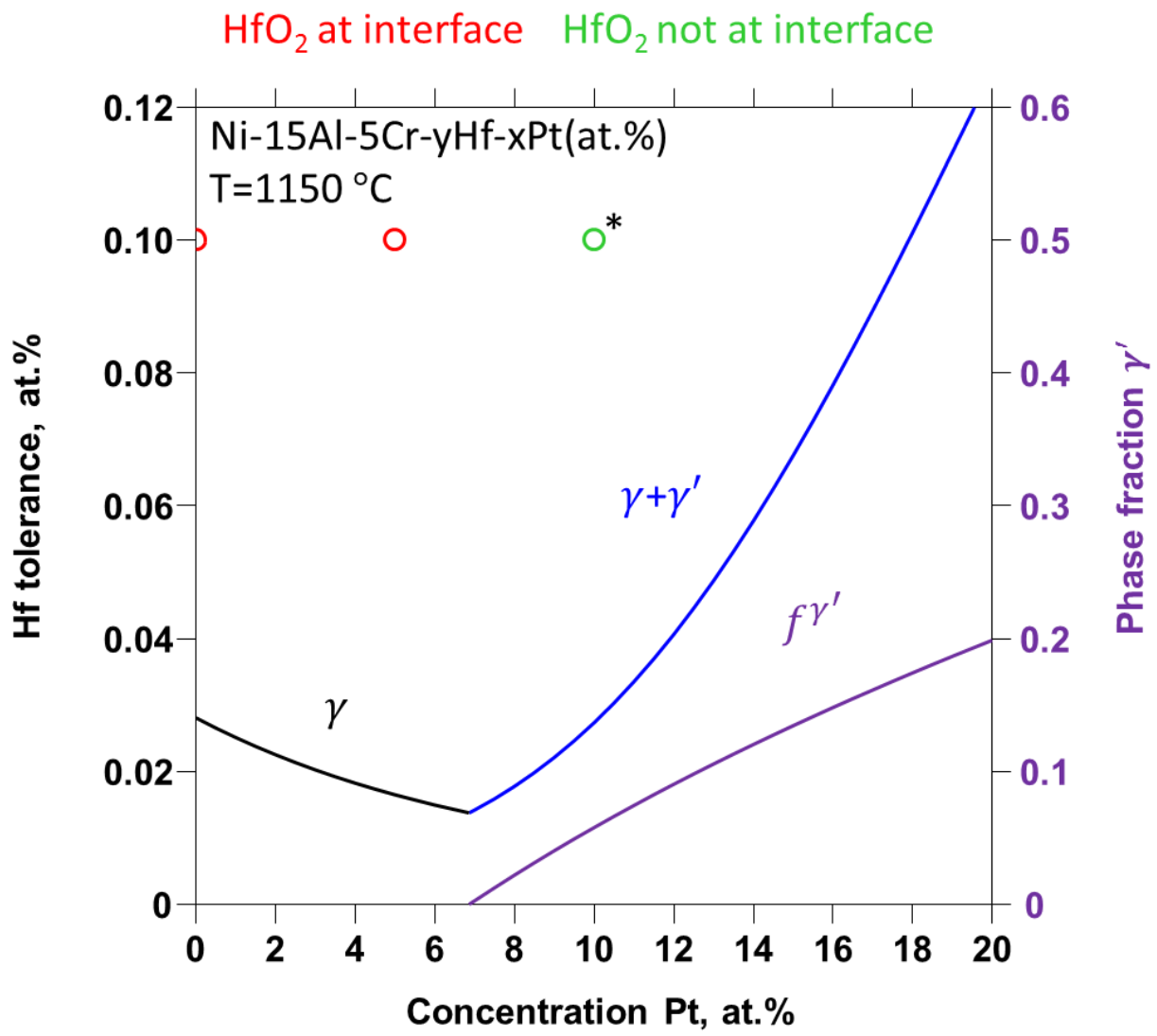

Figure 6.15. Hf tolerance in the Ni-15Al-5Cr-xPt-yHf system at 1150 °C compared to cyclic oxidation experiments by Mu et al.[130] (O). Symbols indicate when HfO_2 was observed at the interface (green) and when it was not observed at the interface (red). An asterisk is added because an internal precipitate is visible in the micrograph but unreported by the author.

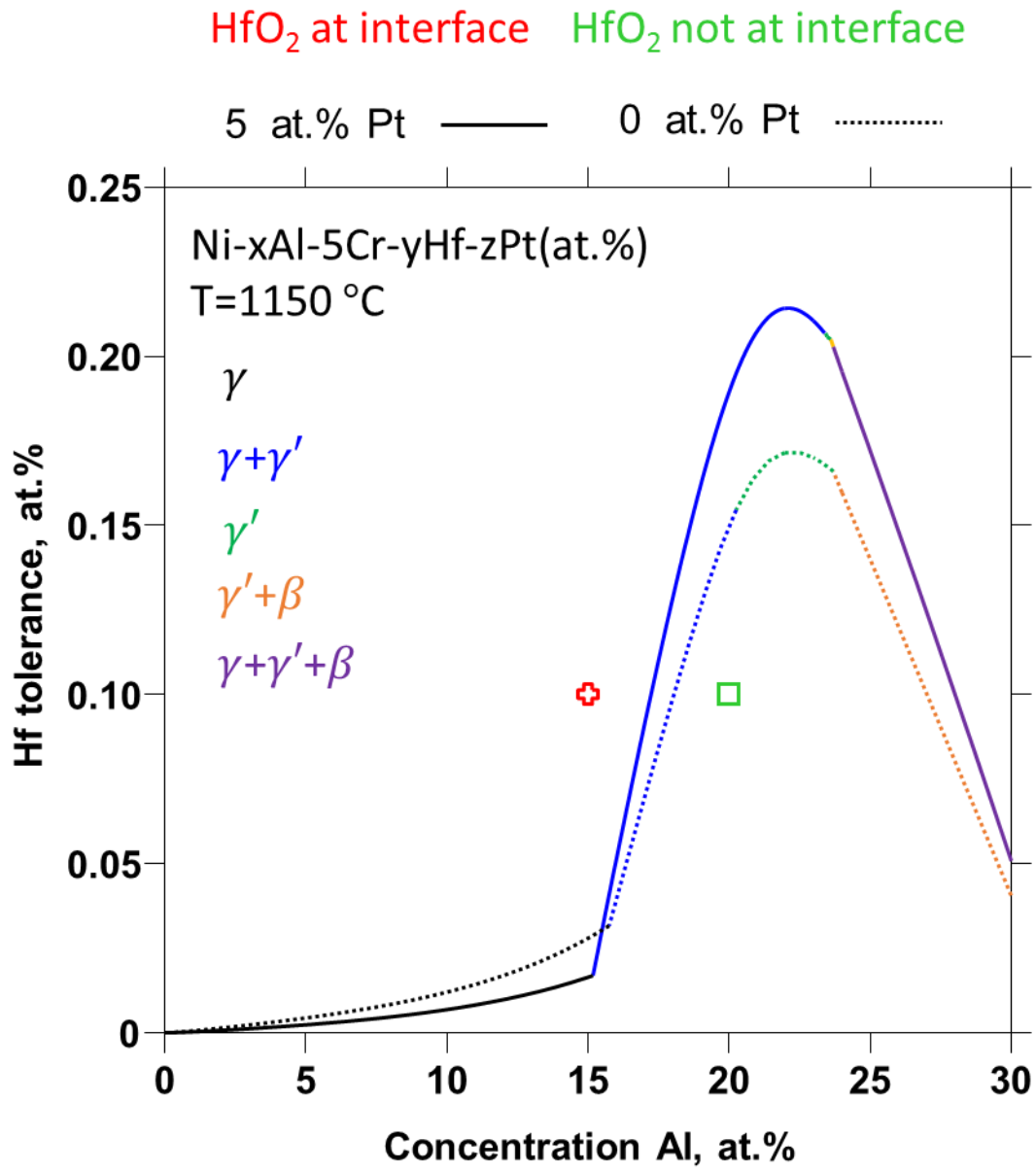

Figure 6.16. Hf tolerance in the Ni-xAl-5Cr-5Pt-yHf system at 1150 °C compared to cyclic oxidation experiments by Mu et al.[130] (✜) and unpublished work by Gleeson(□). Symbols indicate when HfO_2 was observed at the interface (green) and when it was not observed at the interface (red)

7 Conclusions and Future Work

7.1 Conclusions

A comprehensive study of the thermodynamics in the Ni-rich portion of the Al-Cr-Hf-NiPt-O system was performed in the present work using the calculation of phase diagram (CALPHAD) method, aided by first-principles calculations using density functional theory (DFT). Within the scope of this work, the following conclusions are drawn:

I. The Hf solubility in fcc Ni is investigated with a combination of first-principles calculations using SQS and new experiments in the Hf-Ni system. New experiments using high purity Hf are used to establish a greater degree of certainty about the phase boundary between Hf and Ni_5Hf. First-principles calculations using SQS established a stability for the ordered B2 phase in the Hf-Ni system. This has important implications for higher order systems since the B2 phase is often present in significant volume fractions in MRCALY alloys. The $L1_2$ phase is also investigated using finite temperature first-principles in this system since binary terms in the ordered $L1_2$ model play an important role in higher order systems.

II. The phase equilibria is modeled in the Ni-rich portion of the Al-Hf-Ni system and the Cr-Hf-Ni systems using a combination of first-principles calculations and new experiments. Experiments again use high purity Hf to avoid Zr contamination to establish more accurate phase equilibria. Solubility in the γ, γ', β, and η-Ni_7Hf_2 phases is modeled based on experiments at temperatures between 1273.15 K and 1473.15 K. Solubility of Al and Cr in the Ni_3Hf phase was also investigated using first-principles but no apparent solubility is found when using these calculated values in this model. Although most experiments in the literature agree with the present model there are a few sources of

disagreement. The disagreement in each case is suspected to be caused by Zr contamination in those experiments and a subsequent stabilization of Ni_5Hf by Zr.

III. A Ni-rich Al-Cr-Hf-Ni model is constructed out of the Ni-rich models of the Al-Hf-Ni and Cr-Hf-Ni systems and other models in the literature. Only the Al-Cr-Hf ternary model is unavailable in the literature. Since this system does not contain the $L1_2$ phase it is considered unimportant. Experimental equilibria from a quaternary alloy in the literature agreed well with calculations using this model.

IV. The thermodynamic description of the Ni-rich Al-Cr-Hf-Ni model is used to study the activity of Hf in selected quaternary alloys. It is shown that for small Cr concentrations in a Ni-rich Al-Cr-Hf-Ni alloy, the Hf activity decreases appreciably in the two-phase γ-γ' region as the system increases in Al concentration and Al activity. This was due to the large solubility of Hf in the γ' phase relative to the γ phase - since when the system increases in Al concentration it subsequently moves to tie-lines with a lower Hf activity.

V. The thermodynamic description of the Ni-rich Al-Cr-Hf-Ni system is combined with oxides in the binary systems and ternary systems to study the interface equilibrium between the alloy and Al_2O_3 with precipitation of HfO_2 at this interface. This phase boundary is dubbed the Hf-tolerance and is related to the competition between Al and Hf activities. The Hf-tolerance is compared to the oxidation behaviors of alloys in the Ni-rich Al-Hf-Ni and Al-Cr-Hf-Ni systems. Results are favorable in each case, even for cyclically oxidized alloys, and confirmed the performance improvement offered by γ'.

VI. A selection procedure is carried out to study the effects of alloying elements on the Hf-tolerance. The selection procedure targets elements which have a solubility of greater than 5 at.% Hf. These selected elements are Al, Co, Cr, Cu, Fe, Ga, Ge, Hf, Mn, Nb, Ni,

Pd, Pt, Sc, Si, Ta, Ti, V, and Zn. Mixing enthalpies in the γ phase and enthalpies of formation of compounds in the $L1_2$ phase are calculated between Hf and these elements to determine which would have the largest effect on the Hf activity in these phases. Pt, Pd, Ir, Rh and Si are the best candidates, in that order, with the largest negative mixing enthalpies calculated. Interestingly considering their widespread use in MCrAlYs, Co and Cr both had positive mixing enthalpies. Cr had the largest positive mixing enthalpy of all elements considered.

VII. Pt is shown to be the most effective alloying element and is chosen as a case study. A thermodynamic model is constructed for the Ni-rich Al-Cr-Hf-Ni-Pt system based on available data in the literature and ternary SQS data from the first-principles calculations. This model focuses on improving fitting to available phase boundaries and on describing the mixing enthalpy in the $L1_2$ and γ phase. This includes a remodeling of the Cr-Pt system, new modeling of the Hf-Pt system, new modeling of the Al-Cr-Pt and Cr-Ni-Pt systems, and modeling of the Al-Hf-Pt, Cr-Hf-Pt, and Hf-Ni-Pt systems based entirely on data from first-principles calculations. The resulting model agrees well with the available experiments in the Ni-rich Al-Cr-Hf-Ni-Pt system by reproducing the γ' solvus observed experimentally and having excellent agreement with measured phase equilibria for one sample annealed for long times at 1273.15 K.

VIII. Hf-tolerance calculations agree well with the Ni-rich Al-Hf-Ni-Pt and Al-Cr-Hf-Ni-Pt systems. Excellent agreement is found for 20 at.% Al and Pt concentrations up to 10 at.% but some disagreement is found for lower Al concentrations. The present calculations clearly demonstrate the beneficial effects of Pt when added to Ni-rich, oxidation resistant alloys containing Hf.

Overall this thesis provides a thermodynamic means of calculating the maximum concentration of Hf which can be added to an oxidation resistant alloy before massive HfO_2 precipitation occurs. In addition, this work also provides a thermodynamic description of the Ni-rich Al-Cr-Hf-Ni-Pt system which can aid others in designing new, oxidation resistant alloys. The present approach provided in this thesis should help target new oxidation resistant alloys for future study.

7.2 Future work

Based on the knowledge gained in this study, the following is recommended for future work:

I. The remaining elements to be studied are Y and Zr in the case of interfacial reaction with Al_2O_3. However, Y has very little solubility in the γ' phase and its oxide is so stable that the presented concept probably does not apply to the design of Y containing alloys. In-fact, the Y-Al-Oxides are so stable that it is far more likely that the more Y added to the alloy the worse the oxidation properties will become after some initial amount has been added. In that case the minimum Y needed to benefit Al2O3 growth would be more useful than the maximum needed to precipitate Y-Al-oxides (which, again, will be excessively small.) Zr, on the other hand has some solubility in the γ' phase and has an oxide stability near Al_2O_3 signaling that a similar design concept will be applicable to this element. The bonding between Zr and Hf is also quite similar and their oxides form large solid solutions with each other. This makes the concept of co-doping interesting to study as well and opens up the possibility of also studying the Al_2O_3 scale.

II. Despite its detrimental effects on Hf, it is also of interest to add Co to the present alloy system. Many MCRALYs include Co to aid in thermal expansion matching and to improve the corrosion resistance of the underlying alloy. However, this would be another five component system when added to the Ni-rich Al-Cr-Hf-Ni system and, as was seen in this thesis, it is important to have an excellent model of the phase boundaries involving Hf and the γ' phase. Hence, care should be taken when constructing this database. In addition, further thermodynamic experiments may be needed in this case and in the case to develop this database.

III. Since Pt has proved successful within this model of predicting the Hf-tolerance it is likely that Pd, Ir, Rh and Si will all have varying degrees of effectiveness as well. However, in each case it is important to have well described equilibria in nearly every system involved. There were several thermodynamic experiments available to guide the construction of the the Ni-rich Al-Cr-Hf-Ni-Pt system but there are far fewer for systems involving Pd, Ir, Rh and even Si. A combination of high accuracy first-principles calculations and experiments are probably needed to qualify any future databases involving these elements.

References

[1] R. C. Reed, *The Superalloys: Fundamentals and Applications*. Cambridge University Press, 2006.

[2] D. J. Young, *High Temperature Oxidation and Corrosion of Metals*, vol. 1. Elsevier, 2008.

[3] P. Kofstad, *High Temperature Corrosion*, 1st ed. Barking, Essex, Engliand: Elsevier Applied Science Publishers LTD, 1988.

[4] J. R. Nicholls, "Advances in Coating Design for High-Performance Gas Turbines," *MRS Bull.*, vol. 28, no. 9, pp. 659–670, Jan. 2011.

[5] B. A. Pint, J. R. DiStefano, and I. G. Wright, "Oxidation resistance: One barrier to moving beyond Ni-base superalloys," *Mater. Sci. Eng. A*, vol. 415, no. 1–2, pp. 255–263, Jan. 2006.

[6] G. C. Wood, "High-temperature oxidation of alloys," *Oxid. Met.*, vol. 2, no. 1, pp. 11–57, 1970.

[7] M. P. Brady, I. G. Wright, and B. Gleeson, "Alloy design strategies for promoting protective oxide-scale formation," *JOM*, vol. 52, no. 1, pp. 16–21, Jan. 2000.

[8] C. S. Tedmon, "The Effect of Oxide Volatilization on the Oxidation Kinetics of Cr and Fe-Cr Alloys," *J. Electrochem. Soc.*, vol. 113, no. 8, p. 766, Aug. 1966.

[9] D. J. Young and B. A. Pint, "Chromium Volatilization Rates from Cr2O3 Scales into Flowing Gases Containing Water Vapor," *Oxid. Met.*, vol. 66, no. 3–4, pp. 137–153, Nov. 2006.

[10] F. S. Pettit, "Oxidation Mechanisms for Nickel-Aluminum Alloys at Temperatures between 900 and 1300 Degrees C," *J. Met.*, vol. 20, no. 1, p. A9-, 1968.

[11] D. A. Woodford, “Gas phase embrittlement and time dependent cracking of nickel based superalloys,” *Energy Mater.*, vol. 1, no. 1, pp. 59–79, Mar. 2006.

[12] M. Bensch, A. Sato, N. Warnken, E. Affeldt, R. C. Reed, and U. Glatzel, “Modelling of High Temperature Oxidation of Alumina-Forming Single-Crystal Nickel-Base Superalloys,” *Acta Mater.*, vol. 60, no. 15, pp. 5468–5480, Sep. 2012.

[13] F. Pettit, “Oxidation Mechanisms for Ni-Al Alloys at Temperatures Between 900 And 1300 C,” *AIME Met Soc Trans*, 1967.

[14] C. S. Giggins and F. S. Pettit, “Oxidation of Ni-Cr-Al Alloys Between 1000° and 1200°C,” *J. Electrochem. Soc.*, vol. 118, no. 11, p. 1782, Nov. 1971.

[15] B. Gleeson, “Thermal Barrier Coatings for Aeroengine Applications,” *J. Propuls. Power*, vol. 22, no. 2, pp. 375–383, Mar. 2006.

[16] P. Y. Hou, “Impurity Effects on Alumina Scale Growth,” *J. Am. Ceram. Soc.*, vol. 86, no. 4, pp. 660–68, Apr. 2003.

[17] N. Mu, “High temperature oxidation behavior of gammaNi+gamma’Ni3Al alloys and coatings modified with Pt and reactive elements,” Iowa State University, 2007.

[18] B. A. Pint, “Optimization of Reactive-Element Additions to Improve Oxidation Performance of Alumina-Forming Alloys,” *J. Am. Ceram. Soc.*, vol. 86, no. 4, pp. 686–95, Apr. 2003.

[19] L. Kaufman and H. Nesor, “Coupled phase diagrams and thermochemical data for transition metal binary systems-IV,” *Calphad*, vol. 2, no. 4, pp. 295–318, Jan. 1978.

[20] Z.-K. Liu, “First-Principles Calculations and CALPHAD Modeling of Thermodynamics,” *J. Phase Equilibria Diffus.*, vol. 30, no. 5, pp. 517–534, Oct. 2009.

[21] P. Hohenberg and W. Kohn, “Inhomogeneous Electron Gas,” *Phys. Rev.*, vol. 136, no. 3B,

pp. B864–B871, Nov. 1964.

[22] W. K. and L. J. Sham, “Self-Consistent Equations Including Exchange and Correlation Effects,” *Phys. Rev*, vol. 140, p. A1133, 1965.

[23] J. P. Perdew, K. A. Jackson, M. R. Pederson, D. J. Singh, and C. Fiolhais, “Atoms, molecules, solids, and surfaces: Applications of the generalized gradient approximation for exchange and correlation,” *Phys. Rev. B*, vol. 46, no. 11, pp. 6671–6687, Sep. 1992.

[24] J. P. Perdew, K. Burke, and M. Ernzerhof, “Generalized Gradient Approximation Made Simple,” *Phys. Rev. Lett.*, vol. 77, no. 18, pp. 3865–3868, Oct. 1996.

[25] V. L. Chevrier, S. P. Ong, R. Armiento, M. K. Y. Chan, and G. Ceder, “Hybrid density functional calculations of redox potentials and formation energies of transition metal compounds,” *Phys. Rev. B*, vol. 82, no. 7, p. 75122, Aug. 2010.

[26] Z.-K. Liu, “First-Principles Calculations and CALPHAD Modeling of Thermodynamics,” *J. Phase Equilibria Diffus.*, vol. 30, no. 5, pp. 517–534, Sep. 2009.

[27] S. L. Shang, Y. Wang, D. Kim, and Z. K. Liu, “First-principles thermodynamics from phonon and Debye model: Application to Ni and Ni3Al,” *Comput. Mater. Sci.*, vol. 47, no. 4, pp. 1040–1048, 2010.

[28] Y. Wang, Z.-K. Liu, and L.-Q. Chen, “Thermodynamic properties of Al, Ni, NiAl, and Ni3Al from first-principles calculations,” *Acta Mater.*, vol. 52, no. 9, pp. 2665–2671, May 2004.

[29] S. Shang, Y. Wang, and Z.-K. Liu, “First-principles elastic constants of α- and θ-Al[sub 2]O[sub 3],” *Appl. Phys. Lett.*, vol. 90, no. 10, p. 101909, Mar. 2007.

[30] A. van de Walle and G. Ceder, “The effect of lattice vibrations on substitutional alloy thermodynamics,” *Rev. Mod. Phys.*, vol. 74, no. 1, pp. 11–45, Jan. 2002.

[31] A. A. Quong and A. Y. Liu, “First-principles calculations of the thermal expansion of metals,” *Phys. Rev. B*, vol. 56, no. 13, pp. 7767–7770, Oct. 1997.

[32] A. van de Walle, M. Asta, and G. Ceder, “The alloy theoretic automated toolkit: A user guide,” *Calphad*, vol. 26, no. 4, pp. 539–553, Dec. 2002.

[33] V. L. Moruzzi, J. F. Janak, and K. Schwarz, “Calculated thermal properties of metals,” *Phys. Rev. B*, vol. 37, no. 2, pp. 790–799, 1988.

[34] S.-L. Shang, Y. Wang, D. Kim, and Z.-K. Liu, “First-principles thermodynamics from phonon and Debye model: Application to Ni and Ni3Al,” *Comput. Mater. Sci.*, vol. 47, no. 4, pp. 1040–1048, Feb. 2010.

[35] X. L. Liu, B. K. VanLeeuwen, S.-L. Shang, Y. Du, and Z.-K. Liu, “On the scaling factor in Debye–Grüneisen model: A case study of the Mg–Zn binary system,” *Comput. Mater. Sci.*, vol. 98, pp. 34–41, Feb. 2015.

[36] Q. Chen and B. Sundman, “Calculation of debye temperature for crystalline structures—a case study on Ti, Zr, and Hf,” *Acta Mater.*, vol. 49, no. 6, pp. 947–961, Apr. 2001.

[37] C. Kittel and P. McEuen, *Introduction to solid state physics*. 1976.

[38] M. Hillert, “The compound energy formalism,” *J. Alloys Compd.*, vol. 320, no. 2, pp. 161–176, May 2001.

[39] H. L. Lukas, G. S. Fries, and B. Sundman, *Computational Thermodynamics: The Calphad Method*, 1st ed. Cambridge CB2 8RU, UK: Cambridge University Press, 2007.

[40] M. Hillert, *Phase equilibria, phase diagrams and phase transformations: their thermodynamic basis*. 2007.

[41] A. T. Dinsdale, “SGTE data for pure elements,” *Calphad*, vol. 15, no. 4, pp. 317–425, Oct. 1991.

[42] T. Gheno, B.-C. Zhou, A. Ross, X. Liu, G. Lindwall, Z.-K. Liu, and B. Gleeson, “A Thermodynamic Approach to Guide Reactive Element Doping: Hf Additions to NiCrAl,” *Oxid. Met.*, pp. 1–14, Jan. 2017.

[43] B. A. Pint, K. L. More, and I. G. Wright, “Effect of Quaternary Additions on the Oxidation Behavior of Hf-Doped NiAl,” *Oxid. Met.*, vol. 59, no. 3/4, pp. 257–283, 2003.

[44] B. Gleeson, N. Mu, and S. Hayashi, “Compositional factors affecting the establishment and maintenance of Al2O3 scales on Ni–Al–Pt systems,” *J. Mater. Sci.*, vol. 44, no. 7, pp. 1704–1710, Feb. 2009.

[45] G. . Firstov, J. Van Humbeeck, and Y. . Koval, “Comparison of high temperature shape memory behaviour for ZrCu-based, Ti–Ni–Zr and Ti–Ni–Hf alloys,” *Scr. Mater.*, vol. 50, no. 2, pp. 243–248, Jan. 2004.

[46] V. N. Yeremenko, E. L. Semenova, L. A. Tretyachenko, and V. M. Petyukh, “Constitution of the Hf-Ni system up to 50 at.% Ni,” *J. Alloys Compd.*, vol. 191, no. 1, pp. 117–119, Jan. 1993.

[47] Y. Kim and R. Ashbrook, “Directionally solidified pseudo-binary eutectics of Ni-Cr-(Hf, Zr),” 1975.

[48] V. Khorunov, V. Ivanchenko, and V. Kvasnitskij, “Structure and phase composition of Ni-Cr-Zr and Ni-Cr-Hf alloys used as brazing alloys,” *Avtom. Svarka*, 1999.

[49] A. Berche, J. C. Tédenac, and P. Jund, “Phase diagram and enthalpy of formation of Hf-Ni-Sn,” *Comput. Mater. Sci.*, vol. 125, pp. 271–277, Dec. 2016.

[50] T. Wang, Z. Jin, and J.-C. Zhao, “Experimental study and reassessment of the Ni-Hf binary system,” *Zeitschrift für Met.*, vol. 92, no. 5, pp. 441–446, 2001.

[51] C. Zhang, J. Zhu, Y. Yang, H.-B. Cao, F. Zhang, W.-S. Cao, and Y. A. Chang,

"Thermodynamic modeling and experimental investigation of the Ni-rich corner of the Ni?Al?Hf system," *Intermetallics*, vol. 16, no. 2, pp. 139–147, Feb. 2008.

[52] X. Yang, C. Pin, and A. Fane, "Separation of hafnium from zirconium by extraction chromatography with liquid anionic exchangers," *J. Chromatogr. Sci.*, 1999.

[53] M. Hajjaji, "Solid solubility of hafnium in nickel," *J. Alloys Compd.*, vol. 274, no. 1–2, pp. 185–188, 1998.

[54] V. N. Svechnikov, A. K. Shrin, and G. P. Dmitriyeva, "The Hafnium-Nickel Equilibrium Diagram," *Izv. Akad. Nauk SSSR, Met.*, vol. 6, pp. 176–179, 1967.

[55] L. Bsenko, "The Hf-Ni and Zr-Ni systems in the region 65 – 80 at.% Ni," *J. Less Common Met.*, vol. 63, no. 2, pp. 171–179, 1979.

[56] N. Selhaoui, J. C. Gachon, and J. Hertz, "Enthalpies of formation of some solid hafnium nickel compounds and of the Ni-Rich HfNi liquid by direct reaction calorimetry," *Metall. Trans. B*, vol. 23, no. 6, pp. 815–819, 1992.

[57] L. Bencze and K. Hilpert, "Thermochemistry of the Ni-Hf system—Intermetallic phases," *Metall. Mater. Trans. A*, vol. 27, no. 11, pp. 3576–3590, 1996.

[58] D. Shin, R. Arróyave, and Z.-K. Liu, "Thermodynamic modeling of the Hf–Si–O system," *Calphad*, vol. 30, no. 4, pp. 375–386, Dec. 2006.

[59] Q. Guo and O. J. Kleppa, "Standard Enthalpies of Formation of Ni3V, Ni3Hf, PdsHf, and Pt3Sc and Systematics of AHof for Ni3Me (Me = La, Hf, Ta), Pd3Me (Me," *J. Phys. Chem.*, vol. 99, no. 9, pp. 2854–2856, Mar. 1995.

[60] Q. Guo and O. J. Kleppa, "Standard enthalpies of formation of some alloys formed between group IV elements and group VIII elements, determined by high-temperature direct synthesis calorimetry," *J. Alloys Compd.*, vol. 269, no. 1–2, pp. 181–186, 1998.

[61] V. N. Yeremenko, E. L. Semenova, L. a. Tretyachenko, and V. M. Petyukh, “Constitution of the Hf-Ni system up to 50 at.% Ni,” *Journal of Alloys and Compounds*, vol. 191, no. 1. pp. 117–119, 1993.

[62] V. V. Sudavtsova, N. V. Podoprigora, and M. A. Shevchenko, “Thermodynamic properties of Ni-Hf melts,” *Powder Metall. Met. Ceram.*, vol. 49, no. 7–8, pp. 478–483, 2010.

[63] N. V. Podoprigora and V. S. Sudavtsova, “Thermodynamic properties of liquid alloys of the Ni-Hf system,” *Russ. Metall.*, vol. 2009, no. 2, pp. 107–112, 2009.

[64] V. Sudavtsova and N. Sharkina, “Interaction in liquid alloys of Fe–Hf and Ni–Hf systems,” *Neorg. Mater*, 1998.

[65] O. Levy, G. L. W. Hart, and S. Curtarolo, “Hafnium binary alloys from experiments and first principles,” *Acta Mater.*, vol. 58, no. 8, pp. 2887–2897, 2010.

[66] N. N. Eremenko, E. L. Semenova, L. A. Tret’yachenko, and V. . Petyukh, “Reaction of equiatomic binary compounds in ternary systems formed by group-IV transition metals with nickel,” *Inorg. Mater.*, vol. 28, pp. 923–927, 1992.

[67] P. Nash and D. R. F. West, “Phase equilibria in Ni-rich region of Ni–Cr–Hf system,” *Met. Sci.*, vol. 15, no. August, pp. 347–352, Aug. 1981.

[68] P. Nash and D. R. F. West, “Phase equilibria in Ni-rich region of Ni-AI-Hf system,” *Met. Sci.*, vol. 15, no. August, pp. 347–352, 1981.

[69] K. Lee and P. Nash, “The Al-Hf-Ni system (Aluminum-Hafnium-Nickel),” *J. phase equilibria*, 1991.

[70] P. Nash and D. R. F. West, “Phase equilibria in Ni-rich region of Ni–Cr–Hf system,” *Met. Sci.*, vol. 15, no. August, pp. 347–352, 1981.

[71] I. Ansara, N. Dupin, H. L. Lukas, and B. Sundman, “Thermodynamic assessment of the Al?Ni system,” *J. Alloys Compd.*, vol. 247, no. 1–2, pp. 20–30, Jan. 1997.

[72] N. Dupin, I. Ansara, and B. Sundman, “Thermodynamic re-assessment of the ternary system Al-Cr-Ni,” *Calphad*, vol. 25, no. 2, pp. 279–298, Jun. 2001.

[73] A. Kusoffsky, N. Dupin, and B. Sundman, “On the compound energy formalism applied to fcc ordering.,” *Calphad*, vol. 25, no. 4, pp. 549–565, Dec. 2001.

[74] G. Kresse, M. Marsman, and J. Furthmuller, “VASP the Guide,” *http://cms.mpi.univie.ac.at/vasp/vasp/vasp.html*, 2016. [Online]. Available: http://cms.mpi.univie.ac.at/vasp/vasp/vasp.html. [Accessed: 01-Jan-2017].

[75] Y. Wang, Z. K. Liu, and L. Q. Chen, “Thermodynamic properties of Al, Ni, NiAl, and Ni3Al from first-principles calculations,” *Acta Mater.*, vol. 52, no. 9, pp. 2665–2671, 2004.

[76] S. Shang, Y. Wang, and Z.-K. Liu, “First-principles elastic constants of α- and θ-Al2O3,” *Appl. Phys. Lett.*, vol. 90, no. 10, p. 101909, Mar. 2007.

[77] C. Jiang, C. Wolverton, J. Sofo, L.-Q. Chen, and Z.-K. Liu, “First-principles study of binary bcc alloys using special quasirandom structures,” *Phys. Rev. B*, vol. 69, no. 21, p. 214202, Jun. 2004.

[78] C. Wolverton, “Crystal structure and stability of complex precipitate phases in Al–Cu–Mg–(Si) and Al–Zn–Mg alloys,” *Acta Mater.*, vol. 49, no. 16, pp. 3129–3142, Sep. 2001.

[79] C. Jiang, L.-Q. Chen, and Z.-K. Liu, “First-principles study of constitutional point defects in B2 NiAl using special quasirandom structures,” *Acta Mater.*, vol. 53, no. 9, pp. 2643–2652, May 2005.

[80] “Materials Preparation Center, Ames Laboratory USDOE, Ames IA, USA.” .

[81] S. Kirklin, J. E. Saal, B. Meredig, A. Thompson, J. W. Doak, M. Aykol, S. Rühl, and C. Wolverton, “The Open Quantum Materials Database (OQMD): assessing the accuracy of DFT formation energies,” *npj Comput. Mater.*, vol. 1, no. 1, p. 15010, Dec. 2015.

[82] A. D. Pelton, S. A. Degterov, G. Eriksson, C. Robelin, and Y. Dessureault, “The modified quasichemical model I—Binary solutions,” *Metall. Mater. Trans. B*, vol. 31, no. 4, pp. 651–659, Aug. 2000.

[83] V. N. Svechnikov, A. K. Shrin, and G. P. Dmitriyeva, “The Hafnium-Nickel Equilibrium Diagram,” *Izv. Akad. Nauk SSSR, Met.*, vol. 6, pp. 176–179, 1967.

[84] W. J. Zhu, L. I. Duarte, and C. Leinenbach, “Experimental study and thermodynamic assessment of the Cu–Ni–Ti system,” *Calphad*, vol. 47, pp. 9–22, Dec. 2014.

[85] N. Wang, C. Li, Z. Du, and F. Wang, “Experimental study and thermodynamic re-assessment of the Ni–Zr system,” *Calphad*, vol. 31, no. 4, pp. 413–421, Dec. 2007.

[86] J. Stringer, “The reactive element effect in high-temperature corrosion,” *Mater. Sci. Eng. A*, vol. 120–121, pp. 129–137, Nov. 1989.

[87] L. Kaufman and H. Nesor, “Calculation of the Ni-Al-W, Ni-Al-Hf and Ni-Cr-Hf systems,” *Can. Metall. Q.*, vol. 14, no. 3, pp. 221–232, Jul. 1975.

[88] R. R. Nagarajan, A. K. Jena, and R. K. Ray, “Phase Equilibria in the gamma-prime-Rich Region of the Ni-Al-Hf System,” *Zeitschrift für Metallkunde*, vol. 88. pp. 87–90, 1997.

[89] T. Wang, Z. Jin, and J.-C. Zhao, “Thermodynamic assessment of the Al-Hf binary system,” *J. Phase Equilibria*, vol. 23, no. 5, pp. 416–423, Oct. 2002.

[90] J. Pavlů, J. Vřešt’ál, and M. Šob, “Thermodynamic modeling of Laves phases in the Cr–Hf and Cr–Ti systems: Reassessment using first-principles results,” *Calphad*, vol. 34, no. 2, pp. 215–221, Jun. 2010.

[91] P. Suprunenko and V. Markiv, “Magnetic and X-ray structural study of Laves phases in -Cr-Al ternary systems,” *Izv. Akad. Nauk*, 1984.

[92] V. Raghavan, “Al-Hf-Ni (Aluminum-Hafnium-Nickel),” *J. Phase Equilibria Diffus.*, vol. 30, no. 1, pp. 64–66, Feb. 2009.

[93] V. Raghavan, “Al-Hf-Ni (Aluminum-Hafnium-Nickel),” *J. Phase Equilibria Diffus.*, vol. 27, no. 5, pp. 491–492, Oct. 2006.

[94] G. Ghosh and Materials Science International Team, MSIT®, “Al-Hf-Ni Ternary Phase Diagram Evaluation {·} Phase diagrams, crystallographic and thermodynamic data: Datasheet from MSI Eureka in SpringerMaterials (http://materials.springer.com/msi/docs/sm{_}msi{_}r{_}10{_}012751{_}02).” MSI Materials Science International Services GmbH.

[95] S. Miura, Y.-M. Hong, T. Suzuki, and Y. Mishima, “Liquidus and solidus temperatures of Ni-solid solution in Ni-Al-X (X: Ti, Zr, and Hf) ternary systems,” *J. Phase Equilibria*, vol. 20, no. 3, pp. 193–198, May 1999.

[96] M. Albers, M. Sai Baba, D. Kath, M. Miller, and K. Hilpert, “Chemical Activities in the Solid Solution of Hf in Ni3Al,” *Berichte der Bunsengesellschaft für Phys. Chemie*, vol. 96, no. 11, pp. 1663–1668, Nov. 1992.

[97] J. K. Stalick and R. M. Waterstrat, “The Hafnium-Platinum Phase Diagram,” *J. Phase Equilibria Diffus.*, vol. 35, no. 1, pp. 15–23, Feb. 2014.

[98] R. Hu and P. Nash, “Review: Experimental enthalpies of formation of compounds in Al-Ni-X systems,” *J. Mater. Sci.*, vol. 41, no. 3, pp. 631–641, Feb. 2006.

[99] S. Ochiai, Y. Oya, and T. Suzuki, “Solubility Data in Ni3Al with Ternary Additions,” *Bull. P.M.E. (T.I.T.)*, vol. 52, 1983.

[100] R. R. Nagarajan, A. K. Jena, and R. K. Ray, “Phase Equilibria in the γ’-Rich Region of the Ni-Al-Hf System,” *Zeitschrift Fur Met.*, vol. 88, no. 1, pp. 87–97, 1997.

[101] S. I. Mudryi and O. V. Shved, “Structural Transformations and Thermal Expansion in Aluminum Alloys of the Al?Ni?Zr and Al?Ni?Hf Systems,” *Mater. Sci.*, vol. 52, no. 2, pp. 227–232, Sep. 2016.

[102] V. Y. Markiv and V. V. Burnashova, “The Nf-Ni-Al System (In Russian),” *Izv. Akad. Nauk SSSR, Metal.*, vol. 6. pp. 181–182, 1969.

[103] K. P. Gupta, “The Cr-Hf-Ni system (chromium-hafnium-nickel),” *J. Phase Equilibria*, vol. 22, no. 1, pp. 78–84, Jan. 2001.

[104] K. Gupta, “The Cr-Ni-Hf (Chromium-Nickel-Hafnium) System,” *J. Phase Equilibria Diffus.*, 2010.

[105] X. Feng, A. Hope, and J. C. Lippold, “Effect of Cr on eutectic phase formation and solidification temperature range in Ni-Cr-Hf system,” *Mater. Lett.*, vol. 116, pp. 79–81, 2014.

[106] L. Kaufman and H. Bernstein, “Computer calculation of phase diagrams. With special reference to refractory metals,” 1970.

[107] A. Dinsdale, “SGTE Data for Pure Elements,” *CALPHAD*, vol. 15, no. 4, pp. 317–425, 1991.

[108] O. Redlich and A. Kister, “Algebraic Representation of Thermodynamic Properties and the Classification of Solutions,” *Ind. Eng. Chem.*, vol. 40, no. 2, pp. 345–348, Feb. 1948.

[109] I. Ansara, N. Dupin, H. L. Lukas, and B. Sundman, “Thermodynamic assessment of the Al-Ni system,” *J. Alloys Compd.*, vol. 247, no. 1–2, pp. 20–30, Jan. 1997.

[110] V. Markiv and V. Burnashova, “Hf--Ni--Al SYSTEM.,” *Izv. Akad. Nauk SSSR, Met. No.*

6, 181-4 (, 1969.

[111] I. Ansara, B. Sundman, and P. Willemin, “Thermodynamic modeling of ordered phases in the Ni□Al system,” *Acta Metall.*, vol. 36, no. 4, pp. 977–982, Apr. 1988.

[112] T. Abe and B. Sundman, “A description of the effect of short range ordering in the compound energy formalism,” *Calphad-Computer Coupling Phase Diagrams Thermochem.*, vol. 27, no. 4, pp. 403–408, 2003.

[113] B. Jansson, “Trita-Mac-0234,” Stockholm, Sweden.

[114] S. Shang, Y. Wang, D. Kim, C. Zacherl, Y. Du, and Z. Liu, “Structural, vibrational, and thermodynamic properties of ordered and disordered Ni(1-x)Pt(x) alloys from first-principles calculations,” *Phys. Rev. B*, vol. 83, no. 14, p. 144204, 2011.

[115] C. Jiang, C. Wolverton, J. Sofo, L.-Q. Chen, and Z.-K. Liu, “First-principles study of binary bcc alloys using special quasirandom structures,” *Phys. Rev. B*, vol. 69, no. 21, p. 214202, Jun. 2004.

[116] C. Jiang, “First-principles study of ternary bcc alloys using special quasi-random structures,” *Acta Mater.*, vol. 57, no. 16, pp. 4716–4726, Sep. 2009.

[117] D. Shin, A. van de Walle, Y. Wang, and Z.-K. Liu, “First-principles study of ternary fcc solution phases from special quasirandom structures,” *Phys. Rev. B*, vol. 76, no. 14, p. 144204, Oct. 2007.

[118] X. L. Liu, G. Lindwall, T. Gheno, and Z. K. Liu, “Thermodynamic modeling of Al-Co-Cr, Al-Co-Ni, Co-Cr-Ni ternary systems towards a description for Al-Co-Cr-Ni,” *Calphad Comput. Coupling Phase Diagrams Thermochem.*, vol. 52, pp. 125–142, Mar. 2016.

[119] A. C. Lieser, C. L. Zacherl, A. Saengdeejing, Z.-K. Liu, and L. J. Kecskes, “First-principles calculations and thermodynamic re-modeling of the Hf–W system,” *Calphad*,

vol. 38, pp. 92–99, Sep. 2012.

[120] A. Togo, “spglib, a C library for finding and handling crystal symmetries,” 2013.

[121] S. Ong, W. Richards, A. Jain, G. Hautier, M. Kocher, S. Cholia, D. Gunter, V. Chevrier, K. Persson, and G. Ceder, “Python Materials Genomics (pymatgen): A robust, open-source python library for materials analysis,” *Comput. Mater. Sci.*, vol. 68, pp. 314–319, Feb. 2013.

[122] A. van de Walle, Q. Hong, S. Kadkhodaei, and R. Sun, “The free energy of mechanically unstable phases.,” *Nat. Commun.*, vol. 6, p. 7559, Jan. 2015.

[123] S. Ong, A. Jain, G. Hautier, M. Kocher, and S. Cholia, “The materials project,” 2011.

[124] A. Janotti, M. Kr?mar, C. L. Fu, and R. C. Reed, “Solute Diffusion in Metals: Larger Atoms Can Move Faster,” *Phys. Rev. Lett.*, vol. 92, no. 8, p. 85901, Feb. 2004.

[125] M. SHUWEI and Z. YUNRONG, “Diffusion behaviour of hafnium in Ni and Ni3Al,” *J. Mater. Sci. Lett.*, vol. 16, no. 21, pp. 1761–1763, 1997.

[126] M. Takeyama and C. T. Liu, “Microstructures and mechanical properties of NiAl–Ni2AlHf alloys,” *J. Mater. Res.*, vol. 5, no. 6, pp. 1189–1196, Jun. 1990.

[127] X. Feng, A. Hope, and J. C. Lippold, “Effect of Cr on eutectic phase formation and solidification temperature range in Ni–Cr–Hf system,” *Mater. Lett.*, vol. 116, pp. 79–81, Feb. 2014.

[128] N. Dupin and B. Sundman, “A thermodynamic database for Ni-base superalloys,” *Scand. J. Metall.*, vol. 30, no. 3, pp. 184–192, Jun. 2001.

[129] C. Zhang, J. Zhu, Y. Yang, H.-B. Cao, F. Zhang, W.-S. Cao, and Y. A. Chang, “Thermodynamic modeling and experimental investigation of the Ni-rich corner of the Ni–Al–Hf system,” *Intermetallics*, vol. 16, no. 2, pp. 139–147, Feb. 2008.

[130] N. Mu, T. Izumi, L. Zhang, and B. Gleeson, “The development and performance of novel Pt+Hf-modified γ′-Ni3Al-γ-Ni bond coatings for advanced thermal barrier coatings systems,” in *Proceedings of the International Symposium On Superalloys*, 2008, pp. 629–637.

[131] J.-O. Andersson, T. Helander, L. Höglund, P. Shi, and B. Sundman, “Thermo-Calc & DICTRA, computational tools for materials science,” *Calphad*, vol. 26, no. 2, pp. 273–312, Jun. 2002.

[132] O. Fabrichnaya and C. Mercer, “Phase relations in the HfO2–Y 2O3–Al2O3 system,” *Calphad*, vol. 29, no. 3, pp. 239–246, Sep. 2005.

[133] S. S. Kim and T. H. Sanders, “Thermodynamic Modeling of the Isomorphous Phase Diagrams in the Al2O3-Cr2O3 and V2O3-Cr2O3 Systems,” *J. Am. Ceram. Soc.*, vol. 84, no. 8, pp. 1881–1884, Dec. 2004.

[134] A. Ross, “The Graduate School College of Earth and Mineral Sciences,” 2015.

[135] L. Kjellqvist, M. Selleby, and B. Sundman, “Thermodynamic modelling of the Cr–Fe–Ni–O system,” *Calphad*, vol. 32, no. 3, pp. 577–592, Sep. 2008.

[136] B. Li and B. Gleeson, “Effects of Silicon on the Oxidation Behavior of Ni-Base Chromia-Forming Alloys,” *Oxid. Met.*, vol. 65, no. 1–2, pp. 101–122, Aug. 2006.

[137] D. F. Susan and A. R. Marder, “Oxidation of Ni–Al-Base Electrodeposited Composite Coatings. I: Oxidation Kinetics and Morphology at 800°C,” *Oxid. Met.*, vol. 57, no. 1/2, pp. 131–157, 2002.

[138] Y. Niu, Y. Wu, and F. Gesmundo, “The oxidation of three Ni–6Si–xAl alloys in 1atm O2 at 1000°C,” *Corros. Sci.*, vol. 48, no. 1, pp. 1–22, Jan. 2006.

[139] B. Gleeson, W. Wang, S. Hayashi, and D. J. Sordelet, “Effects of Platinum on the

Interdiffusion and Oxidation Behavior of Ni-Al-Based Alloys," *Mater. Sci. Forum*, vol. 461–464, pp. 213–222, Jul. 2004.

[140] M. J. Li, X. F. Sun, H. R. Guan, X. X. Jiang, and Z. Q. Hu, "Effect of Palladium Incorporation on Isothermal Oxidation Behavior of Aluminide Coatings," *Oxid. Met.*, vol. 59, no. 5/6, pp. 483–502, 2003.

[141] S. Ochial, Y. Oya, and T. Suzuki, "Alloying behaviour of Ni3Al, Ni3Ga, Ni3Si and Ni3Ge," *Acta Metall.*, vol. 32, no. 2, pp. 289–298, Feb. 1984.

[142] H. J. Monkhorst and J. D. Pack, "Special points for Brillouin-zone integrations," *Phys. Rev. B*, vol. 13, no. 12, pp. 5188–5192, Jun. 1976.

[143] A. Zunger, S. Wei, L. Ferreira, and J. Bernard, "Special quasirandom structures.," *Phys. Rev. Lett.*, vol. 65, no. 3, pp. 353–356, Jul. 1990.

[144] Q. Chen and M. Hillert, "The compound energy model for compound," no. 96.

[145] I. Ansara, B. Sundman, and P. Willemin, "Thermodynamic modeling of ordered phases in the Ni-Al system," *Acta Metall.*, vol. 36, no. 4, pp. 977–982, Apr. 1988.

[146] V. Deodeshmukh, N. Mu, B. Li, and B. Gleeson, "Hot corrosion and oxidation behavior of a novel Pt+ Hf-modified γ′-Ni 3 Al+ γ-Ni-based coating," *Surf. Coatings Technol.*, 2006.

[147] S. Hayashi and B. Gleeson, "Early-stage oxidation behavior of Pt-modified γ′-Ni3Al-based alloys with and without Hf addition," *Oxid. Met.*, 2009.

[148] T. Izumi and B. Gleeson, "Oxidation Behavior of Pt+ Hf-modified γ-Ni+ γ'-Ni3Al Alloys," *Mater. Sci. forum*, 2006.

[149] X. L. Liu, G. Lindwall, R. Otis, H. Kim, and Z.-K. Liu, "Thermodynamic remodeling of the Al–Pt system towards an assessment of the Al–Ni–Pt system," *Calphad*, vol. 55, pp. 88–102, Dec. 2016.

[150] T. Goto, “Effects of the Atomic Environment on the Magnetic Properties of Cr-Pt Alloys,” *J. Phys. Soc. Japan*, vol. 43, no. 6, pp. 1848–1853, Dec. 1977.

[151] J. Baglin, F. d’Heurle, and S. Zirinsky, “Interactions Between Cr and Pt Films: New Cr-Pt Phases,” *J. Electrochem. Soc.*, vol. 125, no. 11, p. 1854, Nov. 1978.

[152] A. Kussmann, K. Müller, and E. Raub, “No Title,” *Z. Met.*, vol. 59, pp. 859–863, 1968.

[153] J. Preußner, S. Prins, R. Völkl, Z.-K. Liu, and U. Glatzel, “Determination of phases in the system chromium–platinum (Cr–Pt) and thermodynamic calculations,” *Mater. Sci. Eng. A*, vol. 510–511, pp. 322–327, Jun. 2009.

[154] P. J. Meschter and W. L. Worrell, “An investigation of high temperature thermodynamic properties in the Pt-Zr and Pt-Hf systems,” *Metall. Trans. A*, vol. 8, no. 3, pp. 503–509, Mar. 1977.

[155] C. E. Jr, “Phase Equilibria and Interdiffusion in Ni-Cr-Al-Pt Alloy Systems,” 2011.

[156] K. E. Kornienko, V. G. Khoruzha, K. A. Meleshevich, and M. V. Karpets, “The Constitution of Alloys and Phase Diagram of the Ternary Al–Cr–Pt System at 50–100 at.% Pt. I. Solidus Surface and Isothermal Section in the Al–Cr–Pt System at 1350 C in the Range 50–100 at.% Pt,” *Powder Metall. Met. Ceram.*, vol. 52, no. 5–6, pp. 314–328, Sep. 2013.

[157] P. . Hill, L. . Cornish, P. Ellis, and M. . Witcomb, “The effects of Ti and Cr additions on the phase equilibria and properties of (Pt)/Pt3Al alloys,” *J. Alloys Compd.*, vol. 322, no. 1–2, pp. 166–175, Jun. 2001.

[158] R. M. Waterstrat, “The chromium-platinum constitution diagram,” *Metall. Trans.*, vol. 4, no. 6, pp. 1585–1592.

[159] A. Van De Walle, Q. Hong, and S. Kadkhodaei, “The free energy of mechanically

unstable phases," *Nat. Commun.*, 2015.

[160] A. J. Heidloff, J. Van Sluytman, T. M. Pollock, and B. Gleeson, "Structural Stability of Platinum-Group-Metal-Modified γ + γ′ Ni-Base Alloys," *Metall. Mater. Trans. A*, vol. 40, no. 7, pp. 1529–1540, Jul. 2009.

[161] S. Hayashi, W. Wang, D. Sordelet, and B. Gleeson, "Interdiffusion behavior of Pt-modified γ-Ni+ γ′-Ni 3 Al alloys coupled to Ni-Al-based alloys," *Metall. Mater.*, 2005.

[162] B. Gleeson, "Unpublished work at the University of Pittsburgh." 2017.

[163] P. Y. Hou, T. Izumi, and B. Gleeson, "Sulfur Segregation at Al2O3/γ-Ni + γ′-Ni3Al Interfaces: Effects of Pt, Cr and Hf Additions," *Oxid. Met.*, vol. 72, no. 1–2, pp. 109–124, Aug. 2009.

[164] L. Topor and O. J. Kleppa, "Enthalpies of formation of equiatomic compounds of titanium, zirconium and hafnium with late transition metals: Systematic aspects and comparisons with predicted values," *J. Less-Common Met.*, vol. 155, no. 1, pp. 61–73, 1989.

Vita

Austin Joseph Ross was born in Philadelphia, Pennsylvania, in 1990. He graduated from Stony Brook University with a B.S. degree in Physics with minors in Mathematics and Chemistry. He went on to attend graduate school at the Pennsylvania State University where he received an M.S. in Materials Science and Engineering before continuing towards a Ph.D. degree. Listed Below are his publications associated with his Ph.D.:

1. Lindwall, G., Liu, X. L., Ross, A., Fang, H., Zhou, B. C., & Liu, Z. K. (2015). "Thermodynamic modeling of the aluminum–iron–oxygen system." *Calphad*,*51*, 178-192.
2. Ross, A.J., Boyer, J.E., Liu, Z. K., & A.C. Cortopassi (2015). "Assessment of thermodynamic and equilibrium phase behavior of the Al-C-O system at elevated temperatures and pressures." *JANNAF: 30th Rocket Nozzle Technology Subcommittee Meeting,* Salt Lake City, Utah December 2015.
3. Cortopassi, A.C., Schirtzinger, S.C., Boyer J.E., Ross, A.J., & Liu, Z. K. (2015). "Chemical Erosion of Carbon in SRMs by Aluminum and Aluminum Oxide." *JANNAF: 30th Rocket Nozzle Technology Subcommittee Meeting,* Salt Lake City, Utah December 2015.
4. Shang, S. L., Zhou, B. C., Wang, W. Y., Ross, A. J., Liu, X. L., Hu, Y. J., Fang, H.Z., Wang, Y., & Liu, Z. K. (2016). A comprehensive first-principles study of pure elements: Vacancy formation and migration energies and self-diffusion coefficients. Acta Materialia, 109, 128-141.
5. Gheno, T., Zhou, B. C., Ross, A.J., Liu, X. L., Lindwall, G., Liu, Z. K., Gleeson, B. (2017) "A thermodynamic approach to guide reactive element doping: Hf additions to NiCrAl" *Oxidation of Metals* 87, 297-310.
6. Ross, A. J., Fang, H. Z., Shang, S. L., Lindwall, G., & Liu, Z. K. (2017). "A curved pathway for oxygen interstitial diffusion in aluminum." *Computational Materials Science*, 140, 47-54.